Development of Composite Grinding Wheels for Hard and Soft Metals

Faruk Pruti

A thesis submitted in partial fulfilment of the requirements of the University of East London for the degree of Doctor of Philosophy

November 2011

Director of Studies: Dr S.H. Saidpour

Acknowledgement

I wish to express my sincere thanks and appreciation to my Director of Studies Dr Hossein Saidpour and my previous supervisor Dr Ven Malhotra for introducing me to the subject of this thesis and for spending endless time and effort in providing invaluable advice with continuous guidance and encouragement which have been pertinent in the success of this work. Also, I would like to dedicate this work to my family for their support.

I am also grateful for the help rendered, in many different ways, by the following:

Prof. Roy Perryman (Deputy Head of School)
Dr Mohammad Razmara
Ms Karren Huff (Research and Quality Administrator)
Mr. Ralph Potter (Pipeline Technology Group)
Mr. S.E. Teo (Pipeline Technology Group)
Mr. Fred Dietz
Mr. Steve Ruff
Mr. Trevor Rhoden

Abstract

This research investigates the performance of grinding wheel in terms of its internal granular particles and their effect on the surface finish for both soft and hard metals subjected to both dry and wet conditions of use. The study considers the properties of materials of construction including hardness of the granular particles and their size and distributions that affects the grinding wheel efficiency in abrading of soft and hard metal surfaces. Furthermore, in order to improve grinding performance, the mechanism of clogging the cutting surface of the grinding wheel as a function of for example, the surface properties of granular particles and the chips formed during the grinding operation have been considered.

Objective of this project is to study the overall sharpness of the grinding wheel in terms of its internal granular particles and their effect on the surface finish for both soft and hard metals at different conditions of use. The properties of materials of construction including hardness of the granular particles that affects the grinding wheel efficiency in abrading of soft and hard metal surfaces have been studied.

During this project two novel grinding wheels, namely single grooved and crossed grooved wheels, have been developed and their performance has been compared with a selected commercial grinding wheel, the design of grinding wheels incorporated an innovative surface profile which has been shown to be capable of taking potentially large depths of cut at high wheel and workpiece speeds to create a highly efficient material removal process. This aggressive processing generated high temperatures in the contact zone between the wheel and workpiece. The voltage measured by oscilloscope during grinding of different workpiece materials including mild steel, brass and aluminium bars was related to the temperature generated between wheels and workpiece materials.

Temperatures in the ground surface can be predicted with a knowledge of the specific grinding energy and the grinding parameters used. Specific grinding voltage recorded at high specific material removal rates demonstrated a constant value of specific grinding heat dependent on cutting and contact conditions, improving accuracy of the predictive model.

Cutting and contact conditions in the different grinding wheels vary dependent on their surface patterns. This thesis shows how temperature, contact stresses, material removal rates vary with the surface profile, size and orientation of the abrasive particles of the grinding wheel, affecting the performance of the grinding wheel during the grinding operations. Redesigning grinding wheels by making grooves on surface of wheel, material removal rate was increased and less voltage has been recorded. Also, time for redressing wheels was reduced. The wheel surface of crossed grooves shape showed a significant improvement in grinding of soft materials e.g. aluminium.

Finally, the different stress distribution, including von_Mises, principal stresses and shear stresses, in the grinding wheels and the three workpiece bars during the grinding process were investigated using Finite Element Analysis (FEA) technique. The maximum von-Mises stress value of the brass bar was found to be 173.2 MPa. Hence the strength of produced grinding wheel calculated as 207 MPa which was extensively higher than the maximum von-Mises stress value obtained from FEA profile, resulting 19.5% higher strength in crossed grooves wheel.

Table of content

Nomenclature

A	*Cross sectional area of the unreformed chip;*
A_0	*Interface area of a grain;*
A	*Depth of cut;*
a_c	*Engaged length of a grain;*
A_d	*Dressing area;*
a_d	*Dressing depth;*
A_m	*Mean chip cross sectional area;*
A_p	*Area of the pile-up material;*
A_t	*Real contact area between wheel and workpiece;*
B	*Grinding width, radius of the projected area of grain;*
b_c	*Cutting width of a grain;*
C	*Constant;*
C'	*Constant of constrain;*
C_o	*Constant;*
C_1	*Static cutting edge density;*
d_c	*Diameter of the equivalent grain constant circle;*
d_e	*Equivalent diameter;*
d_g	*Diameter of abrasive grain;*
d_s	*Wheel diameter;*
d_w	*Workpiece diameter*
E	*Energy consumption;*
e_c	*Specific energy;*
e_{cc}	*Specific cutting energy;*
e_f	*Specific energy due to friction;*
e_g	*Specific energy for a single grain;*
F	*Constant;*

F_0	*Initial grinding;*
F_1	*Constant;*
F_2	*Constant;*
f_c	*Cutting force on grain;*
F_d	*Dressing force;*
f_d	*Dressing lead;*
F_e	*Critical grinding force at the end of the secondary grinding stage*
F_n	*Normal grinding force;*
f_n	*Normal grinding force on a grain;*
F_{nc}	*Normal grinding cutting force;*
f_{nc}	*Normal grinding cutting force on a grain;*
f_{nf}	*Normal grinding friction force on a grain;*
F'_n	*Specific normal grinding force*
F'_{no}	*Minimum specific normal grinding force to removal metal;*
F_{ns}	*Normal grinding force;*
G	*Grinding ratio;*
H	*Hardness of workpiece or wheel hardness grade number;*
M	*Grain size number;*
M	*Probability of grain fracture in a unit grinding cycle;*
N	*The number of revolutions of the workpiece;*
n_d	*The number of dressing passes;*
n_w	*Workpiece rotational speed;*
n_s	*Wheel rotational speed;*
P	*Grinding power;*
P'	*Specific power;*
Po	*Constant;*
P_{ch}	*The chip formation component of the grinding power;*
P_{pl}	*The ploughing component of the grinding power;*

P_{sl}	*The sliding component of the grinding power;*
Q_w	*Grinding removal rate;*
R	*Force of of identification ;*
R	*Radius of the workpiece, exponent constant;*
R_c	*Rockwell hardness;*
S	*Wheel structure number;*
T	*Period of one workpiece revolution;*
T	*Grinding time or cutting depth of a grain;*
$T^{\max}$	*Maximum cutting depth of cut of the grains;*
X	*Exponent*
Y	*Component;*
Z	*Component;*
α	*Proportion of grains actually cutting or coefficient of significance*
β	*Proportion of the groove volume removed ;*
γ	*Diamond sharpness ratio;*
Δ	*Average spacing of grains along the co-ordinate axes;*
Δ_r	*Workpiece radius error;*
Δ_{ro}	*Initial workpiece roudness error;*
δ	*Deflection of the grinding system;*
δ_c	*Local workpiece deformation;*
δ_d	*Elastic deflection of a grain in dressing;*
δ_{rt}	*Rotation of the grain;*
δ_w	*Deflection of the grain centre;*
ε	*Constant;*
η	*Constant;*
θ	*Half-angle of the scratch*
λ	*Grinding force ratio* f_t / f_n *or* F_n / F_t *;*
$\lambda(t)$	*Cutting edge density during grinding;*
λ_0	*Cutting edge density after dressing;*

λ_c	*Cutting edge density at the end of the secondary grinding stage*
λ_w	*Metal removal parameter;*
σ_w	*Strength of the grinding wheel;*
τ	*Time constant;*
ϕ	*Tip angle of the dressing diamond;*
μ	*Friction coefficient*

List of Figures

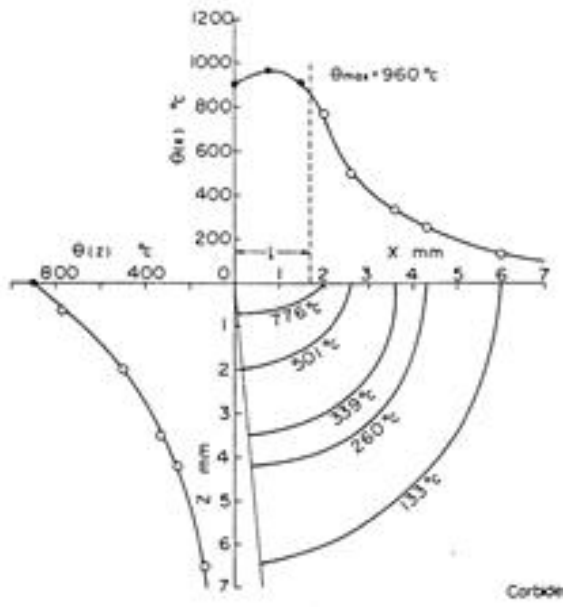

Depth of cut $t_1 = 0.2$ mm
Cutting speed $V_c = 70$ m/min
Cutting time 1 min.

List of Tables

Chapter 1

Introduction

1.1 Background

Grinding wheels are made of natural or synthetic abrasive minerals bonded together in a matrix to form a wheel. While such tools may be familiar to those with home workshops, the general public may not be aware of them because most have been developed and used by the manufacturing industry. In this sector, grinding wheels have been important for more than 150 years.

For manufacturers, grinding wheels provide an efficient way to shape and finish metals and other materials. Abrasives are often the only way to create parts with precision dimensions and high-quality surface finishes. Today, grinding wheels appear in nearly every manufacturing company in the United States, where they are used to cut steel and masonry block; to sharpen knives, drill bits, and many other tools; or to clean and prepare surfaces for painting or plating. More specifically, the precision of automobile camshafts and jet engine rotors rests upon the use of grinding wheels. Quality bearings could not be produced without them, and new materials such as ceramic or material composites would be impossible without grinding wheels to shape and finish parts.

Sandstone, an organic abrasive made of quartz grains held together in natural cement, was probably the earliest abrasive; it was used to smooth and sharpen the flint on axes. By the early nineteenth century, emery (a natural mineral containing iron and corundum) was used to cut and shape metals. However, emery's variable quality and problems with importing it from India prior to its discovery in the United States prompted efforts to find a more reliable abrasive mineral.

By the 1890s, the search had yielded silicon carbide, a synthetic mineral harder than corundum. Eventually, manufacturers Figured out how to produce an even better alternative, synthetic corundum or aluminium oxide. In creating this bauxite derivative, they

developed an abrasive material more reliable than both natural minerals and silicon carbide. Research into synthetic minerals also led to production of the so-called super abrasives. Foremost in this category are synthetic diamonds and a mineral known as *cubic boron nitride* (CBN), second in hardness only to the synthetic diamond. Today, development continues, and a seeded-gel aluminium oxide has just been introduced.

Throughout the grinding wheel's history, the bond that holds the abrasive grains together has proven as important as the grains themselves. The success of grinding wheels began in the early 1840s, when bonds containing rubber or clay were introduced, and by the 1870s a bond with a vitrified or glass-like structure was patented. Since then, bonds used in grinding wheels have been continually refined.

In the grinding operation, the kinematics relationship within the motion(s) of the workpiece and the grinding wheel depends on its cutting grain, the grain size and the distance between two adjacent grains, that is the cutting path-length, which collectively dictates the chip thickness. Also, when the workpiece material can no longer withstand the tearing stress, a chip is formed.

Hence the shape of an idealized chip may be deemed to have been determined by the wheel speed, the removal rate and the distribution of the cutting edges on the wheel surface. Alternatively, the wheel speed and the removal rate may be estimated and/or expressed by the equivalent chip thickness. Equally, the consumption of energy is also influenced by the chip size. In summary, the topography of the inside of a grinding wheel surface and granular particles may be considered to play an important role in the process of grinding.

To select an optimum grinding wheel, a number of factors must be considered. Including the following parameters:

- Type of the materials to be ground
- Kind of abrasive particles used in the wheel
- The amount of stock to be removed
- Wheel speed in operation

For selection of a grinding wheel that allows the abrasive in the wheel to cut efficiently, the wheel must contain the proper bond that is, the material that holds abrasive grains together so that they can cut effectively.

In this project a novel grinding wheel will be made by choosing and mixing appropriate abrasive powder, with a known size distribution of particles, as well as bonding material. This process will be followed by curing process, using an oven. The bonding materials may be mixed with other materials that may be leached out by liquid/solid extraction thus forming a porous novel wheel for study here.

1.2 Brief description of the project

In this study a grinding wheel was selected and fixed on to the machine, Jones Shipman model 540, which will operate at its fixed speed. This rotating grinding wheel will be used to wear off a pre set depth from the top of a work piece. The nature of grinding wheel will be selected to suit the material of construction of the work piece. For each work piece the power consumed during grinding was recorded and analysed versus the surface properties of the grinding wheel that include blinding of the interstices between grinding particles. In this experimental work, effects of lubrication and cooling have been also assessed in order to examine their influence on surface finish.

1.2.1 Grinding Wheels

Conventional grinding wheels are made from mixing measured constituents of a selected abrasive powder followed by other steps. The chosen constituents are placed in a mould and pressed into a wheel shape. The wheel is then fixed in a conventional or electric oven. Aluminium oxide, silicon carbide, bubble alumina, cubic boron nitride are some of the conventional abrasive types particle which commonly have been used in grinding.

For conventional aluminium oxide, perhaps five or six particles are fused together to form the abrasive grain. Silicon Carbide grains are manufactured in a resistance arc furnace using principally silica, coke and carbon electrodes. Both

aluminium oxide and silicon carbide are very hard, but silicon carbide is harder, more brittle and more expensive than aluminium oxide abrasive.

Aluminium oxide is used for grinding steels and steel alloys. Silicon carbide abrasive is used for grinding cost-iron, non-ferrous metals, non-metallic materials. The working of hard and/or brittle materials generally requires a wheel with a fine hard grit size mixed with softer grains. Hard materials resist the penetration of abrasive grains and cause them to dull quickly. The combination of finer grit and softer grade lets abrasive grains brake away as they become dull, exposing fresh, sharp cutting points. Wheels with coarse grit and hard should be chosen for materials that are soft ductile and easily penetrated.

1.3 Summary of Research Contributions

This research program adopts a completely new and innovative investigative approach to the process of optimizing the performance of a grinding wheel during continuous use in any manufacturing operation. The main points of innovative study are as follows.

The arrangement of abrasive particles, hardness and material of construction, size distribution and final porous structure of a selected number of commercially available grinding wheels will be noted under high magnification. The bridging i.e. clogging action of the pores of the grinding wheel by separated particles of the metal surface being removed during grinding will be studied as a function of the above properties. The experimental results will be compared against a numerical FEA model as well as a mathematical model of the grinding process.

A novel structure of a new grinding wheel will be predicted and constructed for continuous testing in a typical industrial grinding process. It is intended to patent the novel structure and construction of the grinding wheels developed.

1.4 Objectives of the investigation

To study the overall sharpness of the grinding wheel in terms of its internal granular particles and their effect on the surface finish for both soft and hard metals at different conditions of use. To study the properties of materials of construction including hardness of the granular particles and their size and distributions that affects the grinding wheel efficiency in abrading of soft and hard metal surfaces. To study the mechanism, in order to improve grinding performance, of clogging the cutting surface of the grinding wheel as a function of for example, the surface properties of granular particles and the chips formed during the grinding operation.

1.5 The methodology to be followed in this study

To achieve a successful outcome of this project and meet the criteria for optimum development of the grinding wheel the following methodology have been pursued:

- To select appropriate grinding wheels, maximum six, that furnish a defined set of properties e.g. the average size of grains, their hardness, materials of construction and bonding.
- To characterise the structure, orientation and size distribution of the particles and pore within a grinding wheel, which are subject of this investigation.
- To develop a mathematical model of the grinding process.
- To develop a three dimensional finite element model of the grinding wheel

This models will include the formation of an idealized chip as a function of the operational parameters of the grinding wheel e.g. depth of cut, rev/min and the linear speed. The established models will be checked from an analysis of the size and shape distribution of the chips formed during grinding. If necessary, the model will be modified in the light of the experimental data collected and analysed.

This model will help to design a novel grinding wheel being constructed from known particles of selected size distribution and chosen materials of construction. These particles will be impregnated and bonded together using an epoxy polymer followed by a curing process in an oven. This approach will be used to produce two novel grinding wheels. One novel grinding wheel will incorporate a single groove profile for removing the chips formed during grinding and retained between edges of the grinding particles and a second grinding wheel will include crossed groove profile. The iteration will be repeated until the predictions of the model closely matches experimentally obtained data.

Thus the mathematical model may need to be modified which includes the process and forces responsible for retaining the chip in the grinding wheel.

- To patent the optimised grinding wheel and its process of construction.

Chapter 2

Literature Review

Manufacturing industry has experienced significant changes in recent years as increasing material and labour costs have taken a necessary toll on its competitiveness. Thus a drive exists for significant reductions in product touch and process time. An effective response to these constraints in the metal cutting field can be to reduce processing times with the use of advanced machining technologies.

By grinding wheel can produce surfaces to very close dimensions and a high degree of smoothness. Hard abrasives can cut hard materials. Often grinding is the only way in which some materials, such as tungsten carbides, may be accurately shaped to final size. Many combinations of abrasive crystals and bonding materials may be used to obtain various rates of cutting and different kinds of surfaces on many type of materials.

2.1 Selection of a grinding wheel

In selecting a grinding wheel, the determining factors are the composition of the work material, the type of grinding machine, the size range of the wheels used, and the expected grinding results, in this approximate order. The Norton Company has developed, as a result of extensive test series, a method of grinding wheel recommendation that is more flexible and also better adapted to taking into consideration pertinent factors of the job, than are listings based solely on workpiece categories. Tool steels and constructional steels are considered in the detailed recommendations presented in this Table 2.1. Recommendations for the selection of grinding wheels are usually based on average values with regard to both operational conditions and process objectives. With variations from such average values, the composition of the grinding wheels must be adjusted to obtain optimum results. Although it is impossible to list and to appraise all possible variations and to define their effects on the selection of the best suited grinding wheels, some guidance is obtained from experience.

The following tabulation indicates the general directions in which the characteristics of the initially selected grinding wheel may have to be altered in order to approach optimum performance. Variations in a sense opposite to those shown will call for wheel characteristic changes in reverse.

Table 2.1: Classification of Tool Steels by their Relative Grindability

Relative Grindability Group	AISI-SAE Designation of Tool Steels
GROUP 1—Any area of work surface	W1, W2, W5
	S1, S2, S4, S5, S6, S7
High grindability tool and die steels	O1, O2, O6, O7
(Grindability index greater than 12)	H10, H11, H12, H13, H14
	L2, L6
GROUP 2—Small area of work surface	H19, H20, H21, H22, H23, H24, H26
(*as found in tools*)	P6, P20, P21
	T1, T7, T8
Medium grindability tool and die steels	M1, M2, M8, M10, M33, M50
(Grindability index 3 to 12)	D1, D2, D3, D4, D5, D6
	A2, A4, A6, A8, A9, A10
GROUP 3—Small area of work surface	T4, T5, T6, T8
(*as found in tools*)	M3, M6, M7, M34, M36, M41, M42, M46, M48, M52, M62
Low grindability tool and die steels	D2, D5
(Grindability index between 1.0 and 3)	A11

GROUP 4—Large area of work surface *(as found in dies)* Medium and low grindability tool and die steels (Grindability index between 1.0 and 12)	All steels found in Groups 2 and 3
GROUP 5—Any area of work surface Very low grindability tool and die steels (Grindability index less than 1.0)	D3, D4, D7 M4 A7 T15

After having defined the grindability group of the tool steel, the proper operation can be find in the first column of Table 2.2. The second column in this Table distinguishes between different grinding wheel size ranges, since wheel size is an important factor in determining the contact area between wheel and workpiece.

Table 2.2: Recommendations for improvements to get good and effective results

Conditions or Objectives	Direction of Change
To increase cutting rate	Coarser grain, softer bond, higher porosity
To retain wheel size and/or form	Finer grain, harder bond
For small or narrow work surface	Finer grain, harder bond
For larger wheel diameter	Coarser grain
To improve finish on work	Finer grain, harder bond, or resilient bond
For increased work speed or feed rate	Harder bond
For increased wheel speed	Generally, softer bond, except for high-speed grinding, which requires a harder bond for added wheel strength
For interrupted or coarse work surface	Harder bond
For thin walled parts	Softer bond
To reduce load on the machine drive motor	Softer bond

Finally, the last two columns define the essential characteristics of the recommended types of grinding wheels under the headings of first and second choice, respectively. Where letters are used preceding A, the standard designation for aluminium oxide, they indicate a degree of friability different from the regular, thus: SF = semi friable (Norton equivalent 16A) and F = friable (Norton equivalent 33A and 38A). The suffix P, where applied, expresses a degree of porosity that is more open than the regular.

To select the best grinding wheel a number of factors must be considered. The first consideration is the material to be ground. The kind of material needs to be ground determines the type of abrasive, which is needed. For example, for grinding steels and the steel alloys, aluminium oxide grinding wheel should be used. For grinding cast iron, non-ferrous metals and non-metallic materials a silicon carbide abrasive must be selected.

A wheel with a fine grit size and a softer grade is required for grinding a hard, brittle material. Hard materials resist the penetration of abrasive grains and cause them to dull quickly. The combination of finer grit and softer grade lets abrasives grains break away as they become dull, exposing fresh, sharp cutting points.

For the soft, ductile and easily penetrated materials wheels with the coarse grit and hard grade are needed. Material can be removed much quicker with coarse grits because they are capable of greater penetration and heavier cuts. Fast cutting can be achieved with wheels having vitrified bonds. If the finish requirements are higher or if a smaller amount of material is to be removed rubber, resin or shellac bond should be used.

American National Standard Grinding Wheel Markings, ANSI Standard B74.13-1990“ Markings for Identifying Grinding Wheels and Other Bonded Abrasives,” applies to grinding wheels and other bonded abrasives, segments, bricks, sticks, hones, rubs, and other shapes that are for removing material, or producing a desired surface or dimension. It does not apply to specialities such as sharpening stones and provides only a standard system of markings.

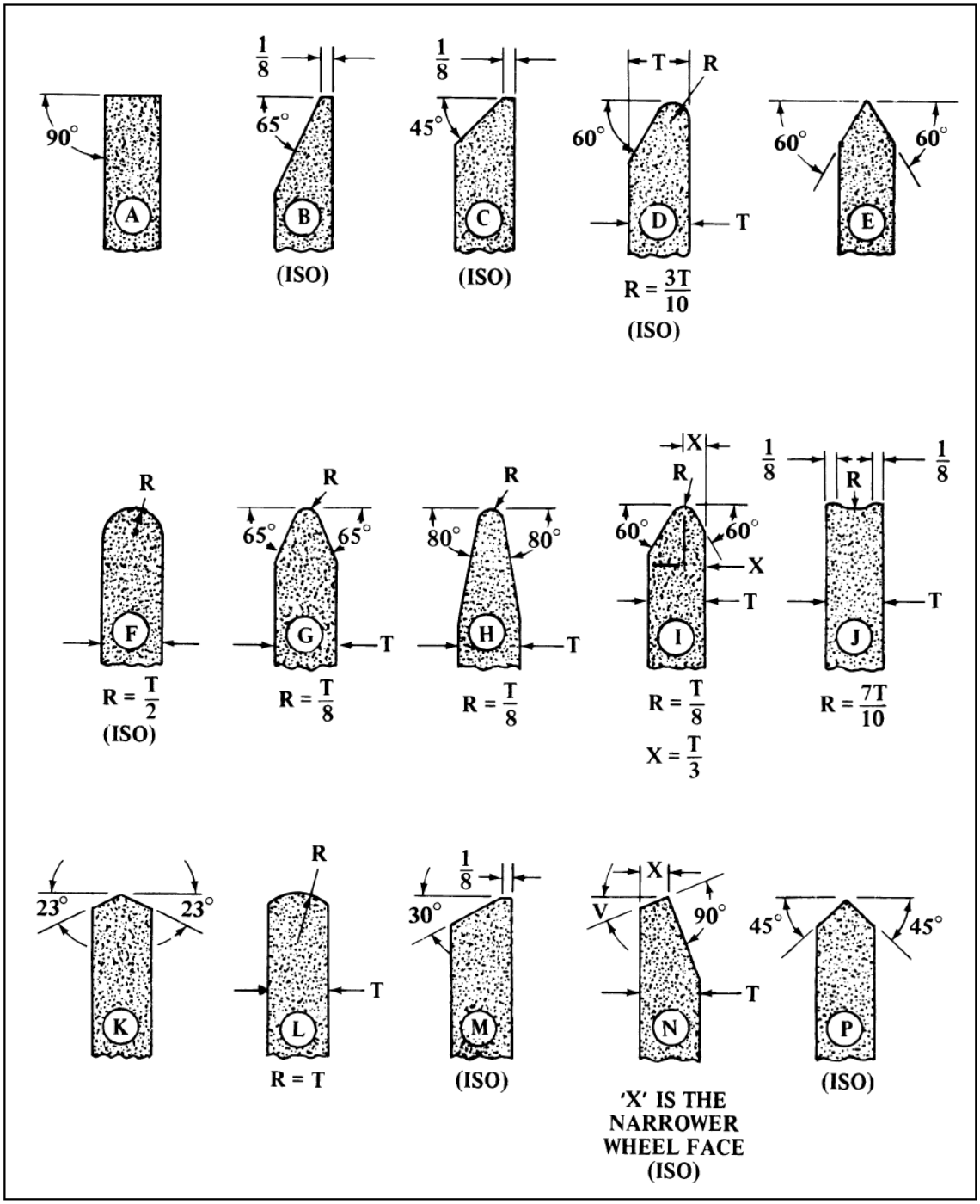

Fig 2.1: Standard Shapes of Grinding Wheel Faces ANSI B74.2-1982

Wheels having the same standard markings but made by different wheel manufacturers may not and probably will not produce exactly the same grinding action. This desirable result cannot be obtained because of the impossibility of closely correlating any measurable physical properties of bonded abrasive products in terms of their grinding action.

Several emergent technologies exist in this field, based around the principle of single set-up, high performance machining; examples of which would include Viper Grinding, Prismatic Machining and High Efficiency Deep Grinding (HEDG).

The literature review will consider the fundamentals of the HEDG process and its predecessors, creep and high speed grinding, as a precursor to the HEDG technology. Following this, temperature measurement techniques employed in both grinding and where relevant alternative metal cutting processes will be considered as a precursor to understanding the development of a temperature measurement methodology for an aggressive environment. Finally the review will consider models of burn threshold applied to the process in terms of the development of the residual stress profile and its prediction via thermal modelling techniques.

2.2 The Grinding Process

According to the U.S. Census Bureau (2006), 2005 saw the shipment of some 792 external cylindrical grinding machines and 564 surface grinding machines with individual values of over $3,025 and a total combined value of over $80 million. Grinding is a major aspect of the production industry, meeting the expectations of Merchant (1971) in terms of both the requirement for grinding processes and the technological advancements attained.

Broadly described by Armarego & Brown (1964), grinding is one of a number of abrasive processes including honing, lapping and super finishing. They have described the abrasive process as a metal cutting process involving hard, sharp and friable abrasive grains, which as a result of their ability to produce a fine surface finish are often considered as finishing processes.

It is stated that there are many instances in which grinding is used for stock removal with the example of rough grinding in foundry work being presented. They go on to consider the earliest forms of abrasive process, which it is suggested began with the use of sandstone for the shaping of tools followed by the use of emery which was found to be more efficient. Emery was suggested to have been originally used as a loose material before it was eventually bonded with clay to form a wheel.

Armarego & Brown (1964) discuss grinding in its role as the most common and best known of the abrasive processes, abrasives are bonded to a wheel or cup, which is power driven. The process consists of a random dispersion of grains in the wheel, taking very small but frequent cuts and producing very small chips. They have divided grinding operations into three major types as shown in Figure 2.2.

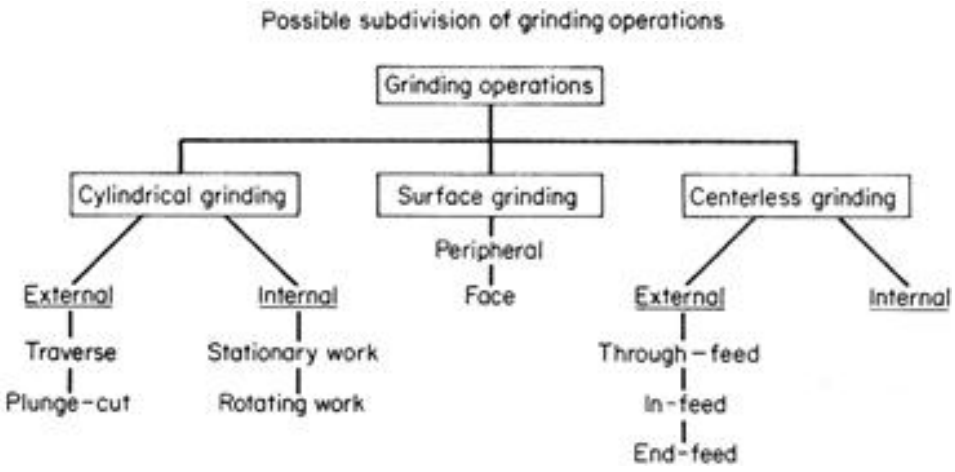

Fig 2.2: subdivision of grinding operations Suggested by Armarego & Brown (1969)

This should be considered in addition to the specialised regimes described in the following pages, which include creep feed, high speed and high efficiency deep grinding primarily utilised in the broad cylindrical and surface grinding operations.

2.2.1 Creep Feed Grinding

Creep feed grinding exhibits a number of benefits over traditional grinding processes. Slow rates of feed with large depths of cut and high levels of coolant application promote a low temperature at the contact and a high quality finished surface.

The creep feed grinding process is described by Malkin (1989) as being characterised by the use of slow workpiece velocities combined with large depths of cut. He describes the increase in depth of cut as a factor of a hundred or thousand times those encountered in regular grinding processes.

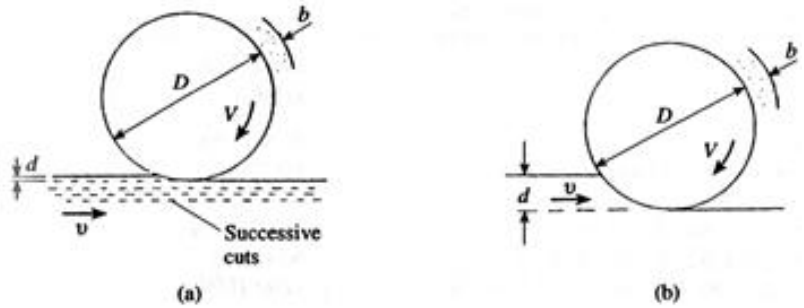

Fig 2.3: Comparison of pendulum and creep feed grinding processes

Shaw (1996) describes the creep feed grinding process in comparison to the conventional pendulum grinding process and presents the schematic comparison of Figure 2.3. He commented on the processes ability to remove the required material in a single pass, when compared to the multiple passes of pendulum grinding and highlights its use in the production of deep slots in hydraulic pumps and fir tree patterns in turbine blade roots.

Shaw (1996) continues to state that the most important aspect of a successful creep feed grinding process is the application of coolant. Coolant must be applied such as to provide uniform coverage of the wheel -work contact zone in order to reduce the high contact zone temperatures generated. The wheel is required to have an open structure such that pockets of fluid can be carried into the contact zone, whilst the use of an air scraper to prevent the boundary layer of air around the wheel deflecting the coolant is advised.

Describing the process, Werner (1979) distinguishes creep feed grinding from conventional grinding regimes by four characteristic features. The total grinding force and wheel-work contact zone temperatures are increased, whilst the individual grit force and work surface temperature are decreased. The increase in total grinding force is described as the result of the increased depth of cut, this increase results in a contact length which increases by a factor of 30 to 100 times. This results in an increased number of grits in the contact zone and hence a decrease in the individual grit force.

The greater energy requirement of the creep feed process results in an increased heat influx per unit contact area. However, the larger contact zone and low heat source velocity result in a greater time for heat dissipation into the work surface, the greater volume yielding a lower overall temperature. It has been already concluded that the creep

feed process can be used to dramatically increase productivity when large amounts of stock have to be removed and the surface requirements are high. It should be noted that in some instances creep feed grinding does not create a greater energy requirement and the slow movement of the heat source can also result in elevated temperatures if uncontrolled.

2.2.2 Wheel speed

Wheel speed in operation is another factor that affects the choice of wheel bond. Usually vitrified wheels are used at speeds less than 6,500 surface revolution per minute. The vitrified bond may break at higher speed. Using wheels with coarser grit and softer grade, for a broad area of contact between the wheel and the work piece, will ensure a free, cool cutting action under the heavier load imposed by the size of the surface to be ground. Smallest areas of grinding contact require wheels with finer grits and harder grades to withstand the greater unit pressure.

2.2.3 High Speed Grinding

For the purposes of this thesis, high speed grinding refers to those grinding processes in which a wheel speed of 60 m/s is exceeded. Increasing the speed of the grinding wheel for a given grinding process produces a number of desirable effects. Knig et al. (1971) presents an early overview of work in the field compiling results from several authors and presenting evidence (Figure 2.4) of the decreasing cutting force, surface roughness and wheel wear as a result of increasing wheel speeds.

High wheel speeds in modern grinding applications are largely the result of improvements in grinding wheel technology. Wheel requirements for successful high speed grinding are described by Jackson et al. (2001).

They have suggested that a wheel exhibiting good damping characteristics, high rigidity and good thermal properties having a thin layer of abrasive material attached to a body of high mechanical strength.

The most suitable abrasive for high speed grinding applications is cubic boron nitride (CBN), Tawakoli (1993) for example highlights the use of electroplated CBN steel wheels, allowing wheel speeds to exceed 200m/s. Jackson et al. (2001) also comment on the suitability of CBN considering its high hardness and thermal and chemical stability to result in an ideal product for high speed ferrous machining. They have continued to describe the application of electroplating as the preferred bonding system with steel wheels and consider cutting speeds in excess of 280 m/s to be possible.

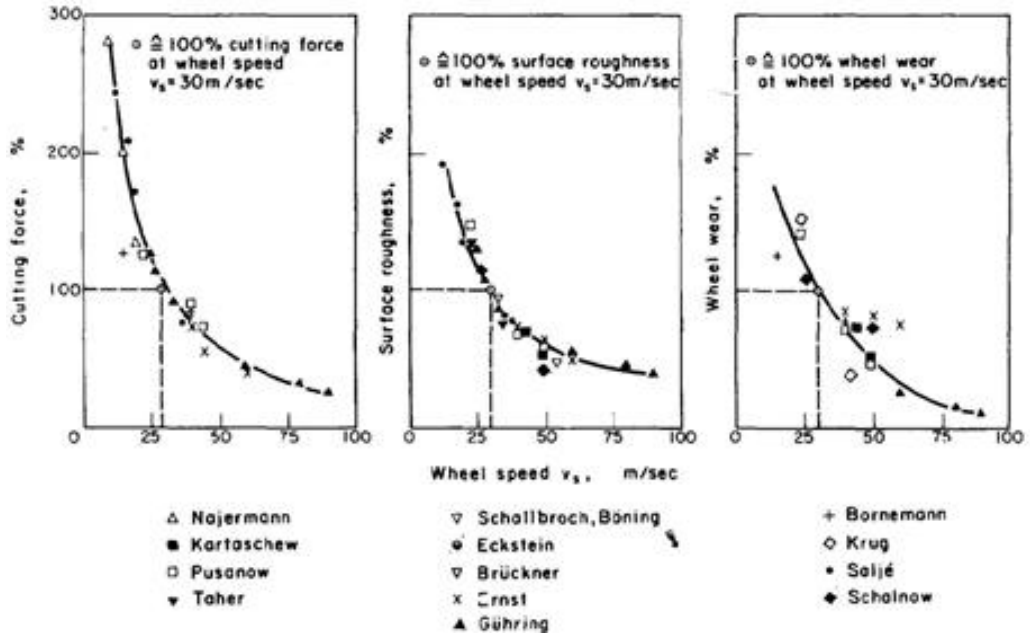

Fig 2.4: Changes in cutting force, surface roughness and wheel wear with increasing wheel speed

2.2.4 High Efficiency Deep Grinding

The High Efficiency Deep Grinding (HEDG) regime is the result of the development of wheel and machine technologies capable of delivering both high wheel and workpiece feed rates with a large depth of cut. The process is the product of the high speed and creep feed grinding regimes utilising the benefits of high wheel speeds at large depths of cut and feed rates to achieve high stock removal rates.

Described by Tawakoli (1993), the process readily achieves specific stock removal rates in excess of 50 $mm^3/mm{\cdot}s$ whilst improving tool wear, specific energy requirement and surface integrity. He also has highlighted that the low workpiece surface temperatures resulting from the HEDG process.

The beneficial contact conditions, high angle of inclination and high wheel and workpiece speeds result in a low workpiece surface temperature and the temperature trend presented in Figure 2.5. It is to be questioned whether the same profile would exist in the sidewall, where no benefit from an angle of inclination is to be found.

Correct selection of the grinding is important for the achievement of stable grinding behaviour and long wheel life. In particular, an appropriate rate of self-sharpening is usually considered to be desirable (King & Hahn, 1986). The total grinding process includes dressing as well grinding.

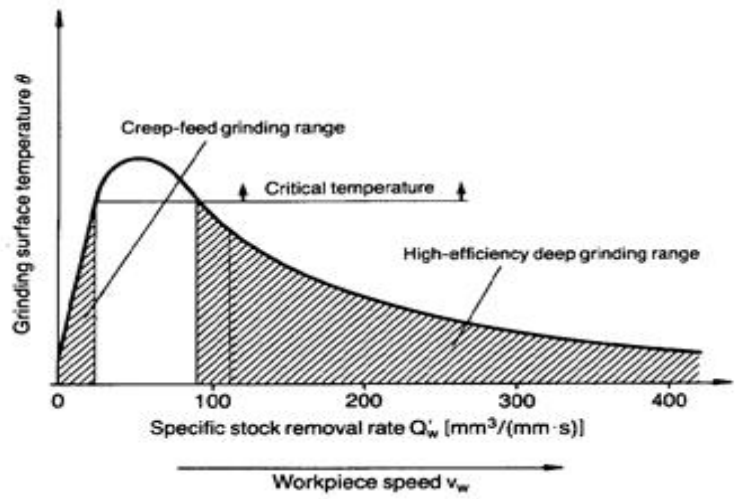

Fig 2.5: low workpiece surface temperature and the temperature trend

Most grinding research is focused on the grinding process rather than the dressing process. Because of the random nature of the grinding wheel topography, the relationships between dressing and grinding parameters are difficult to analyse deterministically. It can be argued that dressing is the least understood but one of the most influential aspects of the grinding process.

Behaviour of the grinding wheel depends partly on its composition and structure and partly on the dressing conditions. The grinding wheel approaches a cutting tool with an infinite number of cutting edges. In grinding operations, if a cutting grit is dull and poorly oriented, it pulls away from the wheel and a new grit is exposed. The hard, sharp-edged grits are randomly located in the matrix of the grinding wheel. Ideally the wheel is much larger than the workpiece so that the effect of wear in negligible when grinding any one piece.

The wheel specification in the standard marking system is defined by the following characteristics (UGWC 1992):

- **Type of abrasive:** The particular abrasive used in a wheel is chosen based on the way it will interact with the work material. The ideal abrasive has the ability to stay sharp with minimal point dulling. When dulling begins, the abrasive fractures, creating new cutting points. Mechanism of each abrasive type is unique with distinct properties for hardness, strength, fracture toughness and resistance to impact.

- **The type of material** to be ground affects the selection of abrasive, grain size and grade. Alumina abrasives (UGWC 1992) are used for grinding high tensile materials such as steel and ferrite cast irons. Silicon carbide abrasives that are even more friable are used for grinding low tensile strength materials and non-metallic materials. CBN abrasive wheels (King & Hahn, 1986) are suitable for grinding high speed steel and high alloy steels. Carbide, ceramic, glass and plastic are often ground using diamond wheels. The harder the workpiece, the harder the grain required. For particular grain hardness, a hard workpiece requires a 'softer' bond than a soft workpiece (UGWC 1992).

- ***Aluminium oxide*** is the most common abrasive used in grinding wheels (Yamaguchi et al., 1999). There are many different types of aluminium oxide abrasives, each specially made and blended for particular types of grinding jobs. Each abrasive type carries its own designation-usually a combination of a letter and a number. These designations do vary from one manufacturer to another. Aluminium oxide are chosen for grinding carbon steel, alloy steel, high speed steel, annealed malleable iron, wrought iron, and bronzes and similar metals. Aluminium oxide crystals are used principally in grinding ferrous and other materials that have a high tensile strength because they are tough and resist fracture to a high degree.

- ***Silicon carbide*** is harder than aluminium oxide, but its crystals are not as tough and break easily. Silicon carbide crystals fracture easily and it is especially adapted to cutting materials with low tensile strength such as brass, aluminium, copper, cast iron, rubber, and plastics. It is also used in grinding hard, brittle materials such as carbide, stone and ceramics.

- ***Ceramic aluminium*** is the newest major development in abrasives. This is a high-purity grain manufactured in a gel sintering process. The result is an abrasive with the ability to fracture at a controlled rate at the sub-micron level, constantly creating

thousands of new cutting points. This abrasive is exceptionally hard and strong. It is primarily used for precision grinding in demanding applications on steels and alloys that are most difficult to grind. The abrasive is normally blended in various percentages with other abrasives to optimize its performance for different applications and materials.

- ***Zirconia alumina*** is abrasive made from different percentages of aluminium oxide and zirconium oxide. The combination results in tough durable abrasive that works well in rough grinding applications, such as cut-off operations, on a broad range of steels and steel alloys. As with aluminium oxide, there are several different types of zirconia alumina from which to choose.

- **Abrasive grain size:** The rate of stock removal and surface texture required affect the choice of abrasive size and bond type. High stock removal rate usually require coarse grain wheels. Fine surface texture and small tolerances need a finer grain size. Extremely fine surface texture usually requires resinoid, rubber or shellac-bonded wheels (UGWC 1992). Selection of the size of grain will depend on the amount of material to be removed, the finish desired and the mechanical properties of the material to be ground, the larger the grains, faster the material will be removed. Coarse grains are better adapted to grinding soft, ductile materials while fine grains are best when fine finishes and close accuracy is required. Selection of size of grain will depend on the amount of material to be removed, the finish desired and the mechanical properties of the material to be ground, the larger the grains, the faster material will be removed. Coarse grains are better adapted to grinding soft, ductile materials while fine grains are best when fine finishes and close accuracy are required.

- **Grade of the wheel**: The letters designating grade indicate the relative strength of the bond that holds the abrasive in place. With given type of bond it is the amount of bond that determines the hardness (grade). When the amount of bond is increased, the size of the bond posts connecting each abrasive grain to its neighbours is increased. A wheel is said to have a soft grade if only a small force is needed to release the grains. It is relative amount of bond in the wheel that determines its grade or hardness.

Hard grade wheels are used for longer wheel life, for jobs on high-horsepower machines, and for jobs with small or narrow areas of contact. Soft grade wheels are used for rapid stock removal, for jobs with large areas of contact, and for hard material such as tools steel and carbides. The accompanying illustration taken from ANSI B74.13-1990

are demonstrated in Figure 2.6, which shows the makeup of a typical wheel or bonded abrasive marking.

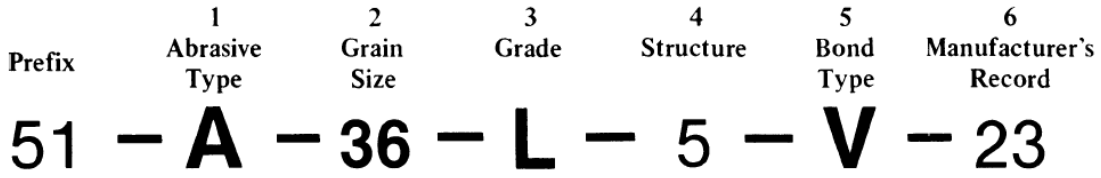

Fig 2.6: Illustration of a typical wheel or bonded abrasive marking

The meaning of each letter and number in this or other markings is indicated by the following complete list.

1) Abrasive Letters: The letter (A) is used for aluminium oxide, (C) for silicon carbide, and (Z) for aluminium zirconium. The manufacturer may designate some particular type in any one of these broad classes, by using exclusive symbol as a prefix.

2) Grain Size: The grain sizes commonly used and varying from coarse to very fine are indicated by the following numbers: 8, 10, 12, 14, 16, 20, 24, 30, 36, 46, 54, 60, 70, 80, 90, 100, 120, 150, 180, and 220. The following additional sizes are used occasionally: 240, 280, 320, 400, 500, and 600. The wheel manufacturer may add to the regular grain number an additional symbol to indicate a special grain combination.

3) Grade: Grades are indicated by letters of the alphabet from A to Z in all bonds or processes. Wheel grades from A to Z range from soft to hard.

4) Structure: The use of a structure symbol is optional. The structure is indicated by Nos. 1 to 16 (or higher, if necessary) with progressively higher numbers indicating a progressively wider grain spacing (more open structure).

5) Bond or Process: Bonds are indicated by the following letters: V- Vitrified, S- Silicate, E- Shellac or Elastic, R- Rubber, RF- Rubber reinforced, B- Resinoid (synthetic resins), BF- Resinoid reinforced, O- oxychloride.

6) Manufacturer's Record: The sixth position may be used for manufacturer's private factory records; this is optional.

If the cutting edges on the grinding wheel tend to glaze and are therefore less likely to be resharpened by fracture, the grinding wheel is described as acting ‘hard’. When the wear of cutting edges on the grinding wheel is mostly due to the fracture of the grains or bonds, the wheel is described as acting ‘soft’.

The effects of the grinding condition on wheel behaviour are summarized in Table 2.3 (UGWC 1992).

Table 2.3: Effect of grinding conditions on wheel hardness behaviour

grinding conditions	behaviour of wheel
High wheel speed	hard
High work speed	soft
High in feed rate	soft

- **Grain structure:**

The grinding contact area also affects the selection of the wheel grade and structure. A large contact area requires a wheel of soft grade and open structure. Vitrified wheels for dry grinding need to be one or two grades softer than for wet grinding (UGWC 1992). The grain structure number indicates the relative spacing of the abrasive grains.

When the grains are close together relative to the grain size, the wheels have low structure numbers such as 1,2,3,4 & 5. Wider spacing relative to grain size is designating by higher numbers. Selection of the proper structure, or spacing between the grains, is governed by the finish required, the nature of the operation, and the mechanical properties of the material to be ground.

A blunted wheel tends to increase grinding force, which may result in grinding chatter or grinding burn (Malkin 1986). If the wheel needs to be dressed too frequently because the grinding force rapidly increases, the wheel is said to be too hard and a softer

grade or coarser grain size is required. When the surface texture and dimensional accuracy of workpiece have deteriorated, the wheel needs to be redressed. If this happens too frequently, the wheel is said to be soft or too coarse, the wheel is said to be too soft or too coarse and either a harder grade wheel or a finer grain size is required.

- **Type of bond:**

Bond is the medium that holds the grains together in the form of a wheel, or on belt or disk. The bond functions in the same way as tool post and holds the grains or cutting tools in position until they become dull and are torn out and fresh grains exposed. Vitrified bonds, organic substances and rubber are three principal types of bonds used in conventional grinding wheels. Each type is capable of giving distinct characteristics to the grinding action of the wheel. The type of bond selected depends on such factors as the wheel operating speed, the type of grinding operation, the precision required and the material to be ground.

- ***Vitrified bonds***

Most grinding wheels are made with vitrified bonds, which consist of mixture of carefully selected clays. At the high temperatures produced in kilns where grinding wheels are made, the clays and the abrasive grain fuse into a molten glass condition. During cooling, the glass forms a span that attaches each grain to its neighbour and supports the grains while they grind.

Grinding wheels made with vitrified are very rigid, strong, and porous. They remove stock material at high rates and grind to precise requirements. They are very hard, but at the same time they are brittle like glass. The pressure of grinding breaks down vitrified bonds.

- ***Organic substances***

Bond made of organic substances softens under the heat of grinding. The most common organic bond type is the resinoid bond, which is made from synthetic resin. Wheels with resinoid bonds are good choices for applications that require rapid stock removal as well as those where better finishes are needed. They are designed to operate at

higher speeds, and they are often used for wheels in fabrication shops, foundries billet shops and for saw sharpening and gumming.

- ***Rubber***

Another type of organic bond is rubber and wheels made with rubber bonds offer smooth grinding action. Rubber bonds are often found in wheels used where a high quality of finish is required, such as ball bearing and roller bearing races. They are also frequently used for cut-off wheels where burr and burn must be held to a minimum.

2.2.5 Vertical Side Face Grinding

One of the most common applications for high performance grinding applications such as creep feed and high efficiency deep grinding is the production of deep slots and profiles. The production of a deep feature using the grinding process results in the development of a vertical sidewall. This sidewall can experience a differing wear and thermal profile to the axis parallel surface.

Both Mindek & Howes (1996) consider the effects of the presence of a sidewall during the grinding process. They discuss the effect of the sidewall in creep feed grinding, they highlight the limitation of coolant access into the sidewall and the wear on the wheel edge radius as detrimental to the heat flux into the sidewall and the holding of tolerance in the bottom of the slot. The heat flux into the sidewall is considered to increase as the wheel begins to gather debris and worn wheel grits are not removed from the wheel.

They develop a model of the thermal and stress considerations in the sidewall for a creep feed grinding application. They suggest that for surface grinding conditions the peak temperature position in the wheel work contact zone will leave a burn strip on the sidewall. This is the result of the process not removing the sidewall material in subsequent passes as would be experienced in cylindrical traverse grinding. Figure 2.10 shows schematically the anticipated location of this burn strip in creep feed grinding. It may be expected that this burn strip exist in HEDG also, as a result of the similar depths of cut and the known high contact zone temperatures experienced.

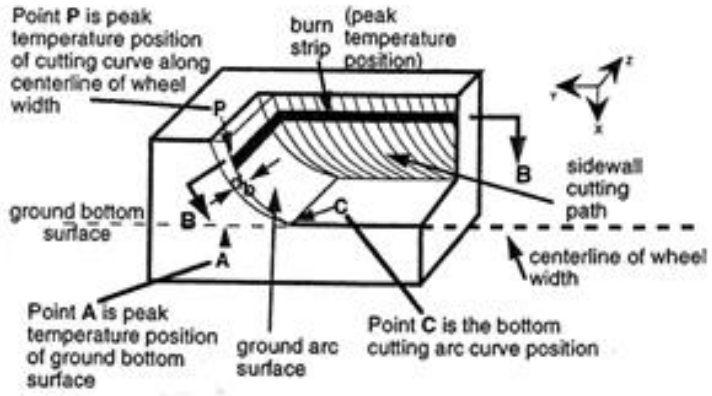

Fig 2.7: Anticipated location of burn in sidewall during creep feed grinding

The application of deep grinding of narrow slots in the HEDG regime is discussed by Werner & Tawakoli (1988b) and considers the application of an optimised wheel geometry for slot grinding. The authors developed a solid wheel, with partial electroplating of the CBN abrasive to the wheel flank or sidewall. This was shown to be the result of experimentation with a fully electroplated wheel and a slotted wheel and permits an improved flow of coolant into the sidewall and reduces sidewall friction. In addition to the benefits of the wheel geometry, a cleaning nozzle arrangement was added to the set-up to remove loaded metal particles from the wheel surface. The use of the optimised wheel geometry is shown to successfully produce slots of 25mm depth by 1.5mm wide in testing.

Snoeys et al. (1978) consider the thermal effects of cut-off grinding, during the cut-off process a vertical sidewall is created as the wheel penetrates the workpiece. The authors suggest that in this case the majority of heat is concentrated in the layer to be imminently ground away. Figure 2.8 (Snoeys et al. 1978) shows a schematic of the theoretical heat flux into the sidewall, the temperature in the sidewall is suggested to be dependent on the workpiece feed rate. The authors also present a theoretical analysis of the temperatures in the workpiece sidewall. Figure 2.9 demonstrates the temperature curves in the sidewall.

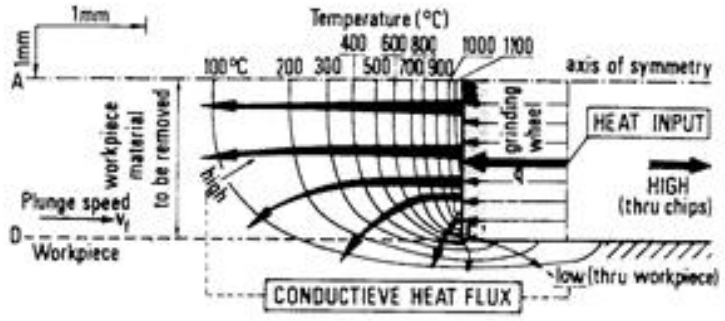

Fig 2.8: Theoretical heat flux to surface and sidewall during abrasive cut-off

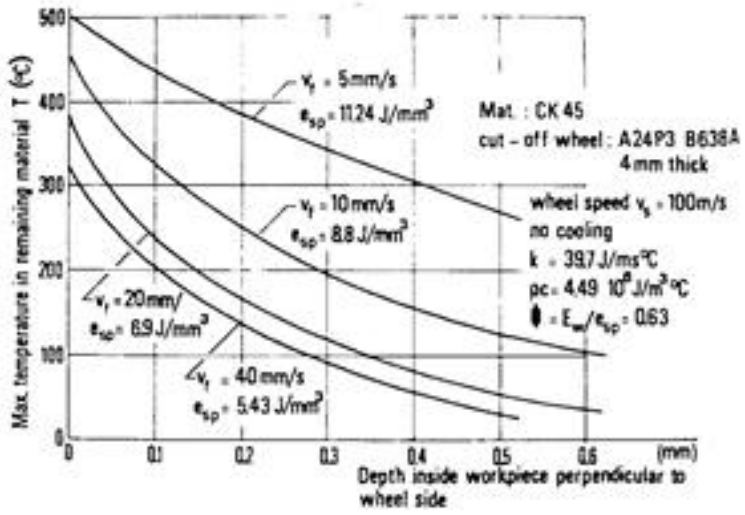

Fig 2.9: Sidewall temperature curves for the abrasive cut-off process

Sainz (2005) made attempts to record the thermal profile where a vertical sidewall was present with the low melting point coating technique. He successfully shows the possibility of recording a complete isotherm in a profile using the technique with the grinding of thin samples and at small widths of cut in the HEDG regime. However the 2mm wide sample was insufficient to contain the entire sidewall isotherm and thermal gradients across the width of the sample due to the cooling at the sidewall face were higher than may be expected. The author concludes that the depth of cut increases the heat flux into the sidewall, with the trend similar for both creep and high efficiency deep grinding regimes. Further no effect on the heat flux to the sidewall as a result of changes in feed rate was found.

2.2.6 Cylindrical Traverse Grinding

Cylindrical traverse grinding is described by Malkin (1989) as grinding with the addition of a crossfeed motion of the workpiece relative to the grinding wheel in a direction perpendicular to the plane of wheel rotation. The author demonstrates the process schematically (Figure 2.10) highlighting the issue of step wear in the wheel as progressive wear is encountered across the wheel width. This may result in a form error, which is cited as a primary reason for the preference of cylindrical plunge grinding in the production environment. The presence of step wear should be limited however by the application of advanced wheel technologies such as electroplated steel CBN wheels, which should exhibit negligible surface wear.

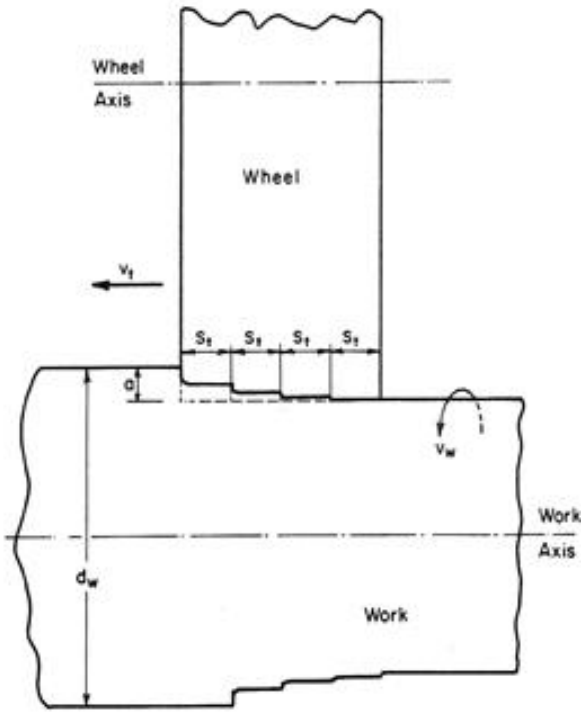

Fig 2.10: Schematic of the cylindrical traverse grinding process

Nakayama et al. (2004) describe an ultra-high speed cylindrical traverse grinding process using CBN wheels. The authors show by experimentation that reducing the traverse feed per workpiece revolution improves the surface roughness. Increasing workpiece speed was shown to suppress the effect of heat in the ground subsurface and could generate compressive residual stress profiles. In conclusion the authors recommend that the increase in work speed allows higher traverse feeds with a small

effective width of cut providing an optimised solution for cylindrical traverse grinding.

In keeping with results for surface grinding with high wheel speeds, both surface roughness and grinding forces are reduced in cylindrical traverse grinding. The work of Nakayama et al. (2004) is limited to a maximum depth of cut of 0.3mm, this delivers a specific material removal rate of 2600mm^3/mm·s and is within the range of high efficiency deep grinding. The work leaves scope for the investigation of larger depths of cut in keeping with stock removal techniques and does not consider temperatures in the surface or sidewall.

Further work in the field of cylindrical traverse grinding has been demonstrated by Weck et al. (2001), Capello and Semeraro (2002) and Bianchi et al. (2003). These reviews consider the application of the cylindrical traverse grinding process to the finish grinding process and do not consider stock removal applications. Stephenson et al. (2002) did however successfully demonstrate the application of the process in the HEDG regime. They considered the use of high rotational speeds with low cross feeds, suggesting that this resulted in a face grinding mode with grinding primarily occurring at the shoulder face of the grinding wheel.

2.2.7 The Application of Grinding Fluid

In grinding, grinding fluids perform a number of functions within the process. Figure 2.14, presented by Brinksmeier et al. (1999) demonstrates the primary effects of lubrication and cooling in the machining process, further to this however it is commonly accepted that coolant also assists in the removal of grinding chips from both the grinding wheel and grinding zone.

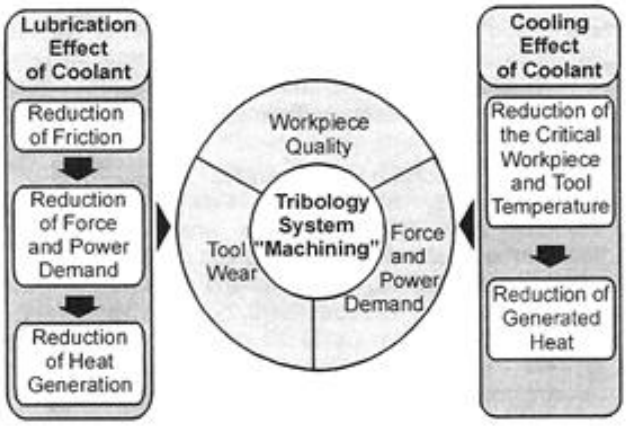

Fig 2.11: Primary effects of lubrication and cooling in the machining process

Ye & Pearce (1983) consider the effect of the type of coolant in the creep feed grinding of a Nickel-base alloy. They demonstrate through experimentation the benefit on surface roughness and profile retention with the use of oil as a cutting fluid. However it is suggested that in this process the use of oil is more likely to result in workpiece burn and therefore if this is a primary consideration, water based coolants are preferred. Further, it is commented that neat oil permitted a greater production rate; this is relevant to the HEDG process as the high production rates possible with the process could be facilitated by the coolant selection.

For the application of grinding fluid to be successful, the coolant must be able to reach the required area of the grinding zone where its functionality is most required. Both Brinksmeier et al. (1999) and Ebbrell et al. (2000) consider the application of coolant into the grinding zone. Of particular importance to the HEDG regime is the boundary layer of air, which occurs around the wheel periphery as a result of high wheel speeds.

Discussed by Ebbrell et al. (2000), conventional methods of fluid delivery are thought to fail to penetrate the boundary layer, resulting in insufficient cooling in the grinding zone. The authors suggest the use of a jet nozzle to avoid this problem, however the application of coolant tangential to the wheel surface is suggested to result in deflection by the boundary layer and thus an angular application of coolant is required, further benefits may also be achieved with the use of a scraper plate to spoil the air flow and minimise the effect of the boundary layer. Further to work relating to coolant selection, Carmona Diaz (2002) presented an optimised geometry for nozzle positioning in the HEDG regime using the Edgetek SAM at Cranfield University.

The author suggests that the leading edge nozzle should be inclined at a shallow angle to the horizontal for surface grinding, which ensures good application of coolant to the contact zone. Considering high performance grinding, Brinksmeier & Minke (1993) suggest the braking effect of the grinding fluid on the grinding wheel is a major limiting factor on the process. When wheel speeds approach 180 m/s, the authors note that only 25% of the total grinding power is actually being used for cutting, the remainder being utilised to drive the coolant (Figure 2.12). The authors also demonstrate the effect of grinding fluid supply on grinding force (Figure 2.13), concluding that the application of coolant in the high performance grinding process is a trade off between the reduction in coolant supply to minimise grinding forces and the minimum quantity of coolant required to cool and

lubricate the process.

Carmona Diaz (2002) studied the influence of grinding fluids on HEDG with a 51CrV4 low alloy steel. His research concluded that the most appropriate selection of grinding fluid for the HEDG regime was neat or synthetic oil. This supports the work of Ye & Pearce (1983), who, working in the creep feed regime, intimated the suitability of neat oil for high stock removal rate processes. It is accepted that this would be true for cylindrical grinding also, as the benefit appears to be the result of the favourable lubrication qualities of oil.

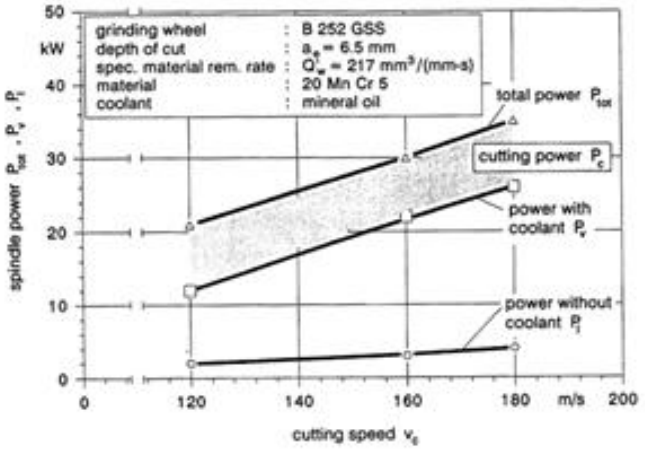

Fig 2.12: The effect of grinding fluid on grinding power

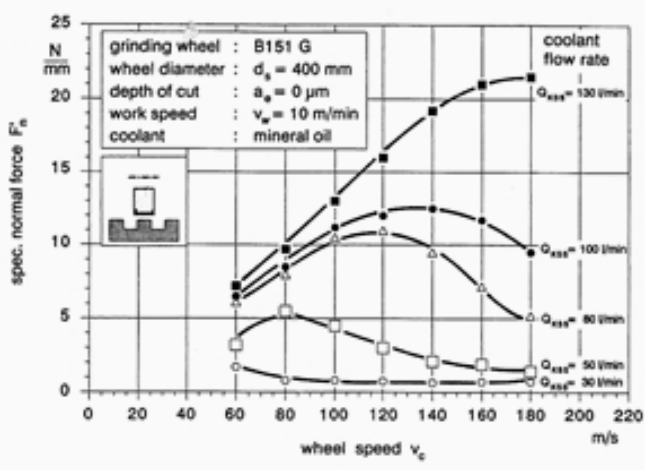

Fig 2.13: The effect of grinding fluid on grinding

2.2.8 Temperature Measurement

The measurement of temperature in any manufacturing process is complicated by issues of accessibility to and the dynamics of the process in question. When considering machining processes, the accurate measurement of temperature is further frustrated by the addition of lubrication to and the removal of swarf from the cutting zone. This is of particular concern for the grinding process, which in many cases floods the wheel workpiece interface with coolant as in the creep feed grinding process or produces high volumes of waste material as found in stock removal processes.

Reviewed by Komanduri and Hou (2001), a variety of temperature measurement techniques are presently available to the researcher. The authors consider the application of thermocouples, infra-red photography and optical pyrometery, thermal paints, materials of known melting temperature and microstructural change. They conclude that the application of a given temperature measurement technique is dependent on the situation considered. Issues include accessibility, heat source size, dynamics of the process, required accuracy, cost implications, sensor technology and data collection.

The use of thermocouples for temperature measurement in grinding is commonplace. Several examples are available of literature presenting results developed from the process, for example temperature measurements in Rowe (2001) utilised this method for verification of thermal models of HEDG. Tawakoli (1993) presents an example of the use of thermocouples for the development of surface temperatures in grinding regimes. He describes advantages including accuracy, a wide temperature range and the ability to place them in or just below the contact zone via drilled holes. It is also noted that the thermocouples require a reference temperature for set-up.

The author provides a schematic (Figure 2.14) of a thermocouple technique for extrapolating surface temperatures via a series of thermocouples placed at varying depths from the contact surface.

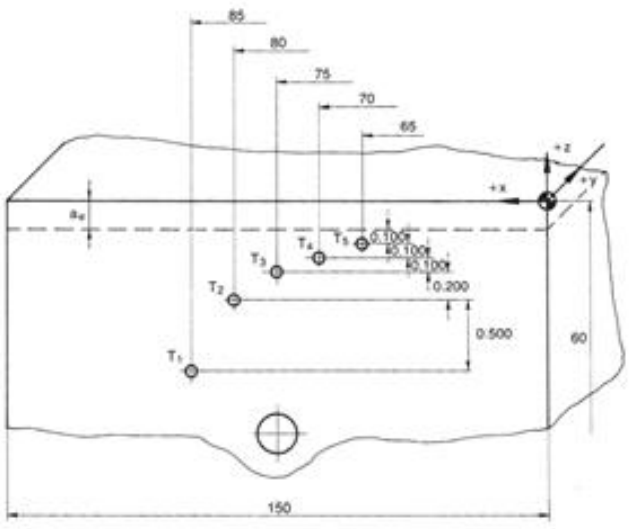

Fig 2.14: Schematic of thermocouple technique for measurement of surface temperatures during grinding

Komanduri & Hou (2001) describe the embedded thermocouple technique process as requiring elaborate preparation, given the requirement for accurate drilling of holes in the surface of an often difficult to machine material. Further, they comment on the disturbance of the heat flow when placed close to the contact surface. They consider that the principal benefits of the system are the ease with which thermocouples can be used and the relatively low cost of the sensors. Kato & Fujii (1997) agree that the termal distortion around the embedded thermocouple may be an issue for the measurement of temperatures at the contact surface in grinding.

Hwang et al. (2003) present an example of the application of an infra-red imaging system to the measurement of temperatures in the grinding process. Trials were performed without the application of coolant by focusing the system onto the sidewall of the grinding sample (Figure 2.15). The authors suggest significant benefits are offered

as a result of the ability to consider temperature measurements over a broader area than the wheel workpiece contact zone; this is highlighted as distinct from other techniques which consider localised temperature measurement only. Issues raised by Komanduri & Hou (2001) relating to the use of infra-red and its requirements for elaborate instrumentation and the possibility of special environments, with the exception of an intolerance for coolant application during trials, appear to have been resolved with technological advancements.

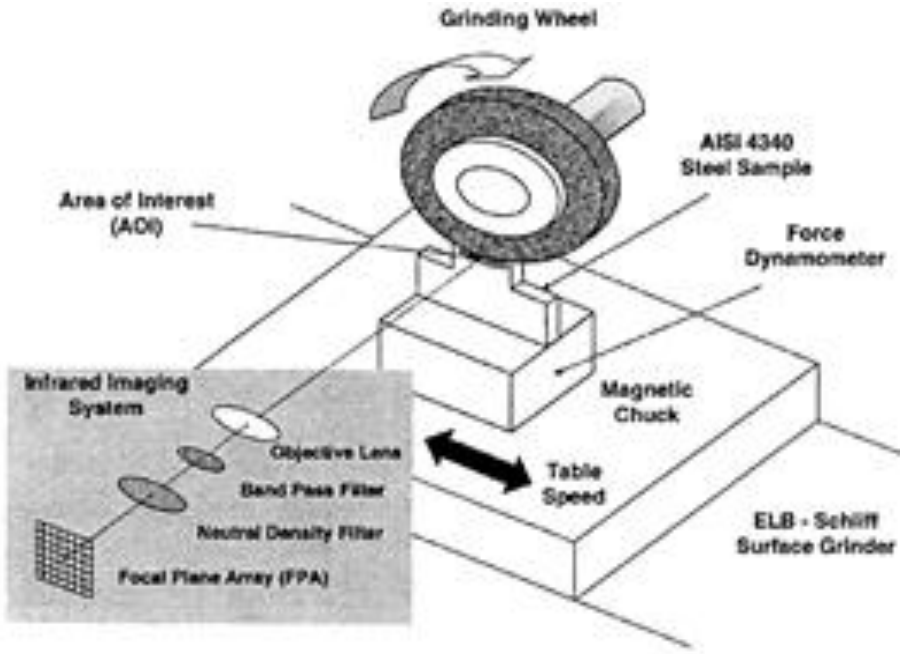

Fig 2.15: Schematic of infra-red temperature measurement system for measurement of grinding temperatures

Earlier measurements of grinding temperature with the use of an infrared radiation pyrometer are presented. An optical fibre is positioned such as to record temperatures at the workpiece surface (Figure 2.16), transferring the data to a remotely located infra-red pyrometer. An experimental set-up utilising a thermocouple for temperature measurement verification was also applied. The chief benefits of the approach are described as the response time and the ability to accurately determine peak temperatures.

Response times of the pyrometer are sufficient to respond to the rapid changes in temperature experienced and thus pick up peak temperatures as well as the average background temperature. More recent work by Müller & Renz (2003) considers the application of an infra-red pyrometer with an optical fibre to a conventional turning process. They agree that the speed of response and the accuracy of the technique are of significant benefit. They describe a metallographic method for determining the temperature gradient in a high speed steel cutting tool. The authors claim that the use of thermocouples and infra-red pyrometry can only provide an indication of the character of the temperature distribution in the tool and that this is inadequate.

The use of the metallographic technique allows for a complete temperature distribution (Figure 2.17) to be developed where applied. By the application of knowledge of the phase transformation temperatures and hence metallographic

changes in the material, the temperature gradient can be determined. Figure 2.18 represents this process schematically, demonstrating the structural changes in high-speed steel as a function of tempering temperature and time. Komanduri & Hou (2001) highlight the limitations of the technique as being the requirement for a suitable material and the increased processing parameters to produce a suitable metallurgical isotherm.

Materials of a known melting point have been applied to machining processes for the measurement of the temperature distribution in cutting tools and surface temperatures in grinding. Kato & Fujii (1997) present the use of powders of a constant melting point to measure tool temperature distribution. The cutting tool was split parallel to the chip flow direction, with the powder applied to the mating surfaces using an aqueous solution of sodium silicate to aid adhesion. The authors conclude that the temperature distributions were measured easily and accurately, with processing resulting in a typical isotherm (Figure 2.19) when surface temperatures were raised as a result of the cutting process. Measurements were recorded graphically as depicted in Figure 2.20, with the technique demonstrated being typical for both powders and pure metals.

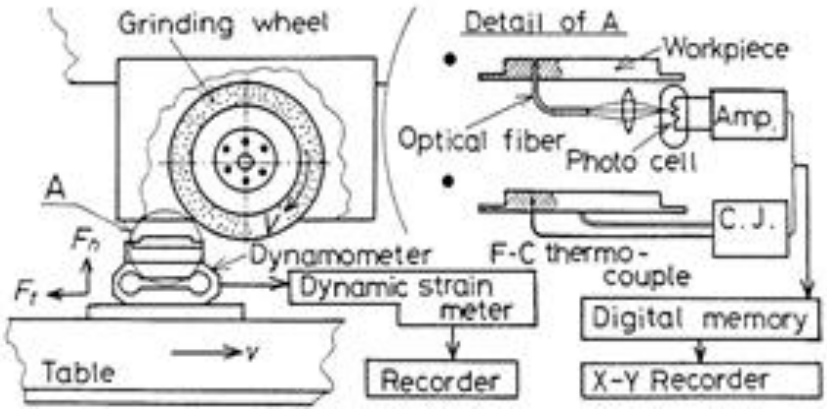

Fig 2.16: Schematic of infra-red pyrometer with local optical fibre temperature measurement system for measurement of grinding temperatures

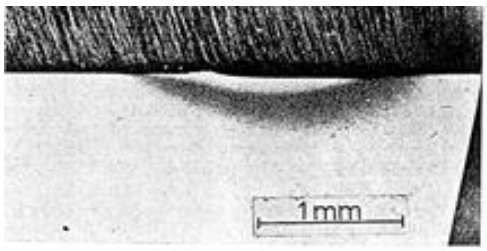

Fig 2.17: Complete temperature distribution shown in metallography of a cutting tool

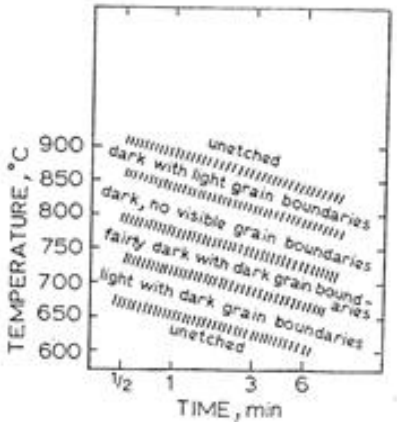

Fig 2.18: Sample time temperature transformation lines for analysis of cutting tools with metallography

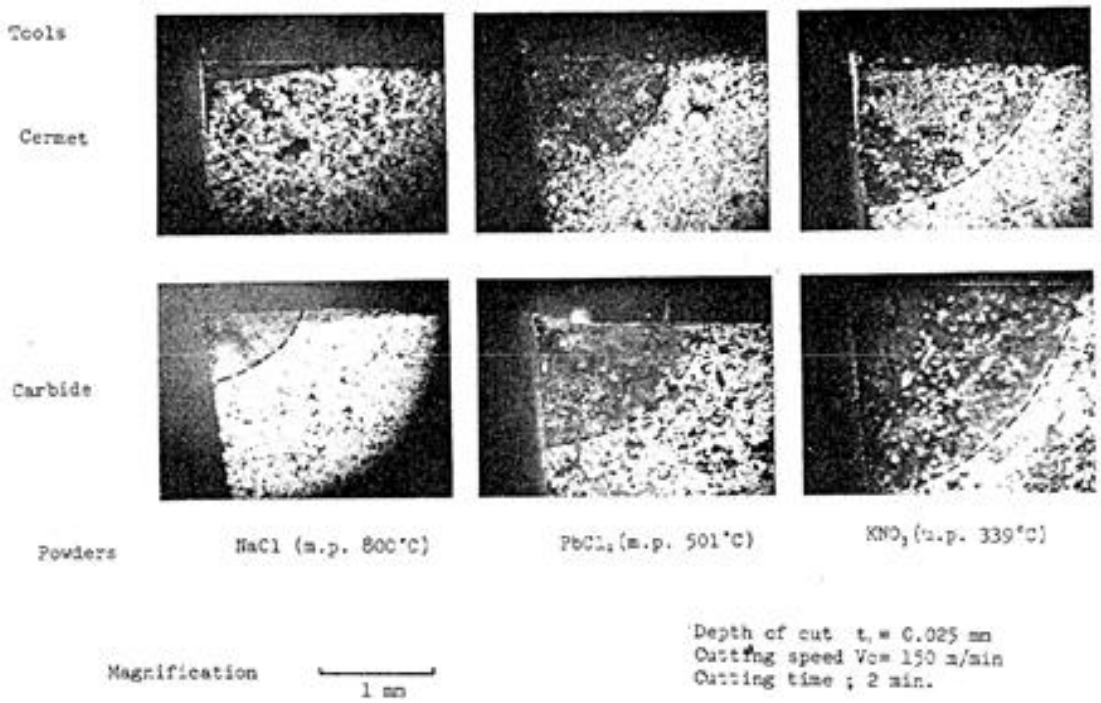

Fig 2.19: Typical isotherms in cutting tools using powders of known melting point

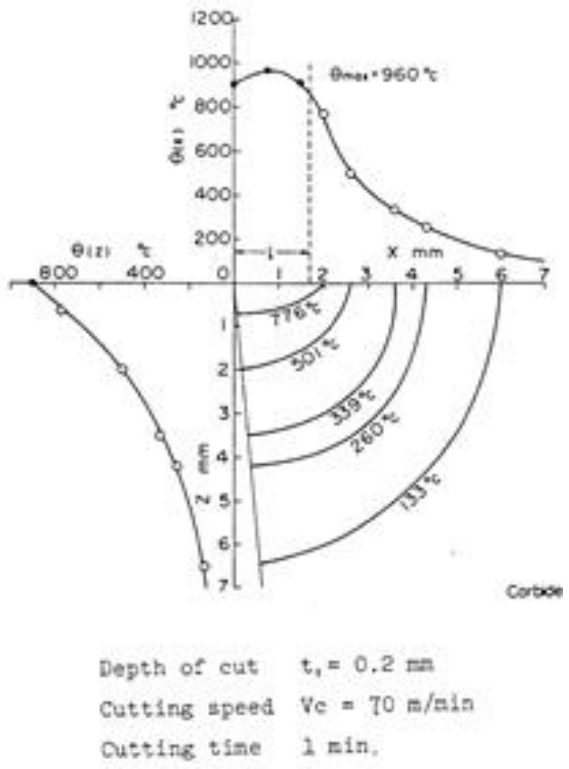

Fig 2.20: Graphical representation of isotherms shown in Figure 2.19

2.2.9 Sharpness of Grinding Wheel

Sharpness of the grinding wheel depends not only on the geometry of the wheel but also on the physical process. A sharpness of grinding wheel is related to sharp grains on the wheel surface. This means the apex angle of the grains is small. A sharp wheel or dull is an ambiguous concept. The definition of Hahn and Lindsay (1969) about wheel sharpness is the high rate of metal removal that wheel can be achieved. On the other hand, the sharpness is being defined as the workpiece surface integrity condition that can be obtained (Hahn 1978).

The wheel sharpness is very important, which influences grinding force, grinding temperature, productivity, accuracy and surface integrity. Since there is no standard definition of wheel sharpness therefore many parameters and methods have been proposed.

To describe the wheel sharpness on the basis of grinding force and stock removal rate the metal removal parameter λ_w was introduced (Lindsay 1986) and defined as equation 2.1.

$$\lambda_w = \frac{Q'_w}{F'_n - F'_{no}} \quad (2.1)$$

Where Q'_w is the volumetric removal rate per unit width, F'_n is the specific normal grinding force, F'_{no} is the threshold value of the specific normal force required to remove metal.

By studying the effects of the grinding parameters, dressing parameters and wheel characteristics, Lindsay (1986) has developed an equation (2.2) for the metal removal parameter in British Imperial Units.

$$\lambda_w = K_{\lambda w} \frac{\left(\frac{v_w}{v_s}\right)^{\frac{3}{19}} \left(1 + \frac{2a_d}{3f_d}\right) f_d^{\frac{11}{19}} v_s}{d_c^{\frac{43}{304}} VOL^{0.47} d_g^{\frac{5}{38}} R_c^{\frac{27}{19}}} \quad (2.2)$$

Where $K_{\lambda w} = 0.021 \frac{inch^{\frac{819}{304}}}{lb, ft}$, d_g is the grain size, d_c is the equivalent diameter, R_c is the Rockwell Hardness, VOL is a volume factor for the wheel, VOL = 1.33H+2.2S-8, H refers to the grade of the wheel hardness, and H= 0,1,2 etc. corresponding to a wheel hardness of H, I, J, etc., S is the wheel structure number, 4,5,6, etc.

Equation 2.2 indicates that an increase in the dressing depth improves the wheel sharpness. The grinding conditions have a strong effect on wheel sharpness.

The time constant τ of the grinding system is a commonly used parameter to indicate the wheel sharpness. The time constant reflects the dynamic response of the system. Time constant represents the combined effect of wheel sharpness and the system stiffness on grinding behaviour. A small value of time constant corresponds to a sharp grinding wheel and stiff machine-workpiece system.

The force ratio F_n/F_t and the specific grinding energy e_c are also used to indicate the wheel sharpness. A sharp wheel corresponds to a small value of force ratio and small value of specific grinding energy. During the grinding process the sharpness of grinding wheel changes and is indicated by the wear of the grinding wheel. The wear of a

grinding wheel in grinding is the combined effect of the wear of individual grains in the wheel. The abrasive grains cut the material and remove small chips when the wheel is rotated at grinding speed.

During the grinding, the forces are imposed on the abrasive cutting points. The magnitude of the forces imposed on the wheel is increased as well as friction and workpiece heating. An increase in the magnitude of grinding force lead to abrasive to fracture and new cutting edges are imposed. Also, this increase in the magnitude, fractures the bond bridges to expose fresh abrasive grains. The wheel is self-sharpening if the fracture wear allows the wheel to remain sharp otherwise wheel has to be dressed more frequently. Loladze and Bokuchava (1985) have been acknowledged three principal mechanisms of wheel wear as follow:

- **Attritions wear**

This occurs on a microscopic scale and enlarges the wear flat area of a grain.

- **Grain fracture**

This is the sharpening mechanism by which a new cutting edge is formed by fracture of an individual grain.

- **Bond failure**

This is a process where dull individual grains break away to reveal fresh grains. The abrasive grains are subject to high temperatures and pressures, as a result of it, chemical reaction, mechanical wear and material bond all play a part. The sharpness of a wheel is reduced by attritions wear of the grains and adhesion of workpiece material.

2.3 Coolant Application

Coolant application is one of the variables in the grinding process. Coolant serves several purposes, removes heat from the work piece, lubricates the grinding and dressing operations, and provides a rust inhibitor for tooling.

Some of the grinding coolants are straight oils, water soluble oils (emulsion type oils), Semi-synthetic fluids and Synthetic fluids.

The continuous dressing keeps the grinding wheel sharp and reduces heat generation. It is critical that a supply of coolant be applied under pressure to the grinding wheel/work piece interface and the grinding wheel/dressing roll interface. Coolant to the grinding zone (interface between the grinding wheel and workpiece) is best applied through jet nozzles. The thermal damage to the workpiece surface can occur during the grinding process and coolant application is used to prevent this.

2.4 Safety in Operating Grinding Wheels:

A damaged grinding wheel can disintegrate during grinding, liberating dormant forces which normally are constrained by the resistance of the bond, thus presenting great hazards to both operator and equipment. To avoid breakage of the operating wheel and, should such a mishap occur, to prevent damage or injury, specific precautions must be applied.

Grinding wheels, although capable of exceptional cutting performance due to hardness and wear resistance, are prone to damage caused by improper handling and operation. Vitrified wheels, comprising the major part of grinding wheels used in industry, are held together by an inorganic bond which is actually a type of pottery product and therefore brittle and breakable. Although most of the organic bond types are somewhat more resistant to shock, it must be realized that all grinding wheels are conglomerates of individual grains joined by a bond material whose strength is limited by the need of releasing the dull, abrasive grains during use.

It must also be understood that during the grinding process very substantial forces act on the grinding wheel, including the centrifugal force due to rotation, the grinding forces resulting from the resistance of the work material, and shocks caused by sudden contact with the work. To be able to resist these forces, the grinding wheel must have a substantial minimum strength throughout that is well beyond that needed to hold the wheel together under static conditions.

2.5 *Characterisation of Grinding Wheels*

Different tests were performed to characterise grinding wheel. Some of the most common tests method used during this study are as follow:

2.5.1 Hardness Tests

The various methods of hardness test are including Rockwell hardness test, Brinell hardness test, Knoop hardness test and Vickers Hardness test.

- **Vickers Hardness test**

To investigate the hardness of different materials, Vickers hardness testing machine was used. It is the standard method for measuring the hardness of metals, particularly those with extremely hard surfaces. The surface is subjected to a standard pressure for a standard length of time by means of a pyramid-shaped diamond. The diagonal of the resulting indention is measured under a microscope and the Vickers Hardness value read from a conversion Table.

The indenter employed in the Vickers test is a square-based pyramid whose opposite sides meet at the apex at an angle of 136º. The diamond is pressed into the surface of the material at loads ranging up to approximately 120 kilograms-force, and the size of the impression (usually no more than 0.5 mm) is measured with the aid of a calibrated microscope. The Vickers number (HV) is calculated using formula 2.3.

$$HV = 1.854(F/D^2) \qquad (2.3)$$

Where F is applied load (measured in kilograms-force) and ***D2*** the area of the indentation (measured in square millimetres). The applied load is usually specified when ***HV*** is cited. The Vickers test is reliable for measuring the hardness of metals, and also used on ceramic materials.

The Vickers indenter is a 136 degrees square-based diamond cone, the diamond material of the indenter has an advantage over other indenters because it does not deform over time and use. The impression left by the Vickers penetrator is a dark square on a light background (Figure 2.21). To perform the Vickers test, the specimen is placed on an

anvil that has a screw threaded base. The anvil is turned raising it by the screw threads until it is close to the point of the indenter. With start lever activated, the load is slowly applied to the indenter. The load is released and the anvil with the specimen is lowered. The operation of applying and removing the load is controlled automatically.

Several loadings give practically identical hardness numbers on uniform material, which is much better than the arbitrary changing of scale with the other hardness machines.

A filer microscope is swung over the specimen to measure the square indentation to a tolerance of plus or minus 1/1000 of a millimetre. Measurements taken across the diagonals to determine the area are averaged. The correct Vickers designation is the number followed "HV" (Hardness Vickers). The advantages of the Vickers hardness test are that extremely accurate readings can be taken, and just one type of indenter is used for all types of metals and surface treatments.

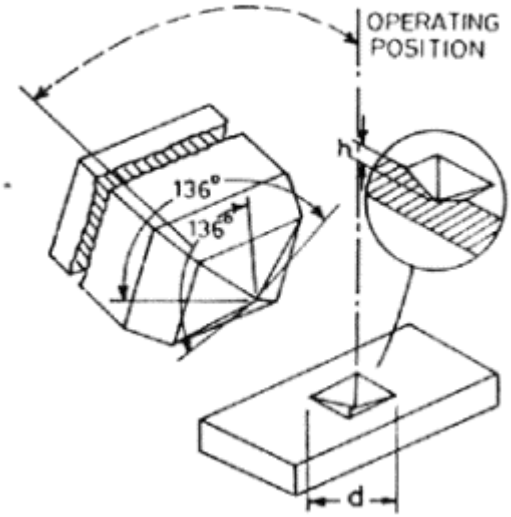

Fig 2.21: Vickers hardness test

2.6 Computer Simulation of the grinding performance

Computer simulation of grinding wheel and bar was performed by using Solidworks 2003/200 and for solid modelling and COSMOSXpress to generate analytical part of this report. Same parameters of Grinding wheels and bar were applied to generate solid modelling. Using of SolidWorks to simulate three dimensional models of grinding

wheel and bars. The programme allowed adequate analysis of designs for functional capability using different analysis tools available, eliminating the traditional separation of design and analysis. The Analysis Advisor wizard allowed user to choose an appropriate analysis for specific tasks and select a correct mesh.

Solid Modelling Processes and FEA Solidworks 2003/2004 was used to draw and extrude the parts in three dimensional objects. Finite element analysis was performed with the support software CosmosXpress.

2.6.1 Finite Element Analysis

Finite Element Analysis (FEA) is a computer simulation technique used to model the physical response of a structure to stress, deformation or temperature. It uses a numerical technique called the finite element method (FEM).

FEA, or finite element analysis, is a technique for predicting the response of structures and materials to environmental factors such as forces, heat and vibration. The process starts with the creation of a geometric model. Then, the model is subdivided (meshed) into small pieces (elements) of simple shapes connected at specific node points. In this manner, the stress-strain relationships are more easily approximated. Finally, the material behaviour and the boundary conditions are applied to each element. Software, such as COSMOS™ FEA software computerizes the process and makes it possible to solve complex calculations in a matter of minutes. COSMOS products can provide the engineer with deep insights to the behaviour of objects. Many of these insights cannot be gained any other way.

There are so many applications of FEA in modern engineering industries. FEA is able to do all that calculations about any structure and stress which is impossible to evaluate manually.

- **Structural Analysis**

FEA is most commonly used in structural and solid mechanics applications for calculating stresses and displacements. These are often critical to the performance of the hardware and can be used to predict failures. The COSMOS STAR module addresses 2D

and 3D linear static problems with state-of-the-art modelling and analysis capabilities. COSMOS STAR calculates stresses, strains and deformations.

- **Thermal Analysis/Heat Transfer**

FEA can be used for thermal analyses to evaluate the temperature distribution, and stresses resulting from uneven heating or rapid temperature changes. Thermal analyses may include convection, conduction, radiation, steady-state, and transient analyses.

The COSMOS HSTAR module helps you model real-world time and temperature-dependent loads and boundary conditions. It helps you analyse thermo-electric coupling to determine the effect of Joule heating on temperature distribution, and element current loading. Figure 2.22 presents a thermal analysis by using COSMOS HSTAR software.

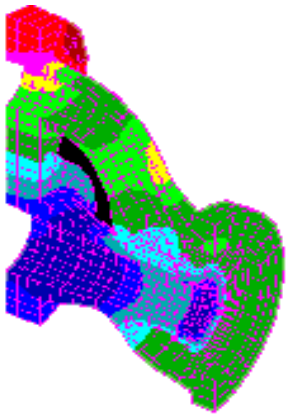

Fig 2.22: Thermal analysis by using COSMOS HSTAR

- **Fluid Flow**

FEA provides insight into complex transient and turbulent flow fields. It allows analysis and optimization of component geometry for efficient fluid flow, as well as allowing users to view velocity, pressure and thermal conditions inherent in the modelled flow fields (Figure 2.23). COSMOSFloWorks™ models transonic, supersonic and subsonic compressible and incompressible gases and liquids through a wide range of Reynolds numbers to ensure that you obtain true-to-life results. COSMOSFloWorks is fully embedded inside of SolidWorks, so it is easy to learn and use.

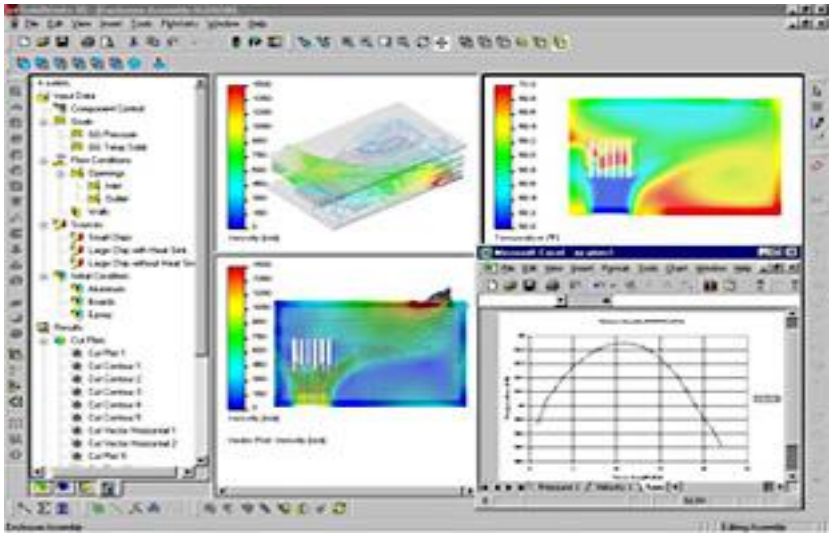

Fig 2.23: FEA of fluid flow by using Solidworks COSMOS Flo works.

- **Advantages of COSMOSWorks**

COSMOSWorks enables faster, less costly, and more optimized product development, as well as more in-depth examination of product performance than would ever be possible using even the most detailed prototypes. Fully integrated with SolidWorks® 3D modelling software, COSMOSWorks allows engineers to test a design and run multiple iterations without ever leaving SolidWorks.

COSMOSWorks shows how a model will perform under real-world conditions before it is built. This allows engineers to predict the physical behaviour of just about any part or assembly under any loading condition.

COSMOSWorks enables designers to meet functional design specifications but not waste materials by over designing; therefore it helps to reduce material costs.

Chapter 3

Dressing Process

3.1 Dressing Grinding Wheels

Dressing may be defined as any operation performed on the face of a grinding wheel that improves its cutting action. Truing the grinding wheel makes it round, concentric with the shaft, and flat across the surface. This means that a fairly large amount of grit is removed from the wheel. Regularly applied truing is also needed for accurate size control of the work, particularly in automatic grinding.

The wheel surface profile formed by dressing is determined by the relative motion between the diamond and the wheel, the characteristics of the wheel and the shape of the diamond. In early research, the dressing process was described as a wheel cutting process. Figure 3.1 shows dressing of grinding wheel by diamond dresser. Chen and Rowe (1996) suggested that the diamond cuts through the abrasive grains to produce cutting points. It has been proposed that the form of the cutting point is determined by the combination of the diamond shape, the dressing lead and the dressing depth.

The perfect grinding wheel operating under ideal conditions will be self sharpening, i.e., as the abrasive grains become dull, they will tend to fracture and be dislodged from the wheel by the grinding forces, thereby exposing new, sharp abrasive grains. Although in precision grinding machine this ideal may be partially attained, it is almost never attained completely. Usually, the grinding wheel must be dressed and trued after mounting on the precision grinding machine spindle and periodically thereafter (Reliance Diamond Tools 2011).

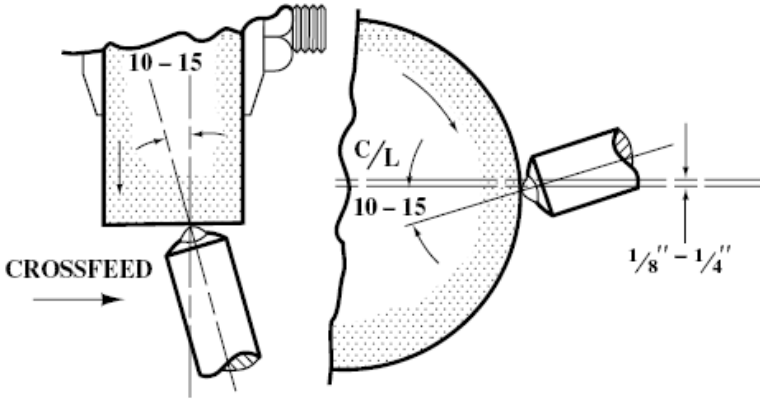

Fig 3.1: Dressing of grinding wheel by diamond dresser.

The simplest kinematic relationship between the grinding wheel and the dressing tool is shown in Figure 3.2. During dressing, the dressing tool moves across the wheel surface with surface with a dressing lead f_d per wheel revolution while XUN removing a dressing depth (Chen & Brian 1996).

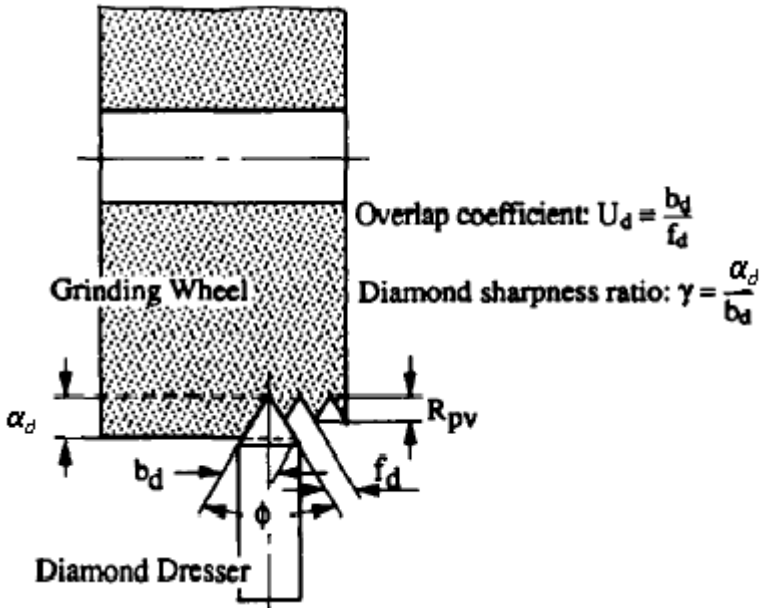

Fig 3.2: Kinematic description of dressing.

A ‘fine’ dressing operation refers to the use of a small dressing lead and small dressing depth. Conversely, α ‘coarse’ dressing operation refers to a large dressing lead and dressing depth. For a dressing diamond with a tip angle Φ, the theoretical peak-to-valley height of the tread profile generated on the wheel can be written as equation 3.1.

$$R_{pv} = \frac{f_d}{2\tan\left(\frac{\phi}{2}\right)} \qquad (3.1)$$

According to this equation, large dressings lead f_d and a sharp dressing tool (tip angle Φ) should lead to a rough wheel surface. When the wheel is used for grinding, the abrasive grains transfer their profile to the workpiece surface since the profile characteristics of the surface of the ground workpiece can be directly attributed to the dressing process (Stephen & Changsheng, 2008).

Accordingly, the dressing traverse rate and the shape of the single-point diamond are particularly important. Torrance and Badger (2000) recorded wheel and workpiece profiles by stylus measurement. Dressing features clearly appeared on the workpiece surface, but could not be detected on the surface of the wheel. They suggested that this was probably because any grooves produced in the grain by the dressing process are very small compared to the roughness of the wheel.

Chen and Rowe (1996) reported that the grain debris size produced during the dressing process and the wheel hardness influenced the size distribution of the dressing particles. The dressing particles for the wheel tested were not much smaller than the grains that went into the wheels, which indicated that the dressing diamond fractured grains to produce relatively large fragments or, possibly, dislodged whole grains from bond. Virtually the entire weight of material dressed off the wheel consists of particles that are much bigger than the dressing depth but smaller than the original grains (Stephen & Changsheng, 2008).

Therefore it must be assumed that the wheel material is mostly removed by brittle fracture to a depth greater than the dressing depth. Although this result throws considerable doubt on the "grain cutting" theory proposed by Malkin and Guo (2008), the "grain cutting theory'' is still helpful in understanding the dressing process.

Abundant cracks can be found in the grain and bond on the dressed wheel surface (Rowe et al., 1993 & Malkin 1989) which supports the conclusion that dressing is a fracture process of abrasive grains and bond. Fracture due to dressing may occur either within a grain or at a bond. Chen and Rowe (1996) suggested that the dressing process consisted of gross fracture and levelling effects, which may be explained by macro and micro action. The micro action refered to the micro fractures on the grain surface.

Allanson (1998) noticed that many of the non-directional micro-cracks on the flat streak of the grain were fragile. The fragile layer had a very low mechanical strength and could not withstand even the 0.5g load of the diamond stylus of the profilometer. This explained why the topography of the wheel cutting surface changed so rapidly during the initial stage of grinding.

The pattern of the wheel topography produced by dressing is transferred, to some extent, to the workpiece surface (Chen & Rowe, 1996). It was assumed that when the dressing diamond passes through the brittle wheel material it causes fracture of the abrasive grains or dislodges them from the bond. It was considered that the wheel profile will not indicate regular features of dressing but will probably contain some points that are coincident with diamond locus. In grinding, a large number of grains on the wheel profile pass through the same section of the workpiece. If each grain profile contains some points that are coincident with the diamond locus, a regular pattern will gradually generate on the workpice surface. Based on this assumption, the envelope of the wheel profile reflects the same features as the workpice produced by the wheel.

The locus traced by the diamond profile replicates onto the abrasive wheel topography which in turn affects the grinding performance. It is shown that (Discos de Diamante 2010) diamond geometry has a significant effect on the stability of the dressing process and thereby influences useful life of the dressing diamond and the efficiency of the grinding wheel operation.

With continued use, a single-point diamond tends to become blunt at its tip and its average radius becomes bigger. This increases the dressing force and the likelihood of bond fracture instead of grain fracture, thereby leaving fewer active grains at the wheel surface. It is reasonable to argue that when a blunt dressing tool cuts plastically through a grain, the top of the remaining grain is flatter (Chen & Rowe**,** 1996). As a consequence, the wheel is less sharp.

The wheel sharpness depends on whether the prevailing effect of dressing is macrofracture or plastic deformation and microfracture. Fracture makes the wheel sharp while plastic deformation makes the wheel blunt. Therefore there is an uncontrolled variation between macrofracture and plastic deformation in the dressing process, which may cause difficulties in grinding process control, especially in automated production.

Sheiko (2007) has stated that the diamond wear in dressing is mainly attributed to abrasive wear and thermal fatigue fracture. When the diamond initially acts on the wheel, the diamond point shatters on impact with abrasive wheel and the diamond loses irregularly shaped particles from the cutting point. This happens almost instantaneously and in most instances is unpredictable. When the diamond is in contact with the wheel and it begin to wear to a shape sympathetic to the profile being traced out. A number of parallel scratches in the direction of the traces of the grains on the wheel are observed. As the wear area increases, the number of cracks on the diamond surface increases, thermal fatigue fracture becomes an important part of the diamond wear. The change of the diamond profile will trace on to the abrasive wheel topography which in turn affects the grinding performance. With diamond wear, dressing chatter may occur. In the event of dressing chatter, the dressing diamond has to be repositioned or replaced.

Shaji and Radhakrishnan (2003) showed that the specific energy in dressing was larger when the dressing lead and depth were decreased. The larger specific dressing energy with finer dressing conditions was attributed to the reduced tendency to fracture and increased plastic deformation.

3.2 Effects of Dressing on the Grinding Wheel Topography

Because of the importance of grinding wheel topography in grinding, a number of researchers (Wan et al., 2006, Koziarski & Golabczak 1985, Fletcher & Maden 1979) focused on the description of the grinding wheel topography. The report reviewed previous research on the relationship between wheel topography and wheel performance. Many techniques for identifying wheel surface topography have been developed. The principal methods for measuring wheel topography are stated below:

Microscopic observation, taper print method, stylus measurement, scratch method, razor blade method, workpiece surface trace method, photo-electric sensing, thermocouple measurement, piezo-electric sensing, thermocouple measurement and piezo-electric dynamometer method. The last two methods can be used to monitor topography during the grinding process and can be used to measure the number of active cutting grains under the dynamic conditions of grinding.

Two dimensional measurement of wheel topography fails to relate to three dimensional functional behaviour of the surface.

Salisbury et al. (2001) have studied the influence of the three dimensional structure of a wheel surface on the final workpiece geometry. In this work, a wheel surface model was developed that can be integrated with a surface grinding process model for simulating workpiece surface texture. The 2-D Fourier forward and inverse transforms are employed to study and model the 3-D surface structure.

Chen and Feng (2009) have been employed 1-D, 2-D and 3-D mainly on abrasive tools topography of wheel surface. Their simplest approach was based on experiment and using the measured tool topography directly in the simulation.

Stout and Sullivan (1989) introduced the technique of measurements and analysis of the grinding process to allow the entire dressing and grinding function to be investigated. By means of these 2-D and 3-D measurements the relationship of the topography of the wheel to the dressing conditions can be discovered. A number of mathematical models were proposed to characterise the surface of the wheel. Statistical methods were widely used to describe the texture of the wheel surface. The parameters commonly used for characterising the wheel topography are the number of cutting points, the probability density distribution of cutting points, the frequency distribution of the cutting points.

Koziarski and Golabzak (1985) investigated the cutting surface of the grinding wheel in relation to the dressing operation. The influence of dressing on cutting edge distribution is expressed as

 (3.2)

The five dressing parameters include, dressing lead f_d, width of dressing tool b_d, dressing depth a_d, grain diameter d_g, and number of dressing passes n_d are represented by X_1 to X_5.

Where;

The coefficients of equation 3.1 were determined by regression analysis at a significance level α=0.10 the vector Y_i is selected in relation to the output required.

The total number of static edges on the wheel surface per unit of the profile length is expressed as

$$Y_1 = 1.645 - 0.049 X_1 - 0.043 X_3 \qquad (3.3)$$

The total number of active edges on the wheel surface per unit of the profile length is expressed as:

$$Y_2 = -1.563 - 0.149 X_1 + 0.107 X_2 + 0.113 X_5 \qquad (3.4)$$

The mean thickness of the undeformed chip is determined as:

$$Y_3 = 0.158 + 0.174 X_1 - 0.095 X_2 - 0.0093 X_3 X_5 \qquad (3.5)$$

According to the above equations, an increase of dressing feed or dressing depth leads to a decrease in the total number of static edges; an increase of dressing depth causes the static cutting edge distribution to penetrate further into the depth of the wheel surface and also increases the depth of active edges; a large diamond tip width results in a concentration of static and active cutting edges close to the nominal wheel surface and increases the number of active edges.

These equations are consistent with the hypothesis that dressing the wheel at a high dressing feed rate or large dressing depth or with a blunt diamond leads to a wheel surface with more fractures of the grain or bond. Dressing a wheel at a slow dressing feed rate, a small dressing depth or with a sharp diamond produces more grain microfractures.

Some of the experiments show that small grain size results in a larger proportion of bond fracture for the same dressing conditions (Brecker 1974). The reasons given are that small grains are tougher than big ones with small grains (Neduet 2011) the dressing lead and depth are larger in proportion to the grain dimensions.

The ratio of the active grains number per unit area to the maximum number is defined as active grain. Malkin and Anderson (1972) found that the number of active grains on the wheel surface increases with a decreasing proportion of bond fractures. Shi and Malkin (2006) on their grinding wheel experiment reported that Wheel wear was

accompanied by a progressive increase in the active grain density and a corresponding decrease in surface roughness. The surface roughness was found to depend mainly on the active grain density and is insensitive to the operating parameters.

The active grains were examined by using microscope. Pattinson and Chisholm (1967) confirmed the density of active grains is increased with decrease of dressing lead, which implied that the proportion of bond fractures is decreased with decrease of dressing lead. However Pande and Lal (1979) gave contradictory results where the proportion of bond fractures increased as dressing lead decreased. By looking into details of the experimental conditions, it was found that the range of dressing lead used by Pattinson and Chisholm was smaller than the range of grains diameter applied by Pande and Lal.

Pande and Lal (1979) also showed that the proportion of bond fracture increases as dressing depth increases. Chen and Rowe **(**1996) quoted same result in their grinding wheel process analysis. This is possibly because increased dressing depth and dressing lead up to the diameter of the grains increase the amount of the wheel material removed during dressing, which produces a larger dressing force on the wheel and a higher probability of bond fracture. When the dressing lead is larger than the diameter of the grains, increasing the dressing lead decreases the length of the dressing path on the wheel surface and decreases the probability of bond fracture.

Besides the influence on the active grain ratio, the dressing operation also affects the shape of the cutting edge. The cutting edges of the wheel are shaped by the fracture and the plastic deformation of the grains. If the bond material is strong enough to withstand the dressing force, the dressing tool will cut through the grain, leaving a relatively large plateau on the top of the grain. With finer dressing conditions, Malkin and Murray (1977) observed larger flattened area formed by plastic deformation on the top of the grains, which was also quoted by Chen and Rowe **(**1996).

It is widely agreed that the mechanics of the grinding process depends on the geometry and distribution of cutting points. Different dressing conditions with different dressing tools make great differences in the topography of the grinding wheel. It was noticed that big changes occur on the wheel surface during the first few dressing passes. Further dressing passes did not yield significant benefit to the wheel surface (Pattinson & Lyon, 1975).

Investigation of the effects of wheel wear (Cai & Rowe, 2004) showed that cutting edges were flattened and distributed closer to the wheel surface with increasing wear. Tsuwa (1972) illustrated the change of cutting edge distribution in the initial stage of grinding due to different dressing conditions. The initial density of cutting edges on the grinding wheel changed and stabilised at a steady state density of cutting edges under particular grinding conditions. Niebel (1990) postulated that optimal dressing would make the cutting point spacing constant throughout the wheel redress life cycle.

3.3 Effects of Dressing on Grinding Behaviour

The shape of the dressing diamond and the dressing conditions have an important influence on the sharpness and topography of the grinding wheel, which subsequently affects grinding force, grinding power, specific energy, grinding temperature, metal removal rate, grinding ratio and wheel wear. The effects of dressing may also be manifested in the quality of the ground product, as defined by size and shape accuracy, surface roughness and surface integrity.

The most important dressing parameters in single diamond dressing operation are dressing lead, dressing depth and the shape of the diamond. The number of dressing passes is also important. A number of researchers (Rowe et al., 1993 & Verkerk 1977) discovered the effects of dressing on grinding force, power, specific energy, metal removal rate and the grinding system time constant. Most of the researchers concentrated on the effects of dressing on grinding behaviour in the steady stage. Little effort has been applied to the effect of dressing on the initial stage of grinding. A larger dressing lead produces a more open wheel surface, leaving sharper grains on the wheel surface with a lower density of active cutting points. With a sharp wheel surface, the metal removal rate is high and grinding force and temperature is low. However, the surface roughness of the workpiece is likely to be larger than with a small dressing lead. The effect of dressing depth on grinding behaviour is similar to that of dressing lead. A large dressing depth produces a rough surface on the wheel because of more macrofracture in dressing.

The effects of dressing are not only evidenced in the grinding behaviour but also in the development of wheel wear. Pattinson and Chilsolm (1967) summarized the strong influence of dressing lead on the initial stage of wheel wear. It has been found that a

larger dressing lead increased the initial wear rate. After the initial wear stage, the wear rate is almost independent of the dressing lead. Pacitti and Rubenstein (1972) further examined influence of the dressing depth on wheel performance.It was found that that a larger dressing depth reduced the rate of wheel wear.

Pande and Lal (1979) found that the wheel life was longer when the rate of bond fracture in dressing was high. It was also concluded that flat cutting edges caused poor cutting performance and decreased the useful life of the wheel. Several dressing passes may be required to stabilise the wheel topography. In multi-pass dressing, the extant topography of the wheel surface is erased and replaced by each successive pass of the dressing tool. Since the second and subsequent dressing passes cannot be guaranteed to be in phase with previous passes, subsequent variations in topography may be expected. This can affect wheel behaviour in grinding. It may be assumed that the number of dressing passes should be a minimum to achieve a satisfactory wheel surface. Pattison and Lyon (1975) showed that there seemed to be little merit in a large number of dressing passes. It may be assumed that the number of dressing passes should be a minimum to achieve a satisfactory wheel surface. The experiments by Pattinson and Lyon indicated that four dressing passes are enough. The shape of the dressing diamond has an important effect on wheel wear. More than 300% differences in wheel wear caused by the shape of the diamond were measured. If small changes of diamond shape make large differences in wheal wear, then it makes accurate prediction of grinding behaviour very difficult. Because the shape of the dressing diamond cannot be controlled, dressing remains subject to a large degree of variability. Dressing with a sharp diamond gives a higher G ratio, the reason being that a sharp dressing diamond creates fewer macrofractures on the wheel surface. The dressing operation has a strong effect on surface roughness, size error and roundness of the workpiece. Many researchers concentrated on surface roughness, because surface roughness reflects the geometrical effects of dressing. Coarse dressing gives a coarse surface texture.

The surface roughness and Figure accuracy were measured by Zhao et al. (2009) with an atomic force microscope (AFM) and Taylor–Hobson profilometer, respectively. The subsurface damage was first evaluated which was realized via observing the subsurface damage. Then a common method was used for measuring the subsurface-damage depth and observing subsurface cracks. Furthermore, the energy-spectrum analysis was used to evaluate the surface and subsurface by an x-ray energy spectrometer.

The experimental results showed that the ground workpiece (optical glass BK7) with surface roughness of 6–30 nm and subsurface-damage depth of less than 2.2 μm was generated with the hybrid-bonded diamond grinding wheel.

Scott and Baul (1986) described the effect of dressing on surface roughness by using a spectral analysis method. An important result shown in many papers is the convergence of the surface roughness with grinding time towards a constant value despite differences of the dressing conditions employed.

Chapter 4

Grinding Process

The grinding process is a process where numerous grains of a wheel pass through the work piece surface. The kinematic relationship between the grinding wheel and the workpiece motion apply to each cutting grain. The analysis of the grinding process can be based on the force on an equivalent grain representative of the wheel surface. Some aspects of the process by which a grain grinds can be illustrated by the geometrical relationship between the grain and workpiece during the grinding process (Alden, Geo 1914 & Guest 1915).

4.1 Phases of Grinding Process

There are three phases in the grinding process including rubbing, ploughing and cutting. When a grain engages with the workpiece, in the rubbing stage, the grain slides on the workpiece surface which cause an elastic deformation and negligible plastic deformation on the workpiece surface.

As the stress between the grain and the workpiece is increased, plastic deformation predominates. This is called ploughing. The workpiece material piles up to the front and to the sides of the grain to form a groove. The chip formation process is called cutting.

Cutting can be the most desirable deformation process. Rubbing and ploughing are inefficient, since the energy is wasted in deformation and friction without contributing to metal removal. A high temperature results that produces an excessive rate of wheel wear and the workpiece surface may suffer metallurgical damage.

4.2 Analysis models in machining process

The fundamental parameter for analyzing machining processes is the specific energy that is defined as energy per unit volume of material removal. For plunge grinding the specific energy is obtained by dividing the machining power P by the removal rate Qw.

$$e_c = P/Q_w = P/(\pi d_w v_f b) \qquad (4.1)$$

Where d_w is diameter of the workpiece, v_f is in feed rate and b is grinding width.

Specific energy is much larger in grinding than in turning, milling and drilling. In order to understand the material removal mechanics in grinding, an abrasive grain may be considered as a cutting tool of irregular shape. Theoretical and experimental analyses (Alden & Geo 1914) based on the grains of an equilateral-triangular pyramid shape, a square-pyramid shape, a conical shape and a spherical shape show that the occurrence of rubbing, ploughing and cutting are strongly dependent on the shape of the grain.

The shape of the grain has a strong effect on the specific energy e_c and the force ratio F_n/F_t. The average effective rake angle of the grain could be expected to lie within the range – 45o to –75o and high negative rake angle, which corresponds to a blunt grain, leads to a high force ratio F_n/F_t and a high specific energy.

The size effect is an important phenomenon in grinding. Backer et al. (1952) found that specific energy became much larger when the undeformed chip thickness was decreased, first discussed the size effect. This observation was attributed to the fact that the small chip size reduced the defects in the metal to be removed, and allowed the workpiece material to achieve its theoretical strength.

Von Turkovich (1970), Nakayama and Tamura (1968) threw a doubt on Backer's description (1952); because their researches showed that the shear strength would not be larger as a result of the decrease of underformed chip thickness. Graham and Baul (1972), Kannapan and Malkin (1972) suggested that the size effect in grinding can be attributed to the occurrence of a relatively greater proportion of sliding and ploughing energy when the undeformed chip thickness is decreased.

Another explanation by the Rowe (2001) may be given by the sliced bread analogy. The thinner the loaf is sliced, the more energy is required to slice the whole loaf.

This is because a greater surface area is created. The energy required to deform material near the surface is expended more times as the number of chips is increased and the surface area of chips is increased. For example, if a cube is cut into two equal halves the surface area is increased by at least one third. More energy is required in cutting the material into smaller chips because the surface area of the chips increases. This effect is therefore too large to ignore.

Shaw (1971) suggested that an abrasive grain could be modelled as a sphere. He presented an analysis which predicted that the force per unit area of the groove will increase as the undeformed chip thickness is reduced. Based on the sphere assumption, Lortz (1979) observed the dead zone in the contact area between the grain and the work piece. There is a critical depth of cut before a chip formation process commences and metal is removed. Also using the sphere model, Malkin et al. (1973) showed that a smaller proportion of the groove volume is removed with smaller undeformed chip thickness due to the material piled up at both sides of the grain. Malkin et al. asserted that the specific energy is unequal to the cutting force divided by the intercepted area of the groove. Only chip formation results in material removal.

The rubbing and ploughing actions in grinding do not produce material removal. Because of the existence of rubbing and ploughing in the grinding process, the specific energy in grinding is higher than in large chip removal processes. The size effect in grinding can therefore be related to the relative proportions of sliding, ploughing and cutting that occur in addition to the effect of the grater surface area.

Local elastic deflection around a grain reduces the real cutting depth of the grain. The local deflection of the wheel when the grain is in contact with steel, are the same order of magnitude as the undeformed chip thickness. Saini et al. (1982) assumed that the elastic deformation consists of four components, local workpiece deformation δw, grain tip deformation δg, variation of deflection of the grain center δc and rotation δrt.

From their results, it was concluded that grain tip deformation δg and rotation δrt are relatively small. The local workpiece deformation δw was said to be just a little more than 2μm and could be considered as a part of the total workpiece deflection. The deflection of the grain centre δc was found to be up to 3μm. The variation of the deflection of the grain centre δc has a trend and scale similar to the total deflection.

Nakayama and Brecker (1971) described the deflection of the grain centre as the form of a hertz distribution,

$$\delta c = F_n^{2/3} \qquad (4.2)$$

Where δc is the deflection expressed in microns and F_n is the normal force expressed in Newton's. Only a part of the chip material at the front of a grain forms the chip because of the elastic and plastic deformation. The remaining material will be removed by successive grains.

The grinding process is often analysed by analogy with the milling process. An average grain is considered as a cutting point mounted on the wheel surface .The grain depth of cut is recognized as the most influential parameter in grinding.

The analysis of the grinding force is based on the relationship between the grain depth of cut and the grinding control parameters. Hahn (1964) suggested that the normal grinding force is proportional to the metal removal rate. The grinding force may be expressed as a linear function of grinding depth. This model cannot take account of the size effect in grinding. An alternative way, by Snoeys et al. (1974) to correlate grinding force with basic process parameters is to employ empirical relationships of the form:

$$F_t' = F_1 h_{cq}^{f} \qquad (4.3)$$

$$F_n' = F_2 h_{cq}^{f} \qquad (4.4)$$

Where F_1, F_2 and f are constants and hcq is the equivalent chip thickness which corresponds to the thickness of a continuous layer of material being removed at a volumetric rate per unit width Qw and cutting velocity vs . This parameter is also equal to the volumetric removal rate per unit area of wheel surface passing through the grinding zone.

$$h_{cq} = \frac{v_w a}{v_s} = \frac{Q_w}{v_s} \qquad (4.5)$$

Where v_w is the workspeed and α is a depth of grinding. The exponent f typically lies in the range 0.4 –0.9.

From the previous equations the specific energy is

$$e_c = F_1 h_{cq} \qquad (4.6)$$

The equivalent chip thickness correlates with other performance characteristics including surface roughness and wheel wear. These empirical relationships/equations tend to be of limited practical use for predicting grinding performance because of the constants depend on effects which have not been taken into account like the dressing conditions, grinding fluid, wheel type, dwell period and workpiece material.

The hcq cannot take into account effects of workspeed on the plunge grinding process because the depth of cut 'a' depends on vf/vw so that hcq depends on vf but not v_w.

To understand the effect of the grinding parameter on grinding force, Ono (1961) initially assumed that the average grinding force on a grain was proportional to the mean chip cross sectional area of the grain Am,

$$f_t = k_c A_m \qquad (4.7)$$

$$f_n = \lambda k_c A_m \qquad (4.8)$$

Where ft and fn are tangential and the normal grinding force on a grain respectively and λ is the grinding force ratio fn/ft. From a survey of experiments on the grinding force, Ono discovered that the grinding force coefficient kc can be empirically expressed as a power function. That is

$$k_c = k_0 A_m^{-\eta} \qquad (4.9)$$

Where k_0 and η are constants and η ranges from 0.25 to 0.5. The grinding force coefficient is commensurate with the specific grinding energy ec .When the wheel passes through the grinding zone of contact length l_k , the workpiece material removed by the wheel is

$$V = b\, l_k\, a \qquad (4.10)$$

Where b is the width of the grinding zone. During the period of contact a grain on the wheel surface covers a distance l_s

$$l_s = l_k v_s / v_w \qquad (4.11)$$

If the separation distance of grains distance of grains on the wheel surface is u, the number of the grains in the length l_s is $\frac{bl_s}{u^2}$. The chip volume removed by a grain will be

$$V_c = u^2 \frac{v_w a}{v_s} \qquad (4.12)$$

If the undeformed chip length is equal to the grinding constant length l_k,

$$l_k = \left(1 + \frac{v_w}{v_s}\right)\sqrt{\frac{a}{\frac{1}{d_s} + \frac{1}{d_w}}} \qquad (4.13)$$

The chip cross sectional area A_m is therefore

(4.14)

The total tangential grinding force Ft is the sum of the forces on each individual grain, therefore

(4.15)

and

(4.16)

Ono's equation is the first attempt to interrelate the grinding parameters v_s, v_w, a, ds and dw by a single exponential coefficient η.Since the equivalent wheel diameter dc is

$$\frac{1}{d_e} = \frac{1}{d_s} \pm \frac{1}{d_w} \qquad (4.17)$$

$$F_t = k_3 b^{3/4} d^{1/4} \left(\frac{v_w}{v_s}\right)^{1/4} d_e^{1/4} \qquad (4.18)$$

Werner (1978) modelled the grinding force on a grain based on an empirical rule for the turning process. The cutting force on a grain was assumed to be

$$f_c = k_1 A^n \qquad (4.19)$$

Where k_1 is a proportionality factor, A is the cross sectional area of the underformed chip and n lies in the range 0 to 1. Summing the grinding forces on individual cutting edges, the semi-empirical grinding force equation is given by

$$F = k K_1 \left(\frac{v_w}{v_s}\right)^{2\varepsilon} a^{\varepsilon} d_e^{1-\varepsilon} \qquad (4.20)$$

Where K is a constant and C_1 is the static cutting edge density. By applying the transformation $\eta=2-2\varepsilon$, the effects of the grinding parameters in equation 1.18 and 1.20 are the same. The difference between these two models is the spacing of the cutting edges. Ono (1961) used the average value of the dynamic cutting edge separation u, while Werner used the static cutting edge density C_1. However these two models are the same.

The advantage of the Ono and Werner is that if the effect of one parameter is established, the effect of other parameters is also known. This suggests that wheel speed, workspeed, depth of cut, wheel diameter and workpiece diameter do not have an independent influence of the grinding force , but are closely interrelated. By studying of one grinding parameters, for example depth of cut, the influence of other parameters can also be understood. The deficiency of the equation is that the mechanical significance of the exponential coefficient is not clear. Since the models are semi-empirical models, the relationships only work for the particular range of grinding conditions.

Werner's model expresses the effects of control parameters and the wheel surface condition with two coefficients ε and γ respectively, which may be helpful in

understanding the effect of the wheel characteristics. Werner further stated that the theoretical values of exponential coefficients γ and ε lie in the ranges $0 \le \gamma \le 1$, $0.5 \le \varepsilon \le 1$, Therefore the theoretical value of η lies within the range $0 \le \eta \le 1$.

Combining the Ono and Werner models, equations 18 an 20 can be expressed in the form

(4.21)

At the extreme condition, γ=1 and η=1,

(4.22)

At this condition the grinding force is directly related to the contact area and the specific number of the cutting edges . This may actually mean that the grinding force is generated by friction. At the other extreme , if γ = 0 , and η = 0 ,

(4.23)

This equation shows the grinding force is directly related to the equivalent chip thickness. This is consistent with a situation where the grinding force is generated by chip formation.

4.3 Mechanics of Grinding Process

In order to clarify the function of cutting and friction in grinding, Malkin (1971) suggested that almost all sliding energy is generated at the interface between the wear flat of the grain and the work piece. Both tangential F_t and normal forces F_n consist of two components, one due to cutting $F_{nc} or F_{tc}$ and other due to sliding $F_{ns} or F_{ts}$ on the wear flats.

$$F_n = F_{nc} + F_{ns} \qquad (4.24)$$

$$F_t = F_{tc} + F_{ts} \qquad (4.25)$$

It was assumed that the cutting force components were unaffected by the size of the wear flat. The sliding force components were assumed to be proportional to the area of wear flat.

Since the tangential and normal sliding forces are both linearly related to the wea flat area, the friction coefficient μ and the average contact pressure $\bar{p}$ between the wear flats and the workpiece were assumed to be constant. The normal friction force was assumed to be the result of the wear flat area and average contact pressure. Defining Ac as the real contact area between the wheel and the workpiecce, equations 1.24 and 1.25 become

$$F_n = F_{nc} + A_c \bar{p} \qquad (4.26)$$

$$F_t = F_{tc} + \mu A_c \bar{p} \qquad (4.27)$$

The tangential cutting force can be obtained from the specific cutting energy, which is defined as

$$e_{cc} = \frac{F_{tc} v_s}{v_w a} \qquad (4.28)$$

The normal force of cutting can be calculated if the cutting force ratio F_{nc}/F_{tc} is known.

Buttery (1973) considered the grinding process as an interaction between two surfaces rather than as a conventional cutting process. He derived an expression for the normal force from wear theory,

$$F_n = \frac{2 v_w b a l}{v_s \alpha \beta \Theta} \qquad (4.29)$$

Where H is the hardness of the workpiece, α is the proportion of grains actually cutting β is thew proportion of the groove volume removed Θ is the half- angle of the

scratches form on the abraded surface. This model highlights the effects of grain shape with the scratch angle and the distribution of the grains.

Shaw idealized a grain on the wheel surface as a sphere (1973). The normal force applied to a grain was assumed to be similar to the force in a Brinell hardness test or a Meyer hardness test. The deformation process is constrained by an elastic-plastic boundary. As the sphere moves horizontally, the plastically deformed zone beneath the surface becomes inclined.

The workpiece material is squeezed upwards forming a chip which is subsequently shared from the surface. In this model the horizontal movement of a sphere at a cutting depth t is equivalent to a sphere intended into a surface to the same depth.

In the absence of friction at the surface between the sphere and the workpiece, the force to indent the workpiece is independent of the direction in which is loaded. This implies that the projected area of indentation is independent of the direction of the force. If the radius of the projected area is b , the force to indent the workpiece is

$$R = \pi b^2 H (C'/3) \qquad (4.30)$$

where C' is a constraint coefficient defined as the ratio of the average pressure $\bar{p}$ on the contact area to the uniaxial flow stress σ_b. In the most cases of grinding, C' is about 3.

The specific energy may be defined as

$$e_c = \frac{f_t}{A} \qquad (4.31)$$

Where F_t is the tangential component grinding force on grain A is the cross section area of an undeformed chip. If A is approximated to A = 4/3 bt then

$$e_{cc} = \frac{3R\sin\theta}{4bt} \qquad (4.32)$$

The specific energy due to cutting may therefore be expressed as

$$e_{cc} = \frac{3\tau b}{4t}\left(\frac{C}{3}\right)\sin\theta \qquad (4.33)$$

According to Shaw , the friction force is assumed to be $\mu \bullet R \bullet \cos\theta$ where μ is the mean coefficient of friction at the contact surface. The specific energy due to friction is

$$e_f = \frac{3\tau\mu b}{4t}\left(\frac{C}{3}\right)\cos\theta \qquad (4.34)$$

The total specific energy for a single grain is

$$e_g = \frac{3\tau b}{4t}\left(\frac{C}{3}\right)(\sin\theta + \mu\cos\theta) \qquad (4.35)$$

Generally only a portion of the workpiece material engaged by the grain is removed in grinding. In grinding, some material is removed so that the volume rising above the original surface is equal with the material bulge at the sides of a grain and chip formation.

In a hardness test, the material flows upward along the sides of the indenter. This can be expressed by the upward flow ratio β,

$$\beta = \frac{\textit{Volume rising above original surface}}{\textit{Total volume displaced}} \qquad (4.36)$$

In grinding, the cutting efficiency of a grain (the upward flow ratio ,β, the measure of the cutting efficiency of a grain) may be expressed in terms of a cross section perpendicular to the path of a grain (Torrance 1990),

$$\beta = \frac{A_1 - A_2}{A_1 + A_3} \qquad (4.37)$$

Where A_1, A_2 and A_3 areas of material flow under a grain for an upward flow ratio β less than one , the specific energy for a single grain is

$$e_g = \frac{3\pi bH}{4t\beta}\left(\frac{C}{3}\right)(\sin\theta + \mu\cos\theta) \qquad (4.38)$$

If the average diameter of the grain is d_g and the average depth of cut of the grain is $\bar{t}$

$$b = \sqrt{\left(\frac{d_g}{2}\right)^2 - \left(\frac{d_g}{2} - \bar{t}\right)^2} = \sqrt{\bar{t}\left(d_g - \bar{t}\right)} \qquad (4.39)$$

$$\sin\theta = \frac{2b}{d_g} = \frac{2\sqrt{\bar{t}\left(d_g - \bar{t}\right)}}{d_g} \qquad (4.40)$$

$$\cos\theta = \frac{\sqrt{d_g^2 - (2b)^2}}{d_g} \qquad (4.41)$$

The specific energy of grinding is

$$e_c = \frac{3\pi H}{4\beta}\left(\frac{C}{3}\right)\left(\frac{\sqrt{\bar{t}\left(d_g - \bar{t}\right)}}{d_g} + \mu\frac{\sqrt{d_g^2 - 4\bar{t}\left(d_g - \bar{t}\right)}}{d_g}\right) \qquad (4.42)$$

For most practical case $d_g >> \bar{t}$ so that

$$e_c \approx \frac{3\pi H}{4\beta}\left(\frac{C}{3}\right)\left(2 + \mu\sqrt{\frac{d_g}{\bar{t}}}\right) \qquad (4.43)$$

The mechanics of grinding can also be investigated by monitoring and analyzing the grinding power. In plunge grinding the grinding power P can be expressed in terms of tangential force

$$P = F_t(v_s \pm v_w) \qquad (4.44)$$

The positive sign is for upcut grinding and the minus sign is for downcut grinding. When the workpiece speed is much smaller than the wheel speed, the grinding power can usually be simplified with less than 2% error to

$$P=F_t\, v_s \qquad (4.45)$$

Based on the simplification that grinding consists of rubbing, ploughing and chip formation phases, Malkin suggested that the grinding power P can be partitioned into chip formation, ploughing and sliding components

$$P=P_{ch}+P_{pl}+P_{sl} \qquad (4.46)$$

Malkin proposed that the chip formation components P_{ch} can be estimated based on constant specific chip formation energy. The ploughing component $P_{pl\ was}$ assumed to be based on a constant ploughing force per unit width. The sliding power P_{sl} was assumed to be proportional to the area of the wear flats on the surface of the wheel. A linear relationship was found between the grinding force and the area of the wear flats on the wheel. The proportionality factor depends on the grinding conditions and the particular wheel –workpiece –fluid combination.

Mechanics of the grinding process depends critically on the geometry and the distribution of the cutting points on the wheel surface, both of which are affected by dressing (Buttery et al., 79 & Chen 1996). When a grain passes through the workpiece surface, workpiece material is removed, leaving a trace on the workpiece surface. Because the cutting edges are randomly positioned on the wheel surface the path of each grain ids different. Only the outermost active cutting edges on the grinding wheel surface actually cut through the workpiece to generate the workpiece profile. The action leaves irregular rough surface along the direction of grinding. The surface roughness is therefore determined both by the grinding kinematics and the distribution of the cutting edges on the wheel surface.

Both the elastic and plastic deformations have to be considered in view of the physical mechanism involved in the generation of the ground surface. The side-flow material ploughed into ridges increases the workpiece roughness, while rubbing in the grinding zone may improve the surface roughness. Due to the elastic and plastic deformation in grinding, only a proportion of the material in the groove is removed by

the grain. A rough surface can therefore be attributed to the accumulation of grooves, which are generated according to the grinding kinematics and the deformation which occurs in grinding.

Empirical models may also provide a basis for further understanding of the workpiece surface generation in grinding. In cylindrical plunge grinding, the surface roughness may be expressed approximately as a function of equivalent chip thickness (Snoeys et al., 1978).

$$R_a = R_1 \, h^r_{cq} \qquad (4.47)$$

Where R_1 and r are constant for a particular system. The exponent r typically lies in the range 0.15-0.6. Malkin and Murray (1977) found that there is a logarithmic linear relationship between specific energy and surface roughness. This indicates that the generation of the workpiece surface cannot be fully understood without considering the mechanics of the grinding process.

Chapter 5

Experimental details

5.1 Computer modelling of grinding wheel process

Computer simulation of grinding wheel and bar was performed by using Solidworks 2003/2004 available in the university library for three dimensional modelling with support of COSMOS Xpress software to implement Finite Element Analysis (FEA) which is produced the analytical part of this thesis. Same parameters of grinding wheels and bar were applied to simulate three dimensional model of grinding wheel and bars. The programme has allowed adequate analysis of designs for functional capability using different analysis tools available, eliminating the traditional separation of design and analysis. Also an appropriate analysis for specific tasks can be chosen and a correct mesh can be selected in the analysis advisor wizard.

5.2 Material used

5.2.1 Material used in mould preparation and grinding wheel production

During this experiment silicon carbide powder particles manufactured by Saint Gobin with various powder sizes (0.1, 0.2 and 0.25 µm) diameter were used. Table 5.1 presents the property values for silicon carbide at room temperature (Saint-Gobain 2009 & Accuratus Corporation 2011). The silicon powder was mixed with the solution of araldite epoxy resin with density of 1.18 g/Cm^3, felexural strength of 80 MPa and catalyst to make grinding wheels. Dibutyltin dilaurate was used as a catalyst (hardener). The Physical properties of dibutyltin dilaurate can be seen in Table 5.2. Mixing resin and catalyst, delivers an exothermic reaction which enters the mixture into the curing stages. The crosslinking (thermosetting) chemical reaction occurs during the final processing. The network structure results in a rigid through a stage called vitrification, providing a strong

solid material. Properties of thermosets depend mainly on crosslinking density and the length of crosslinkage (Razmara 2008).

Table 5.1: Properties of silicon carbide measured at room temperature

Silicon Carbide Properties		
Mechanical (SI/Metric)		
Density	g/Cm⍰	3. 21
Flexural Strength	MPa	550
Elastic Modulus	GPa	410
Shear Modulus	GPa	—
Bulk Modulus	GPa	—
Poisson's Ratio	—	0.14
Compressive Strength	GPa	3900
Vickers hardness	GPa	29
Fracture Toughness K_{IC}	$MPa \bullet m^{1/2}$	4.6
Typical Temperature resistance in Air	°C	1500
Thermal		
Thermal Conductivity	W/m•°K	50-100
Coefficient of Thermal Expansion	10^{-6}/°C	5
Specific Heat	J/Kg•°K	750
Electrical		
Volume Resistivity	ohm•cm	10^{2}–10^{6}

Table 5.2: Physical data of dibutyltin dilaurate

Appearance	Yellow liquid
Melting point	22 - 24 C
Vapour density	21.8 (air = 1)
Flash point	226 C
Stability	Combustible, Incompatible with strong oxidizing agents. May be air sensitive.
Toxicology	May cause skin irritation.
Personal protection	Safety glasses, adequate ventilation.

Special precautions applied during mixing of both materials before preparation of mould. The safety data sheet can be seen in Table 5.3.

Table 5.3: Safety (MSDS) data sheet Table for dibutyltin dilaurate

Synonyms	Butyl norate, laudran, tinostat, stabilizer D-22
Molecular formula	$C_{32}H_{64}O_4Sn$
CAS No	77-58-7

5.2.2 Materials used to make mould

- Two different wallpaper strips shown in Figure 5.1, used to make same pattern on inner periphery mould and outer of grinding wheel.
- A plastic plate of 40 cm in length, 25 cm in width and 10 mm in thickness to give support to grinding wheel during process.
- A Plastic Ring to hold catalyst material during pouring in the mould.
- Blue tack to avoid leakage of material from the bottom part of the ring.
- An obtained grinding wheel with different pattern on their periphery to make mould of same shape.

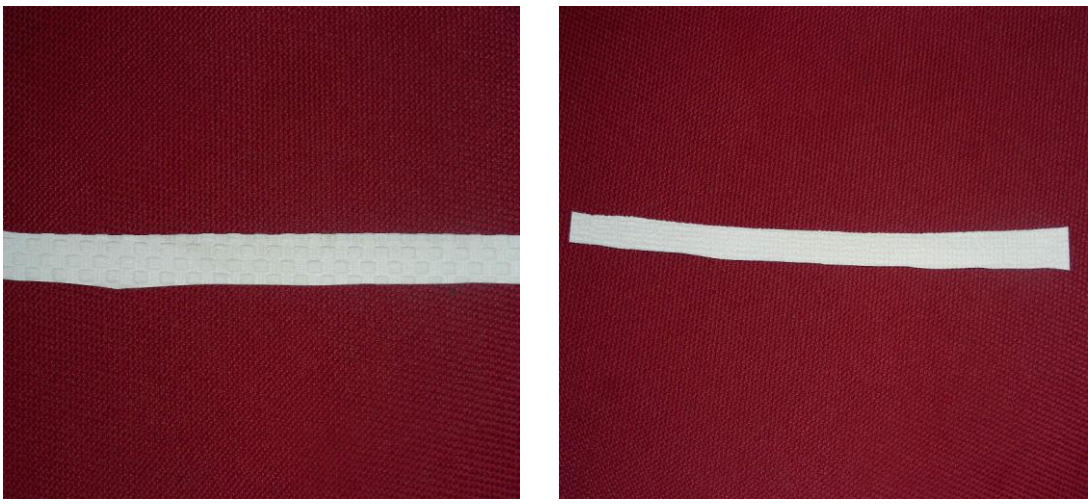

Fig 5.1: Wallpaper strips used to make similar pattern on mould

5.2.3 Other materials used during the experiments

- Using various produced and commercial grinding wheels (W1, W2, W3, and W4).
- Mild steel, brass and aluminium bars have been used, Figure 5.2.

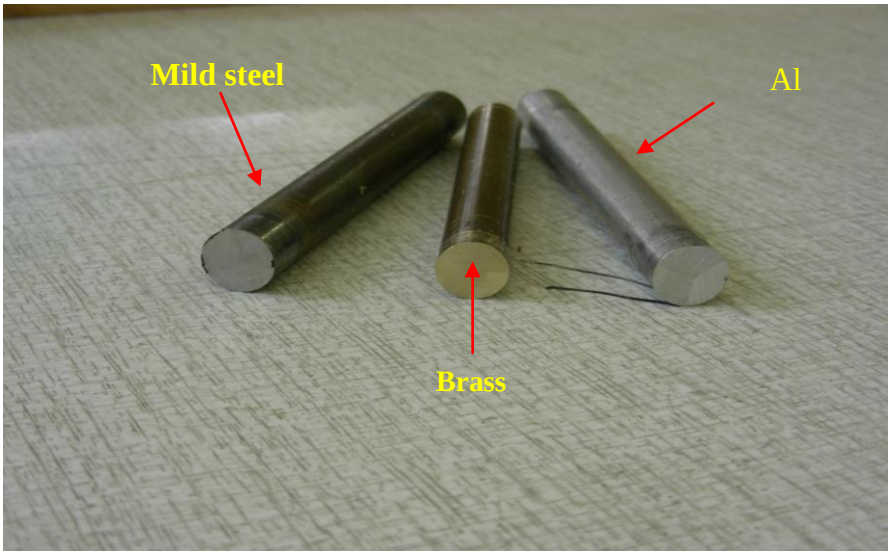

Fig 5.2: Bars used in experiments

In Table 5.4 sizes and hardness properties of various bars shown in Figure 5.2 are displayed.

Table 5.4: Bars Size & Hardness

No.	Bars material	Diameter (mm)	Length (mm)	Hardness (HV)
1	Mild steel	12.96	120	906.2
2	Brass	12.77	120	708.9
3	Aluminium	12	120	509.8

5.3 Equipment used

Equipment used in completion of project divided in three parts-equipment, including equipment for mould preparation, equipment for manufacture grinding wheel and equipment used for experiments by using different commercial grinding wheels.

5.3.1 Equipment used in mould preparation

- ***Electrical Oven*** was used to cure the thermoset and make a grinding wheel. The oven shown in Figure 5.3 provided the temperature range about 50 – 60ºc.

Fig 5.3: Oven used in manufacturing grinding wheel

- Mould formed with the required shape.
- Two aluminium discs to make ring for grinding material on its periphery.
- Two plastic plates used to compress grinding wheel.
- Different tools used to Mix and fill material into the mould and aluminium discs.

5.3.2 Other equipment used during the experiments

Following equipment were used in this study to run the project.

- ***Bench Grinder***, Clarke Heavy duty bench grinder 8", 400 watt, shown in Figure 5.4 helps keep drill bits, chisels and shears etc in tip top conditions as well as being generally useful for metal shaping, smoothing and polishing, built for tough daily industrial / general engineering use. Some other Features of this machine includes:

➢ Adjustable tool rests.
➢ Removable wheel-guards for easy wheel changing.
➢ It is supplied with combined eye shields/spark arrestors, one medium 200x20mm wheel and one wire wheel.

Fig 5.4: Bench grinder used for experiments

- ***Oscilloscope (CRO)*** used to record vibration and grinding operation. The oscilloscope is actually a graph-displaying device. It demonstrates a graph of an electrical signal. In most applications the graph (Figure 5.5) shows how signals change over time: the vertical (Y) axis represents voltage and the horizontal (X) axis represents time. The intensity or brightness of the display is sometimes called the Z axis. By oscilloscope, the following points can be assessed:

- The time and voltage values of a signal.
- To calculate the frequency of an oscillating signal.
- A malfunctioning component which is distorted the signal.
- The extent of the noise into the signal and changes of noise value with time.

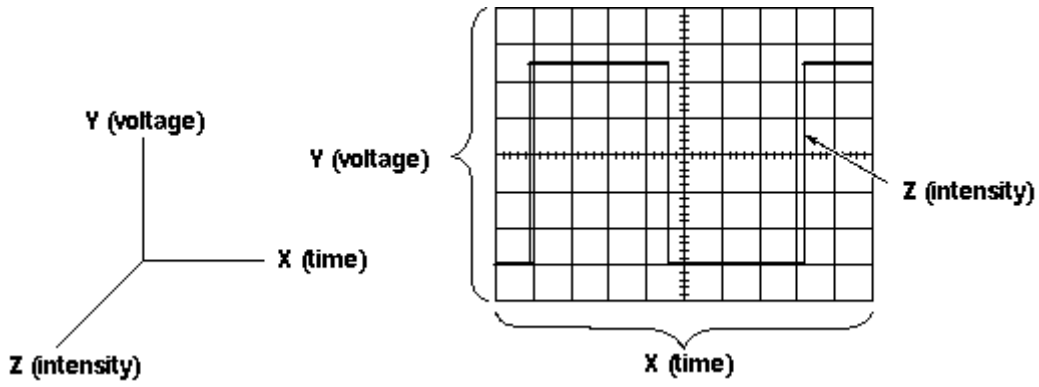

Fig 5.5: X, Y, and Z Components of a Displayed Waveform

- ***Flexiforce pressure sensor*** used to measure deformation during grinding and send data to oscilloscope. Flexiforce pressure sensors (Figures 5.6, 5.9) can measure force between almost any two surfaces and is durable enough to stand up to most environments. Flexiforce has better sensor properties, linearity, hysteresis, and drift and temperature sensitivity than any other thin film force sensor.

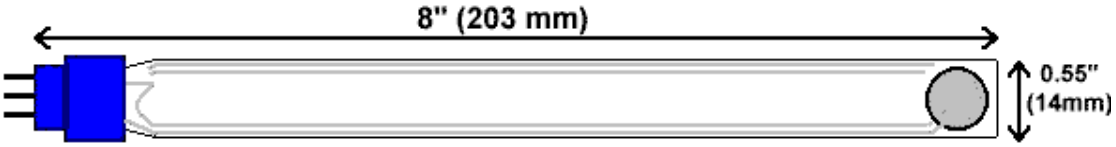

Fig 5.6: Flexiforce pressure sensor

➢ Typical Sensor Response: The Flexiforce single element sensor acts as a resistor in an electrical circuit. When the sensor is unloaded, its resistance is very high. When a force is applied to the sensor, this resistance decreases. The resistance can be read by connecting an ohm meter to the outer two pins of the sensor connector and applying a force to the sensing area. There are many ways to integrate the sensor into an application. One way is to use a circuit which can convert force into voltage. Standard Force Ranges as tested with circuit shown in Figure 5.7.

- PS-01: 0 - 1 lb. (4.4 N)
- PS-02: 0 - 25 lb. (111 N)
- PS-03: 0 - 1000 lb. (4448 N)

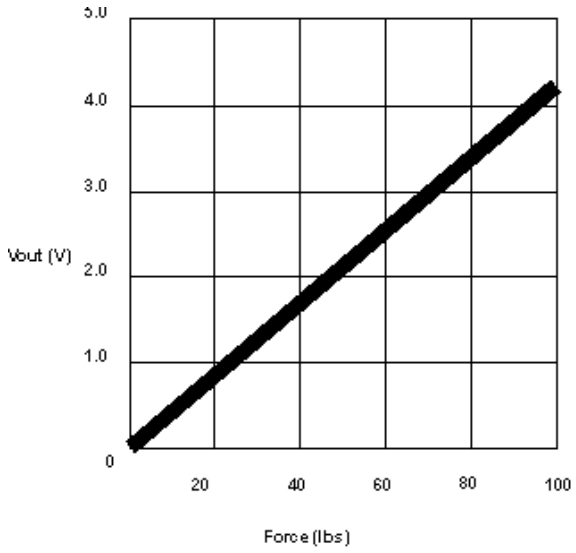

Fig 5.7: Force range against Voltage

➢ A means of calibration have been established to convert the output into the appropriate engineering units. Depending on the setup, an adjustment could then be done to increase or decrease the sensitivity of the sensor. Physical properties and typical performance of the sensor are shown in Tables 5.5 and 5.6 respectively.

Table 5.5: Physical Properties of Flexiforce

Thickness (mm)	0.127
Length (mm)	203 (End of connector to tip of sensor)
Width (mm)	14
Active sensing diameter (mm)	10
Connector	3 pin Berg Clincher

Table 5.6: Typical Performance of Flexiforce

Linearity (Error)	< ±5% (Line drawn from 0 to 50% load)
Repeatability	< ±2.5% of full scale (Conditioned sensor, 80% of full force applied)
Hysteresis	< ±4.5% of full scale (Conditioned sensor, 80% of full force applied)
Drift	< 3% / logarithmic time (Constant load - 25 lb.)
Rise Time	< 20 µsec (Impact load - recorded on oscilloscope)
Operating Temperature	15º F - 140º F (-9º C - 60º C)*

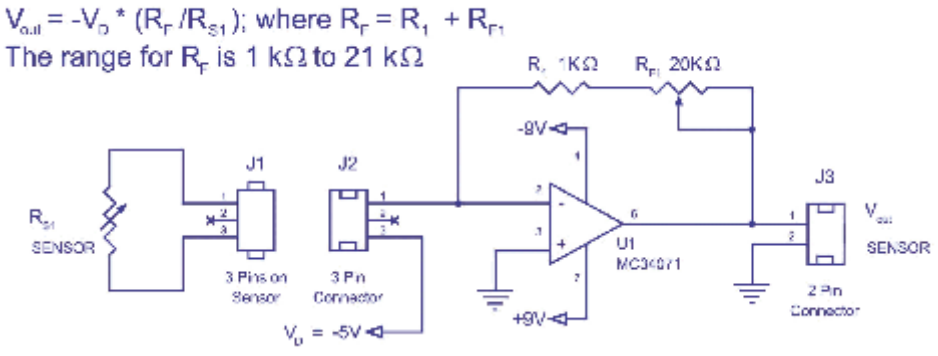

Fig 5.8: Digital diagram of Flexiforce pressure sensor

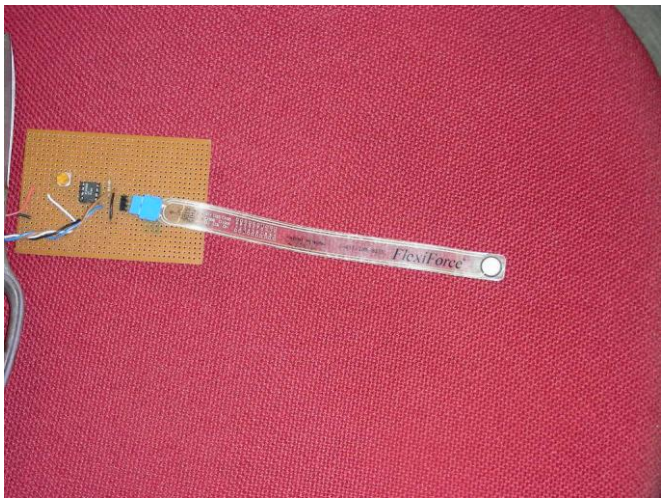

Fig 5.9: Flexiforce pressure sensor

- **Constructed Assembly** to hold bar and to feed it against the grinding wheel. This assembly plays an important role in completion of experiments of grinding. This assembly used to hold and press bars versus grinding wheels. Assembly (Figure 5.10) included a micrometre to give an accurate measurable feed. Two aluminium columns and one base used to support columns and micrometre.

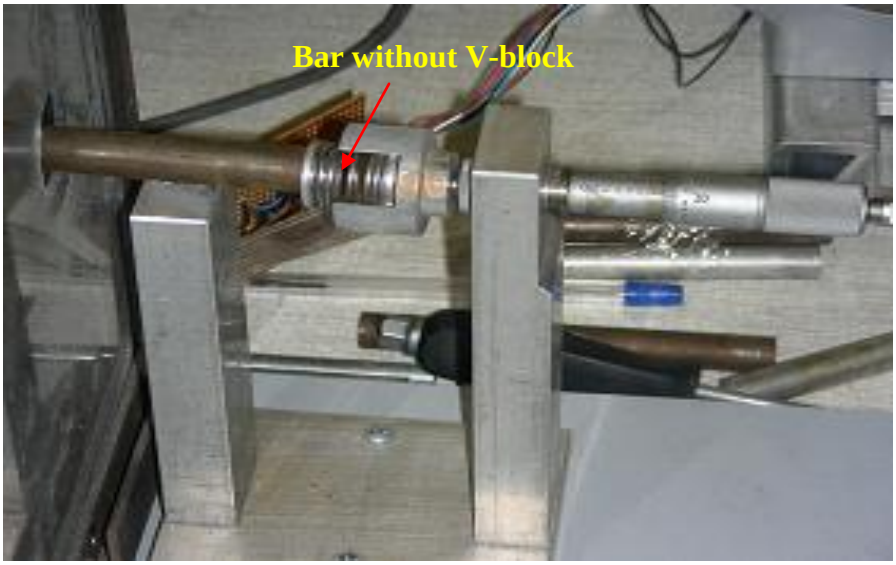

Fig 5.10: Constructed assembly holding bar without V- block

➢ A modification has been made in this assembly. Bar had to be hold and guided by hand against grinding wheel. During grinding operation, bar gets heated and it was very hard to hold bar by hand. Therefore in modified assembly a V- block (Figure 5.11) was used to guide and hold bar versus grinding wheel.

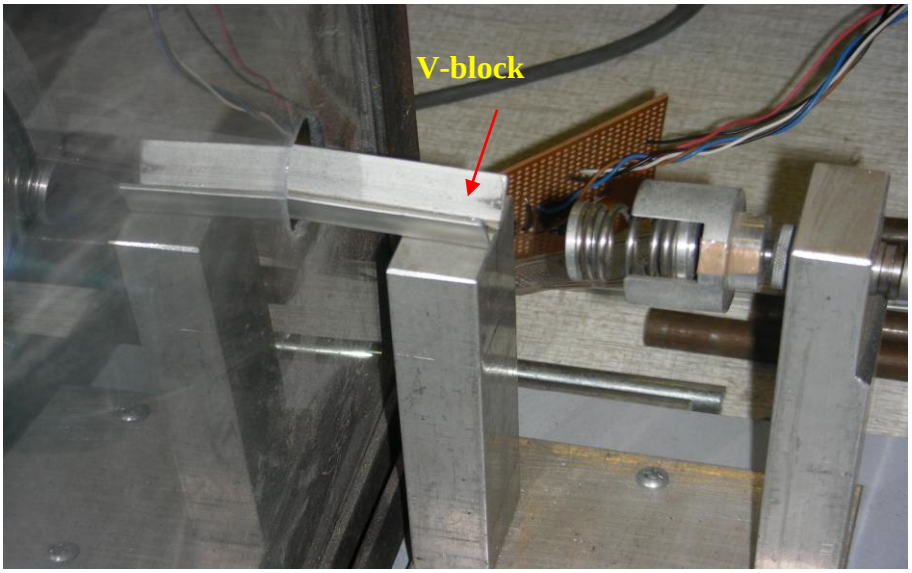

Fig 5.11: Modification of Constructed assembly with V- block.

- **Microhardness Testing machine** (Figure 5.12): A Mitutoyo hardness testing machines was used to obtain the Vickers hardness of the various bars show in Figure 5.5. Also the measured hardness of bars can be found in Table 5.3. The machine was controlled by touch screen display panel set next to it.

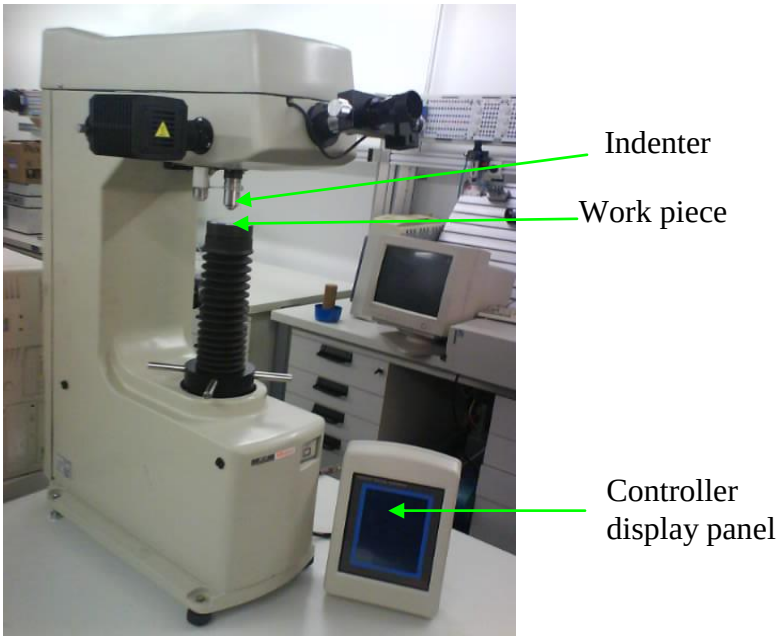

Fig 5.12: Microhardness testing machine

The machine was controlled by touch screen display panel set next to it. Measurements were made on the top surface of each specimen bar and recorded (Figure 5.13).

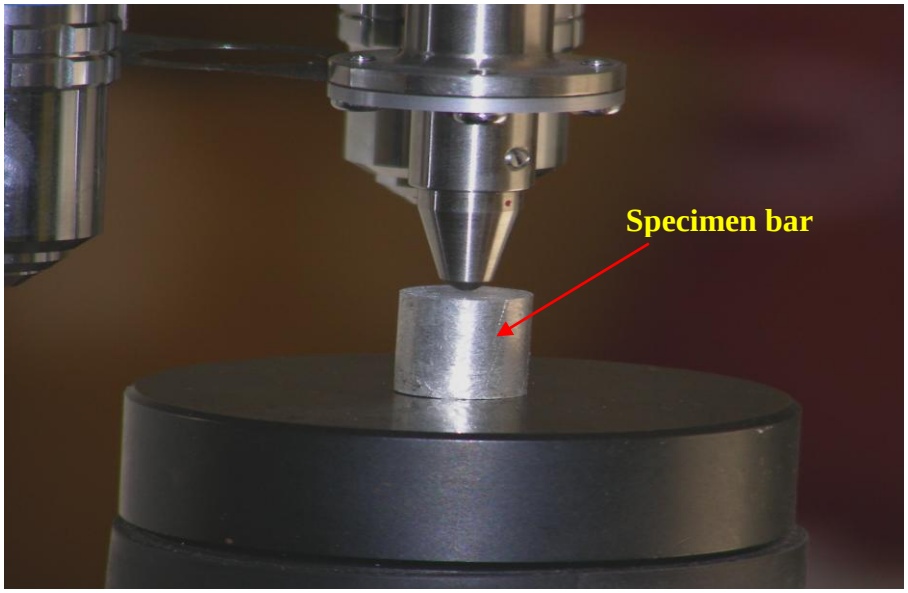

Fig 5.13: Loading of indenter on the specimen bar

The best view of the work piece through the microscopic lens and eye piece was found. The diamond indenter was set on the top of the work piece surface. By pressing indenter, indentation effect was seen in the lens controller on the display screen.

5.1 Preparation of Samples

5.1.1 Mould preparation

A Dibutyltin dilaurate (DBTDL), the typical catalyst was used with an aliphatic isocyanates to make a thermosets mould. According to the data supplied with materials, accurate ratio of both resin and catalyst is very important to produce appropriate mould. In this process, grinding wheel plays a significant role. A previously prepared grinding wheel with wallpaper fixed on its periphery, was used to make a mould.

To begin with the process, resin was poured into the clean container, followed by adding up 36 drops of curing agent, making a mixture with necessary thickness. After curing the mixture, two grinding wheels with different shapes on its periphery were used to make a mould. Wallpaper strips with different pattern were used, making various shapes on

grinding wheels periphery. One of the Grinding wheel was placed on the base plate, surrounded by plastic ring from the outside.

Two different shaped moulds have been made. A clamp (Figure 5.14) has been used on first mould to avoid leakage of mixture. In case of second mould, Blue Tack (Figure 5.15) has been fixed to prevent any leakage of mixture from the mould sides. Plastic ring clamped from the outside to hold grinding wheel. The formulated mixture was poured inside of the ring afterward. Random checking has been done to ensure proper filing of mixed material into the ring. All assemblies were laid in ambient temperature for about 24 hours.

Fig 5.14: Mould preparation by using clamps to hold ring.

Fig 5.15: Another mould Preparation by using catalyst and curing agent

Figure 5.16 presents an image of the mould which was ready to use after 24 hours.

Pattern will be created on periphery of grinding wheel

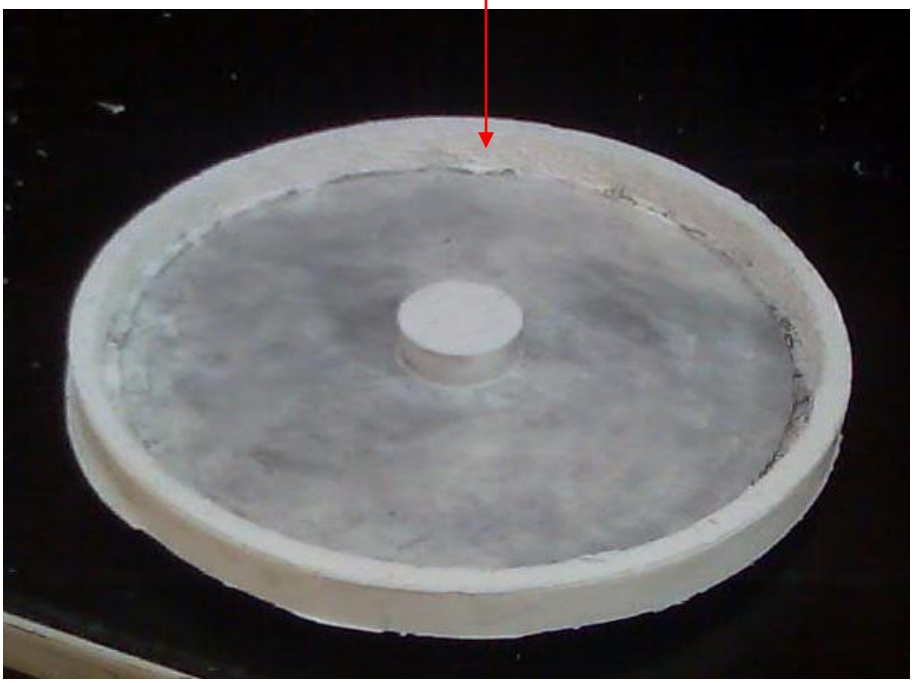

Fig 5.16: mould used to manufacture grinding wheel

5.4.2 Manufacturing grinding wheels:

Four grinding wheels were made from various silicon carbide powder sizes containing 0.1, 0.25 and 0.25 µm and araldite epoxy resin with outer diameter of 175 mm, inside diameter of 32 mm and width of 14 mm. Special precautions upon using silicon carbide powder with regards to health and safety were taken in manufacturing of grinding wheel. Mould which previously produced was used in this process.

Well accurate built mould makes an important effect in manufacturing precise grinding wheel. If mould takes possession of defect or irregular shape, therefore similar deformity will be passing on to grinding wheel periphery. To produce a grinding wheel, mould was placed on the plastic sheet. A plastic ring mounted outside the outer mould periphery. The special care needed to be taken in mixing the accurate ratio of each material. Silicon carbide was weighted (60 g) using digital scale before mixing with 60 g of araldite epoxy resin to ensure using the precise amount of silicon carbide into the mixture (Figure 5.17).

Fig 5.17: Mixing of silicon carbide with araldite epoxy resin

They were appropriately mixed to prevent of any air bubbles inside of the mixture. Then abrasive materials were poured into the mould and the gap between mould and disc was filled using some special tools (Figure 5.18). The second plastic plate was clamped tightly on upper side to pertain a very smooth disc surface. All assemblies were placed inside of the oven in 50^{o}c temperature for about 5-6 hours thereafter.

Fig 5.18: Filling material in the gap between the mould and aluminium disc

After removing the holding assembly from the oven, the grinding wheel was put on lathe chuck to clean. Also sandpaper was applied to trim bits by turning operation.

Using the same process four grinding wheel has been made with various particle size and different pattern on their periphery.

To simplify the analysis of samples the following coding system was adopted for the different grinding wheels.

For Example:

- W1 for the sample with silicon carbide particle size of 0.25 µm
- W2 for the sample with silicon carbide particle size of 0.2 µm
- W3 for the sample made from glass fibre for polishing uses
- W4 for the sample with silicon carbide particle size of 0.1 µm
- W5 for grinding wheel with parallel grooves (Figure 5.19)
- W6 with crossed grooves (Figure 5.20)

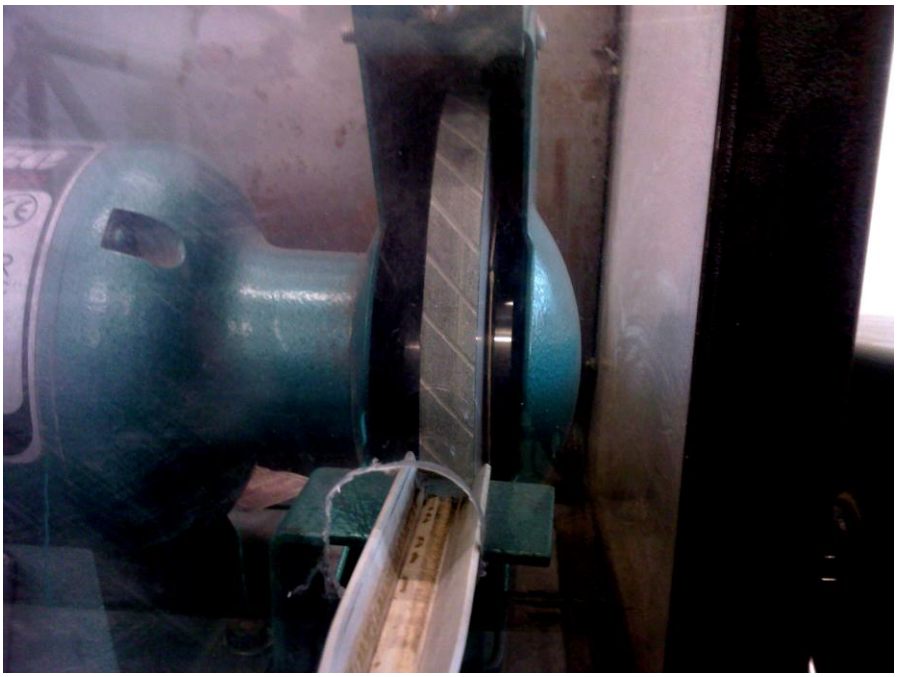

Fig 5.19: Grinding wheel with parallel grooves lines

Fig 5.20: Grinding wheel with cross lines

5.5 Experimental Methods

5.4.2 Various grinding and commercial wheel

All systems explained in section 5.2.3 were set up and happen ready to start the experiment. After removing safety housing, commercial grinding wheel (C) was installed on the grinder machine. Safety housing was moved back on to the machine and all safety precautions of working with grinder were considered subsequently.

Fig 5.21: Installing grinding wheel on grinder

- **Testing procedure:**

For the first experiment, three bars with different materials (mild steel, brass, and aluminium) samples were used. During this experiment, following actions were performed (Figure 5.22).

➢ By installing commercial wheel (C) on grinder, length of all bars before grinding and total grinded materials were calculated.

➢ The mild steel bar was installed inside of the assembly against of grinding wheel.

➢ After 18 s grinding and feeding of 1.28 mm of bar, voltage axis, representing bar load against the wheel versus grinding time were shown on the oscilloscope.

The procedure was followed for the entire bar samples. Same operation was repeated twice to obtain average results.

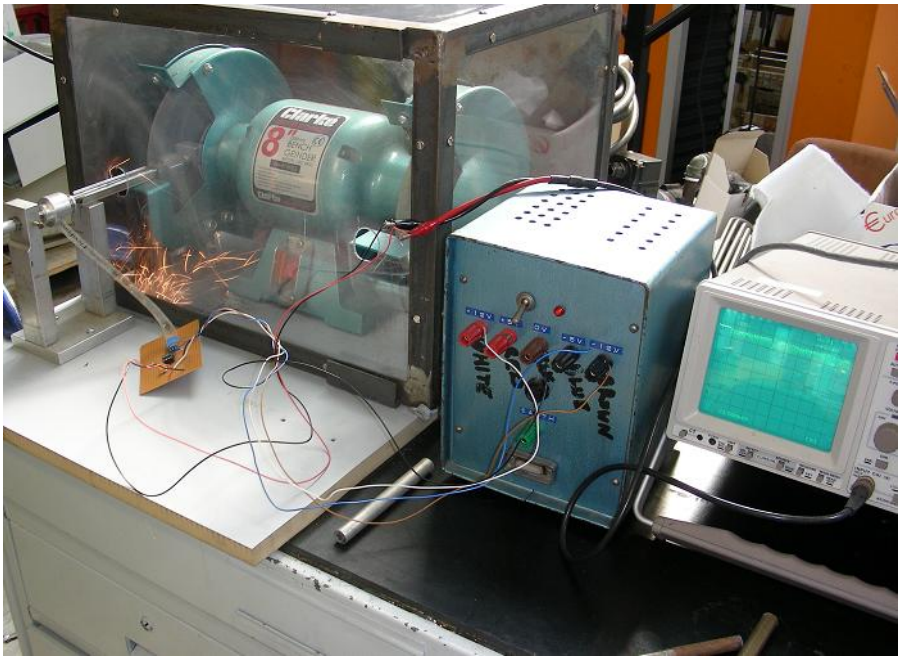

Fig 5.22: Grinding of mild steel bar on commercial wheel

After commercial wheel (C), other grinding wheels were installed. Precautions have been followed while changing the wheels. Same testing procedure was performed for all grinding wheels (W1 to W6) and obtained results have been discussed in chapter 8.

Chapter 6

Results and Discussion

6.1 Experimental Results and Discussion

6.1.1 Wet\Dry cutting experiment

Grinding operation is used for finishing a product because of their ability of miniature cutting and surface roughness. Although water tends to deteriorate the resin and reduce the life of the cut-off wheel, coolants are invariably used in finish grinding to dissipate the heat generated and to protect the workpieces from grinding burn. Effective coolant filtration is necessary for efficient coolant performance.

The surface of wheel (tool) and workpiece are subjected to (a) forces and contact pressure, which range from very low values to multiples of the yield stress of the workpiece material,(b) relative speeds, from very low to very high, and (c) temperatures, which could reach melting point. Metal working fluids are applied in addition to selecting appropriate material and controlling process parameter.

A direct water base coolant, emulsion, was used for the experiment. Direct emulsions are important fluids because the presence of water gives them high cooling capacity. They are particularly effective in high-speed machining where temperature rise has damaging effects on tool life, the surface integrity of workpieces, and dimensional accuracy of parts. The following results were obtained during the wet cutting investigation, using C:

Table 6.1: Talysurf measurement of work piece material mild steel during wet cutting experiment

Particle size	Depth of cut (µm)	Surface finish (µm)
30	10	0.63
46	10	0.44
	20	0.42
60	10	0.35
	20	0.33

Table 6.2: Talysurh measurement of workpiece material MILD STEEL during wet cutting experiment

Particle size	Depth of cut (µm)	Surface finish (µm)
46	10	0.38
	20	0.32
60	10	0.28
	20	0.24

The following readings were recorded during dry cutting experiment:

Table 6.3: Talysurf measurement of workpiece material –Mild steel during dry cutting experiment

Particle size	Depth of cut (µm)	Surface finish (µm)
46KV	5	0.38
	10	0.4
46LVS	10	0.56
	20	0.37
60LVS	10	0.35
	20	0.32

Table 6.4: Talysurf measurements of Mild steel *workpiece* during dry cutting experiment

Particle size	Depth of cut (µm)	Surface finish (µm)
46LVS	10	0.35
	20	0.32
60LVS	10	0.34
	20	0.28

Above Tables (6.1 and 6.4) show clearly that grinding operation carried out on both workpiece materials at the same depth of cuts resulted in better surface finish for mild steel due to its higher hardness and higher ductility than mild steel.

Grinding of mild steel using the wheel of grit size 60 at 20µm depth of cut had more metal chips adhere to its grain it still resulted in giving the best surface finish from the results obtained during the course of performing the experiment due to the fact more grain actually participated in the cutting operation.

The investigations indicated that the parameters feed rate, depth of cut, grit size types and applications of coolant are the primary influencing factors which affect the surface integrity of the grinding wheel during the grinding operation.

6.1.2 Dimensional Analysis

The grinding force for a given set of wheel-workpiece system can be considered to be the function of the following easily controllable factors:

$$F\,g = f\,(Vs,Vw,d,w,Su,G,P\,) \qquad (6.1)$$

Where Fg is grinding force, Vs spindle speed, Vw work speed d depth of cut, w width of cut, Su is tensile strength of the workpiece material, G groove on grinding wheel, P particle size. These variables are listed in Table 6.5 together with three primary units that is mass M, length L and time T.

The Buckingham's π- theorem of dimensional analysis indicates that the relationship among the variables in the functional form can be expressed as:

$$f\,1\,(\,Fg,Vs,Vw,d,w,Su,G,P\,) = 0 \qquad (6.2)$$

The above 8 variables contain 3 primary units M, L, T. According to the π-theorem, there exist 3 independent dimensionless products or π-terms.

Table 6.5: Different variables together with M, L & T

No.	Name	Symbol	Dimensional formula
1	Grinding force	Fg	ML*1/T*T
2	Spindle speed	Vs	L*1/T
3	Work speed	Vw	L*1/T
4	Depth of cut	D	L
5	Width of cut	W	L
6	Tensile strength	Su	M*1/L*1/T*T
7	Groove	G	L
8	Particle size	P	L

The construction of the 3 π-terms rests upon the fact that the best set should provide most insight to the problem under investigation. Based on these, for the present surface grinding process, the above equation can be written as

$$f_2(\pi_1\pi_2\pi_3) = 0 \qquad (6.3)$$

or

$$f_2\left(\frac{V_w}{V_s}, \frac{dG}{wP}, \frac{F_g V_s}{V_w dw S_u}\right) = 0 \qquad (6.4)$$

or

$$\pi_3 = \frac{F_g V_s}{V_w dw S_u} = f_3\left(\frac{v_w}{V_s}, \frac{dG}{wP}\right) \qquad (6.5)$$

Where

$$\pi_1 = V_w / V_s, \pi_2 = dG / wP, \pi_3 = F_g V_s / V_w d_w S_u \qquad (6.6)$$

The π-theorem of dimensional analysis suggests that the functional relationship between the response/dependent parameter (π_3) and independent parameters ($\pi_2\pi_3$) can be written as:

$$\hat{\pi}_3 = C\left(\frac{V_w}{V_s}\right)^{\alpha}\left(\frac{dG}{wP}\right)^{\beta} (1) \qquad (6.7)$$

Where $\hat{\pi}_3$ = is the predicted response (dependent dimensionless parameter) and C, α, β are the model parameters to be determined by experiment.

Taking natural logarithm converts the intrinsically linear type non-linear model into standard linear form of the first –order regression model as:

$$\hat{y} = b_0 x_0 + b_1 x_1 + b_2 x_2 \qquad (6.8)$$

Where $\hat{y}$ is the predicted response on natural logarithmic scale, x_0 =1 (a dummy variable) , x_1, x_2 are coded values (logarithmic transformations) of Vw/Vs , dG/wP respectively, and b_i (I = 0,1,2) are parameters to be estimated by linear multiple regression.

- **Estimation of test regions (coding) for independent variables**

To simplify the calculation, the independent variables are coded so that their values are found in the interval (-1, 0, 1). The levels of independent variables and coding identifications used in the design of experiment are presented in Table 6.6. The coded values of the variables for use in Equation (6.8) are obtained from the following transforming Equations (Lo and Chen, 1977)

$$x_1 = \frac{\ln(V_w / V_s) - \ln(7.5/(25*60))}{\ln(10/(25*60)) - \ln(7.5/(25*60))} \qquad (6.9)$$

$$x_2 = \frac{\ln(dG/wP) - \ln(10/25*10^3)}{\ln(15/25*10^3) - \ln(10/25*10^3)} \qquad (6.10)$$

Where x_1 is the coded value of the factor corresponding to its natural value Vw/Vs,(7.5/(25*60)) natural value of this factor corresponding to the base or 0 level value , (10/(25*60)) the natural value of this factor at the +1 level, and x_2 is the coded value of the factor corresponding to its natural value d/w, ($10/(25*10^3)$) the natural value of this factor corresponding to the 0 level, (15/(25*60) the coded value of this factor at +1 level.

Table 6.6: Coding and levels of Factors

Factors	Units	Symbol	Coding	Low (-1)	Medium (0)	High (1)
Work speed / Spindle speed	m/sec	Vw/Vs	X1	5.6/25*60	7.5/25*60	10/25*60
Depth of cut / Width of cut	mm/mm	dG/wP	X2	6.5/25*1000	10/25*1000	15/20*1000

- **Estimation of parameters**

On the basis of the data the values of regression coefficients (b_0, b_1, b_2) in the regression model were estimated by the least square method, using the following basic formula written in matrix form.

$$b_m = (X_m^T X_m)^{-1} X_m^T Y_m \qquad (6.11)$$

Where b_m is the matrix of parameters, X_m the design matrix of levels of independent variables x, X^T the transpose of matrix X_m and Y_m are the matrix of logarithm of the measured response y.

The X_m and Y_m matrices can be written in the following form:

$$X_m = \begin{bmatrix} 1 & -1 & -1 \\ 1 & +1 & -1 \\ 1 & -1 & +1 \\ 1 & +1 & +1 \\ 1 & 0 & 0 \\ 1 & 0 & 0 \\ 1 & 0 & 0 \\ 1 & 0 & 0 \end{bmatrix} \quad \text{and} \quad Y_m = \begin{bmatrix} 4.2940 \\ 3.8160 \\ 4.3451 \\ 3.9025 \\ 4.2993 \\ 4.1707 \\ 4.2092 \\ 4.0675 \end{bmatrix}$$

The vector of the estimated regression coefficients is found to be

$$b_m = \begin{bmatrix} 4.1380 \\ -0.2302 \\ +0.0344 \end{bmatrix}$$

The differences between measured and predicted unit grinding force are illustrated in Figure 6.1.

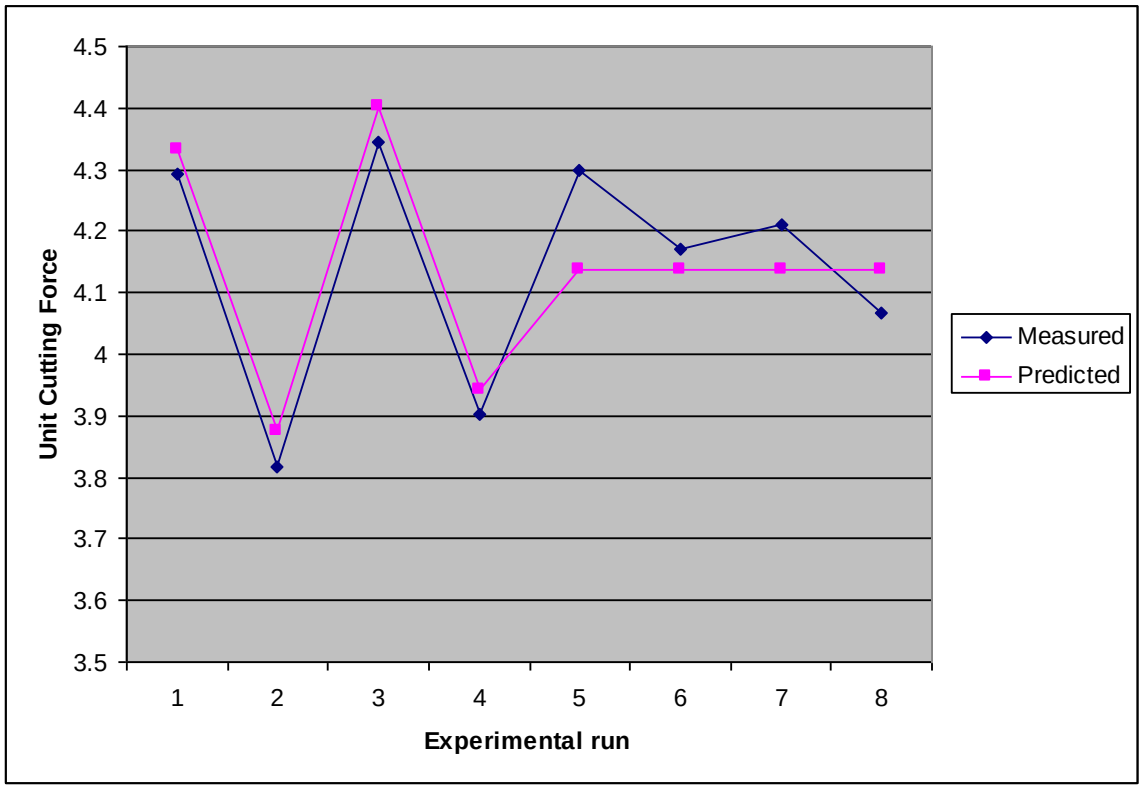

Fig 6.1: Measured versus predicted unit grinding force (J/sec)

To analyse the above results, the predictive model can be used by substituting the estimated parameters into Equation (6.8), which gives rise to

$$\hat{y} = 4.1380 - 0.2302\, x_1 + 0.0344\, x_2 \qquad (6.12)$$

This equation can be transformed using Equations (6.9) and (6.10) to provide the dependent dimensional parameter as the function of two independent dimensionless parameters, which is

$$\hat{\pi}_3 = \frac{F_c V_s}{V_w d w S_u} = 1.8868 \left(\frac{V_w}{V_s}\right)^{-0.7865} \left(\frac{d}{w}\right)^{0.0849} \qquad (6.13)$$

From Equation (6.14) the predicted unit grinding force (work done per unit volume of material removed) $\hat{k}_s$ can be shown to be

$$\hat{k}_s = \frac{\hat{F}_c V_s}{V_w d w} = 1.8868 S_u \left(\frac{V_w}{V_s}\right)^{-0.7865} \left(\frac{d}{W}\right)^{0.0849} \qquad (6.14) \qquad (8)$$

Equation (6.14) indicates that an increase in the ratio of the feed rate to wheel speed decreases the unit grinding force while an increase in the ratio of depth of cut to width of cut increases the unit grinding force.

Grinding power, time constant surface roughness and roundness converge with grinding time despite differences in the dressing conditions employed. This implies that dressing has most effect on the initial grinding stage, while the grinding conditions affect the whole wheel life cycle. Selection of dressing conditions and grinding conditions may be separated. The dressing conditions may be selected to adjust the initial grinding behaviour after dressing and the grinding conditions selected to adjust the grinding behaviour in other stage stages of a wheel redress life cycle. This conclusion is considered to be important for the design of a dressing strategy.

When dressing with very coarse conditions or with a very blunt dressing diamond, more bond fracture is generated on the wheel surface. The result is that wheel wear is increased and workpiece size errors are increased in a positive sense.

After dressing with very fine conditions, the wheel wear may mainly be attributed to attritions wear and microfracture. The wheel wear volume was small. Force and deflection reduction and thermal expansion cause the workpiece size errors to increase in a negative sense. It is concluded that a good dressing operation makes grinding behaviour more stable and gives better grinding quality.

One of the most interesting aspects of the grinding process is that the grinding behaviour can be very different even for the same value of control parameters, such as $v_s, v_w, v_f, a_d f_d$ .This is attributed to uncontrollable parameters involved in the grinding operation. The dressing width of the diamond is an uncontrollable parameter and has a strong effect on grinding behaviour. Due to insufficient control of the shape of the dressing diamond, it is necessary to develop a strategy for the selection of dressing parameters, so that effect of the effect of the dressing diamond can be compensated.

6.1.3 Grinding Wheels experimental comparison

During grinding procedures, the set up was connected to the oscilloscope to record voltage consumed to wear bars. The experiments have been performed using commercial wheel (C), following by W1, wheel made of silicon carbide grain, size 0.25, W2 with grain size of 0.2 (silicon carbide), thereafter W3 Polishing wheel made of glass fibre has been used. Wheel W4 made of very fine & small silicon carbide grain size of 0.1 was used subsequently.

Then W5 and W6 made of silicon carbide grain size of 0.2 were used with different surface shapes of parallel grooves and crossed grooves respectively.

Time given for all grinding operation= 18 sec

Feed given = 1.28 mm

Diameters and Cross-sectional area of all bars are given in Table 6.7.

Table 6.7: Cross- sectional area of different bars

No.	Bars Material	Diameter (mm)	Cross sectional area (mm^2)
1	Mild Steel	12.96	131.8
2	Brass	12.77	113
3	Aluminium	12	128

During this experiment the amount of removed material of ground bars was recorded against the consumed voltage. The data obtained for commercial grinding wheel (C) are presented in Table 6.8.

Table 6.8: Experimental Data of commercial grinding wheel (C)

No.	Workpiece Materials	Hardness (HV)	Grinding time (S)	Commercial Wheel (C)			
				Voltage (V)	Cross sectional area (mm^2)	Removed length (mm)	Total material removed (mm^3)
1	Mild Steel	906.2	18	2.29	131.8	1.66	210.7
2	Brass	708.9		1.95	113	3.5	395.5
3	Aluminium	509.8		1.77	128	0.79	101.1

To ease of comparison the total volume of materials removed and voltages consumed during grinding of various bars using C are plotted in Figure 6.2 and 6.3 respectively.

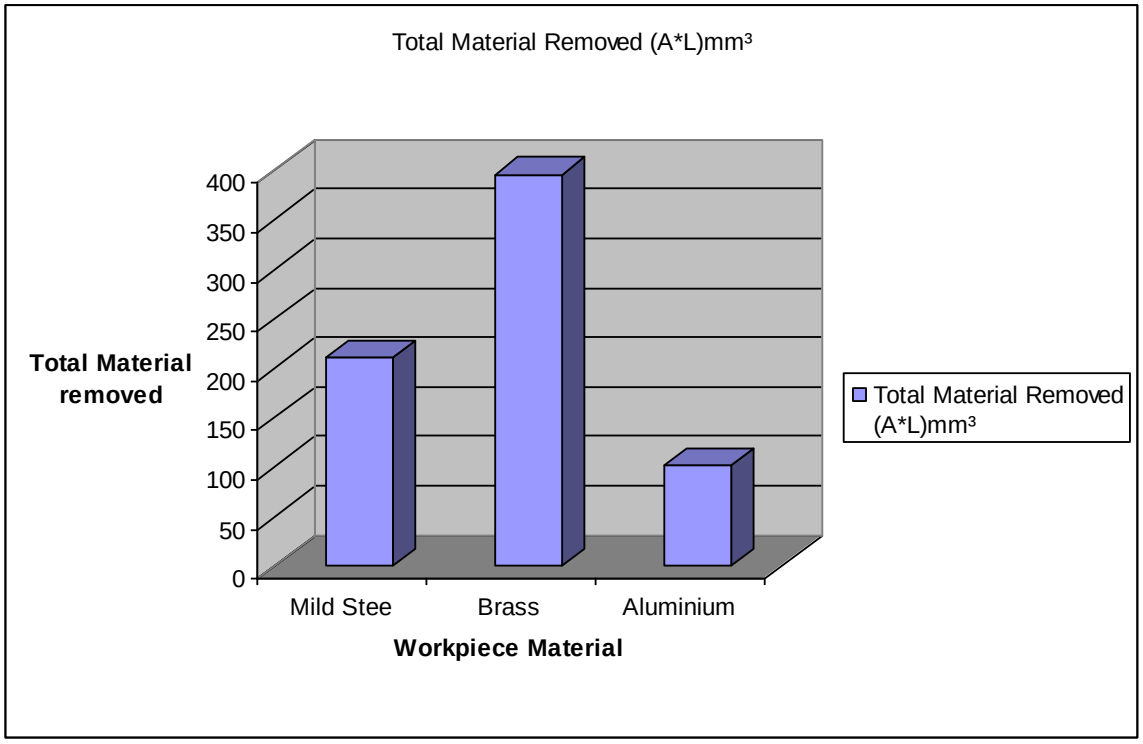

Fig 6.2: Total materials removed by C

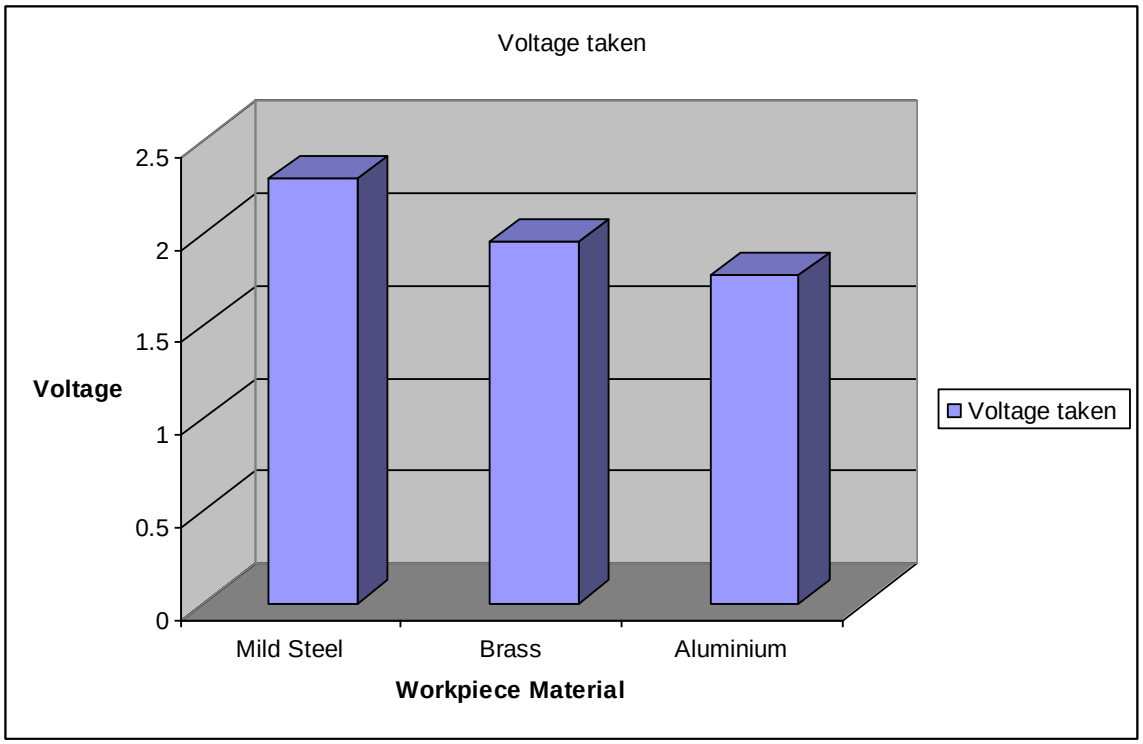

Fig 6.3: Total consumed voltage during grinding of a variety of workpieces

From the experiment it has been found that by using C, maximum voltage of 2.29, 1.95 and 1.77 v was consumed to grind the mild steel, brass and aluminium respectively. Rate of material removed for all workpieces are different due to the materials hardness. Aluminium has the lowest hardness property and the grinding rate of aluminium is lower than brass and mild steel. After grinding operation some bits of aluminium material stuck on the periphery of wheel (Figure 6.4), which proves that C is not a suitable wheel to grind aluminium and other soft materials.

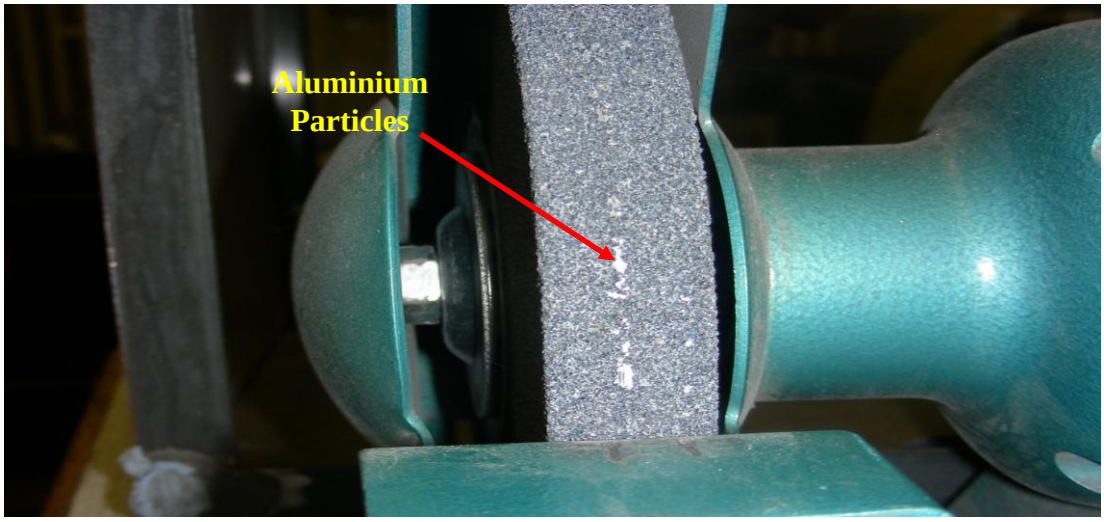

Fig 6.4: Aluminium particles stuck on C.

For brass workpiece removal rate is approximately double than mild steel. It seems the grinding rate of brass is increased considering lower voltage utilised, emphasising an optimised usage of C is for grinding of materials with same properties of brass.

Table 6.9 shows the average voltage utilised during grinding of different bars using W1. It is evident that using silicon carbide particle with 0.25 Nm in W1 is significantly effective in grinding of materials with similar hardness of brass through lower voltage consumption. Given that amount of voltage used in this experiment is related to the heat produced during grinding process, consequently affecting the thermal stresses on the wheel surface. An increase in thermal stresses may cause strength fall and further failure of breaking apart in wheel structure. To get to an optimum grinding process, minimum voltage usage needs to be considered by suitability of grits size and materials in wheels design thus the properties of materials to be grinded by same wheel.

Table 6.9: Voltage consumed and total materials removed by W1

Sr. No	Bar material	Voltage Taken (v)	Average Voltage (v)	Total material removed (mm^3)
1	Mild Steel	1.63	1.74	56.6
		1.85		
2	Brass	1.52	1.54	220
		1.57		
3	Aluminium	1.15	1.11	86.6
		1.07		

Figure 6.5 and 6.6 presents the graphs of total materials removed and voltages consumed during grinding of various bars using W1 respectively.

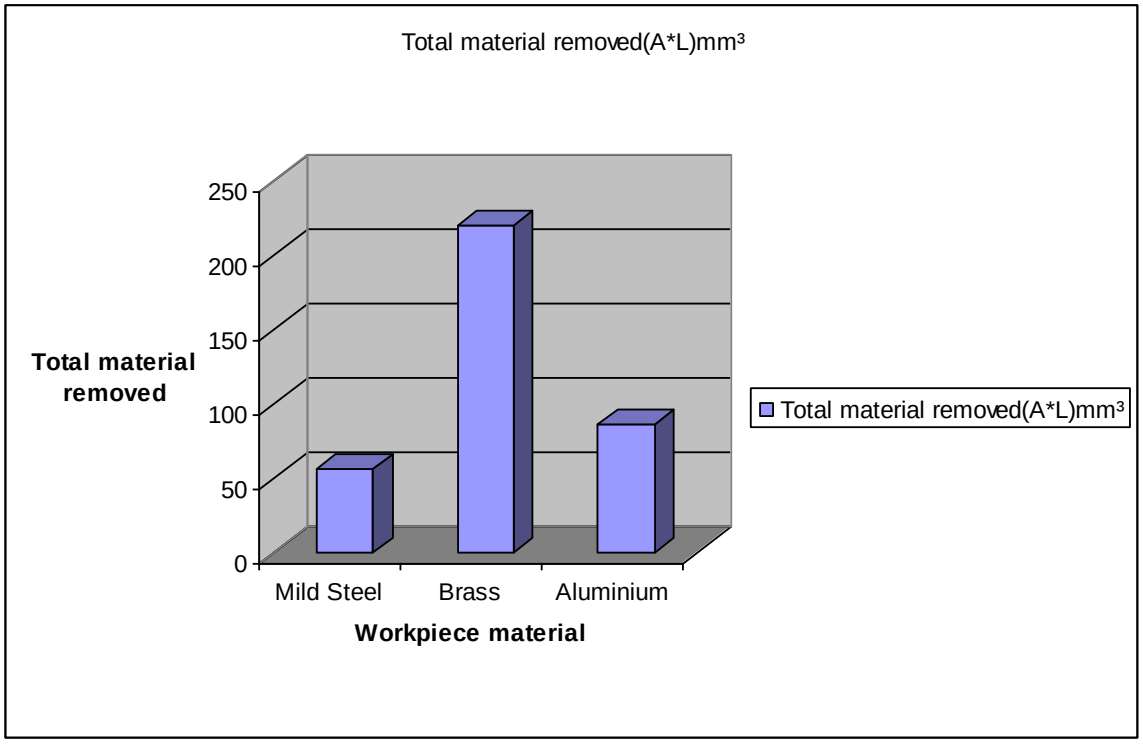

Fig 6.5: Graph of material removed by wheel made of grain size 0.25

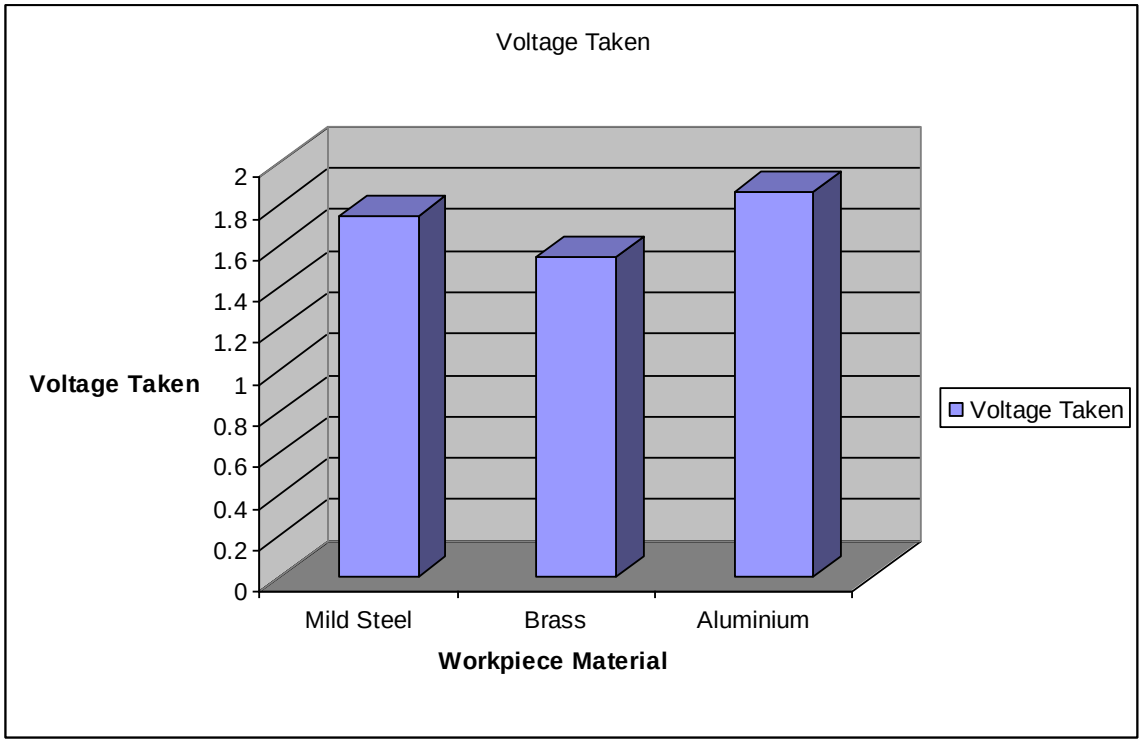

Fig 6.6: Graph of voltage taken by grinding wheel made of grain size 0.25

The voltage recorded during grinding of mild steel was 1.74 v. Table 6.10 shows that the material removal rate of aluminium bar has relatively improved. W2 made by silicon carbide grain size 0.2. Although aluminium particles did not stuck on outer surface of W2 which is very important in grinding process, it was noted that W2 didn't improve grinding process significantly.

Table 6.10: Voltage taken and total material removed by W2

No	Bar material	Voltage Taken (v)	Average Voltage (v)	Material removed (mm^3)
1	Mild Steel	2.06	2.02	18.45
		1.98		
2	Brass	1.7	1.7	24.4
		1.69		
3	Aluminium	1.72	1.68	14.08
		1.65		

Figure 6.7 and 6.8 shows the graphs of total material removed and voltage respectively by W2. It can be seen that W2 consumed maximum voltage of 2.02, 1.7 and 1.68 v to grind the mild steel, brass and aluminium bars respectively.

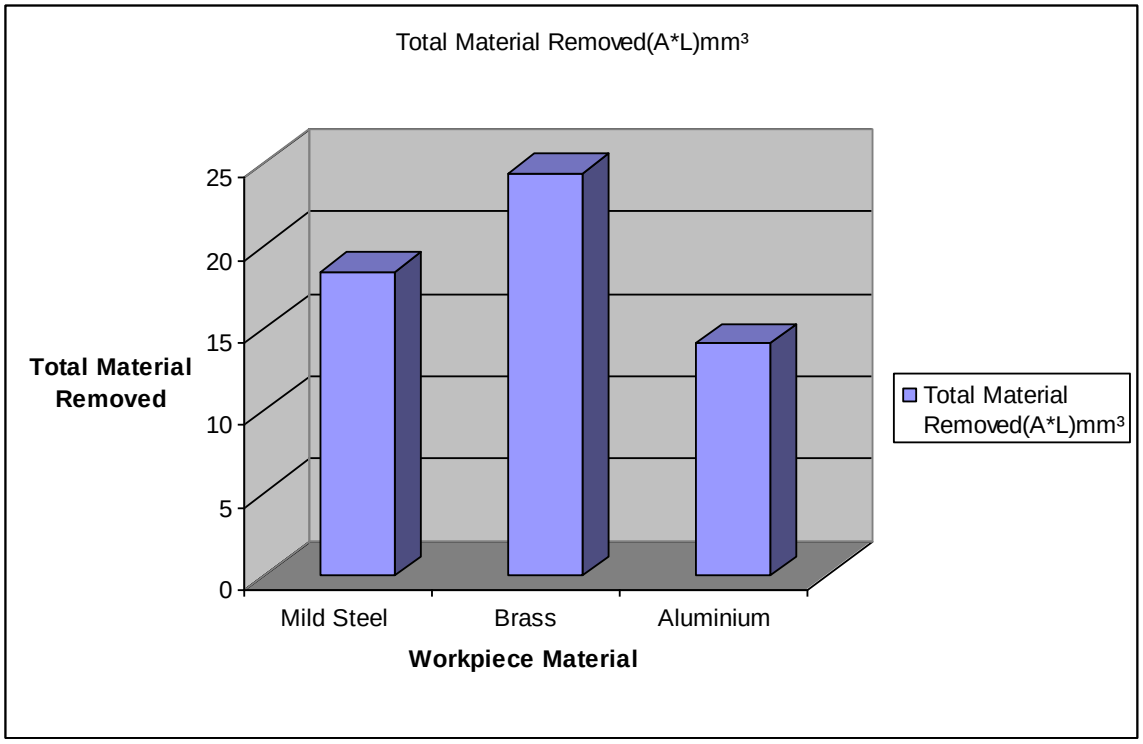

Fig 6.7: Total Material removed by W2

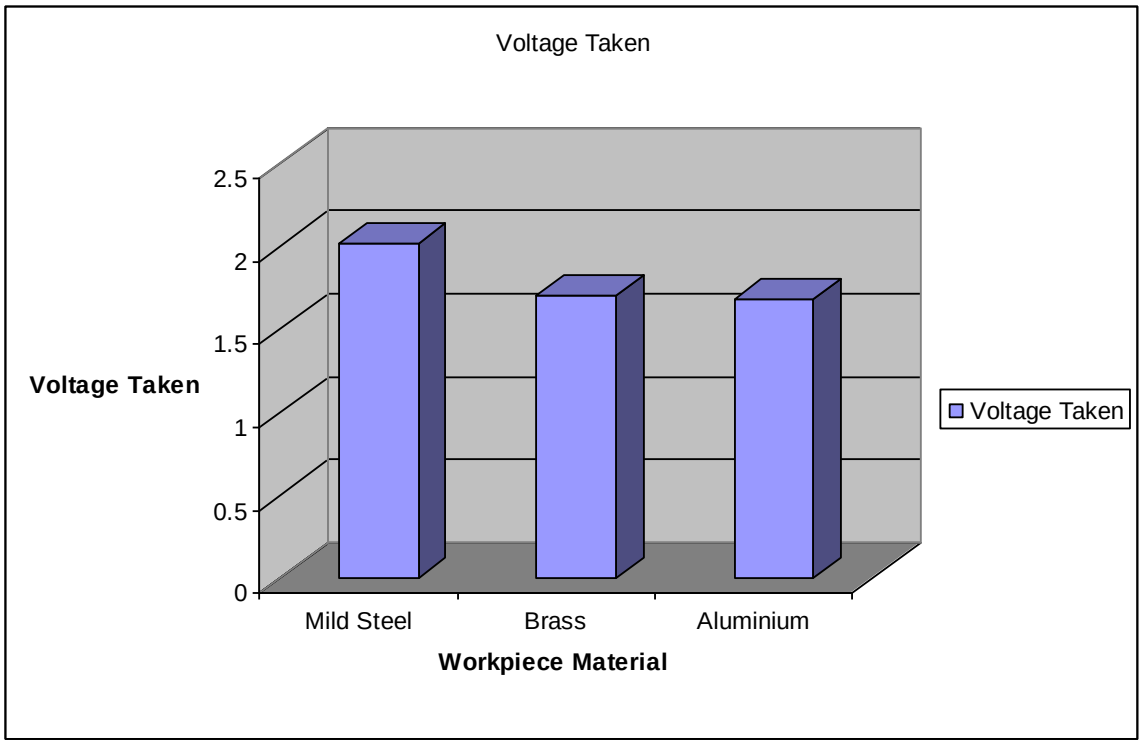

Fig 6.8: Voltage utilised during grinding of different bars by W2

The whell made by glass fibre was used as a polishing wheel (W3). The information obtained during polishing of different bars by W3 is presented in Table 6.11.

Table 6.11: Voltage used and total materials removed by W3

No	Bars	min. & max. voltage (v)	Average Voltage (v)	Total material removed (mm^3)
1	Mild Steel	1.63	1.66	6.59
		1.69		
2	Brass	1.43	1.43	9.04
		1.43		
3	Aluminium	1.33	1.31	7.68
		1.3		

The maximum voltage of 1.66, 1.43 and 1.31 v consumed to grind the mild steel, brass and aluminium bars respectively. It was observed that more brass was grinded than aluminium and mild steel bars workpiece respectively. It is found that material removal rate of aluminium bar is approximately same as brass. It is shown that W3 utilised less voltage to grind more brass and aluminium than mild steel. To simplify and of better understanding of W3 behaviour, the volume of material removed and consumed voltage were plotted in Figures 6.9 and 6.10 respectively.

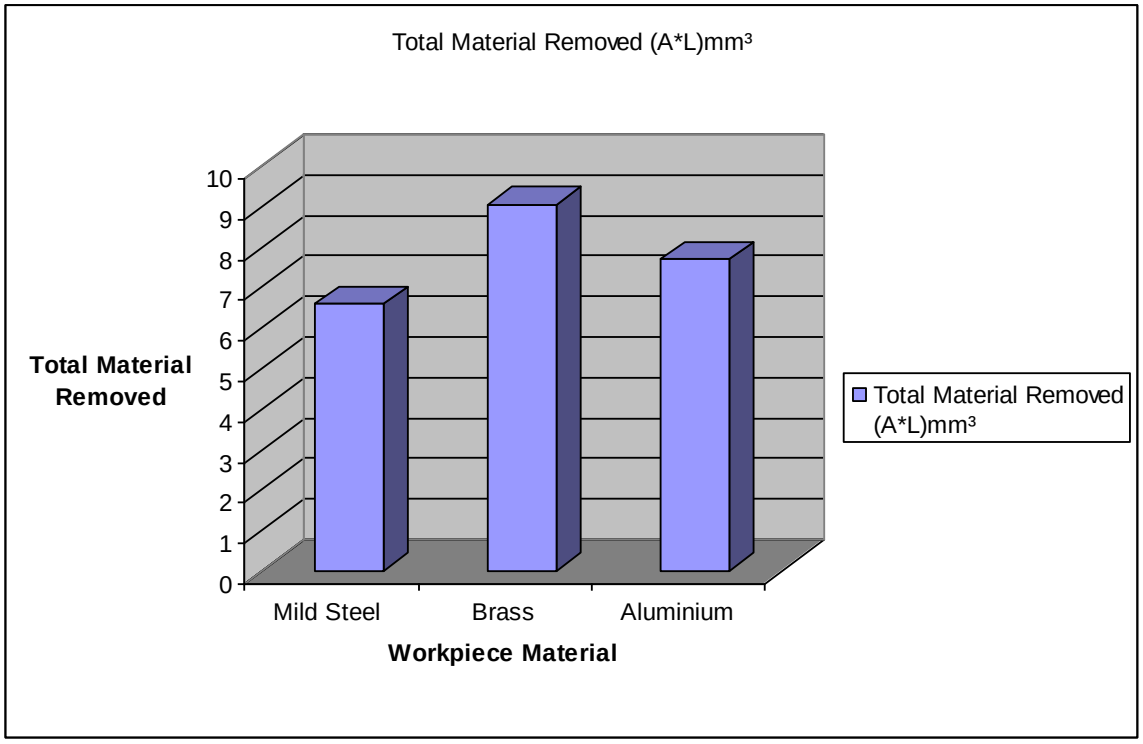

Fig 6.9: Material removed by W3

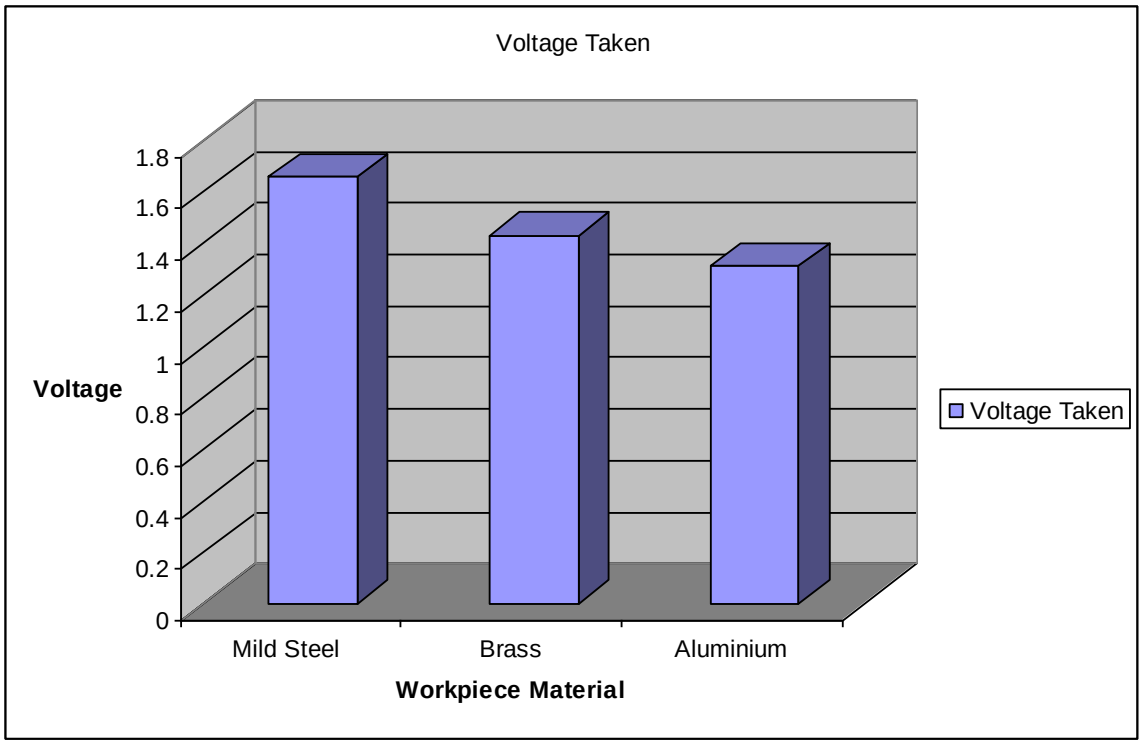

Fig 6.10: Consumed voltage by W3

W4 was made of very fine & small grain size 0.1 of silicon carbide. The information collected from grinding of various bars using W4 is gathered in Table 6.12. It shows that the maximum voltage used by W4 was 1.88, 1.5 and 1.37v for grinding of mild steel, brass and aluminium bars, respectively.

Table 6.12: Voltage taken and total materials removed by W4

Sr. No	Bar material	Voltage Taken (v)	Average Voltage (v)	Total material removed (mm^3)
1	Mild Steel	1.87	1.88	126.5
		1.89		
2	Brass	1.43	1.5	28.2
		1.57		
3	Aluminium	1.32	1.37	103.6
		1.43		

It can be noted that W4 has grinded mild steel more than other materials. Hence more voltage was taken while grinding of mild steel than brass and aluminium, which may be related to the hardness of material.

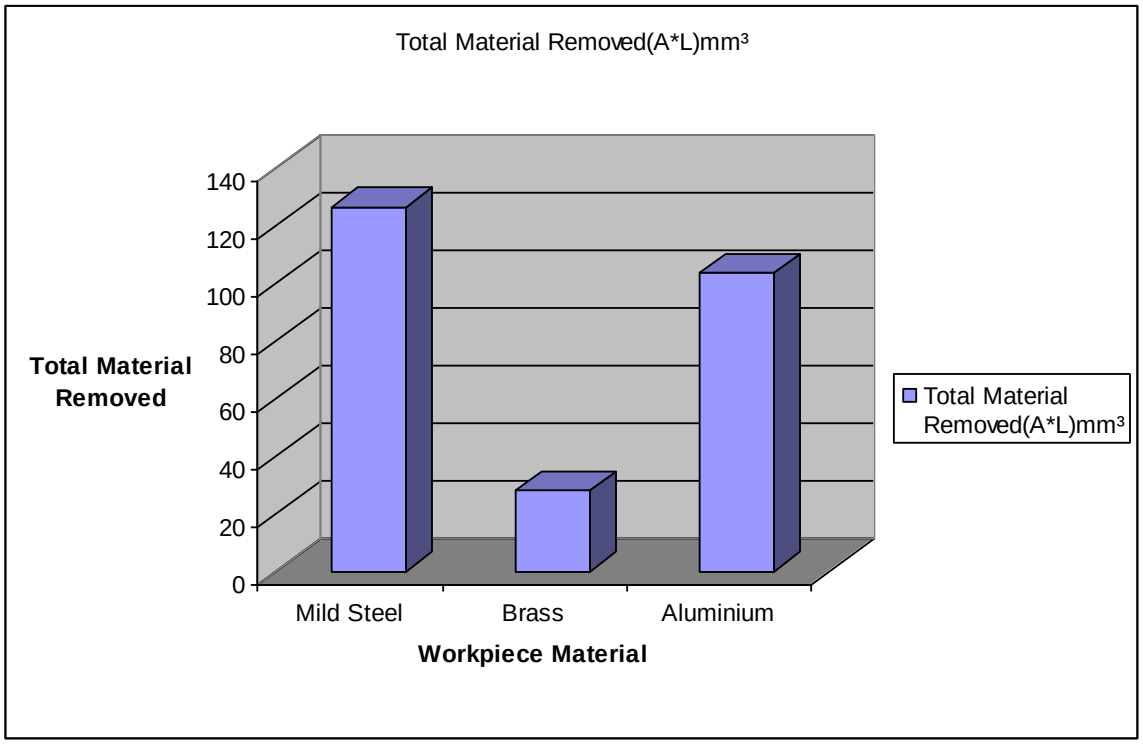

Fig 6.11: Total material removed by grinding W4

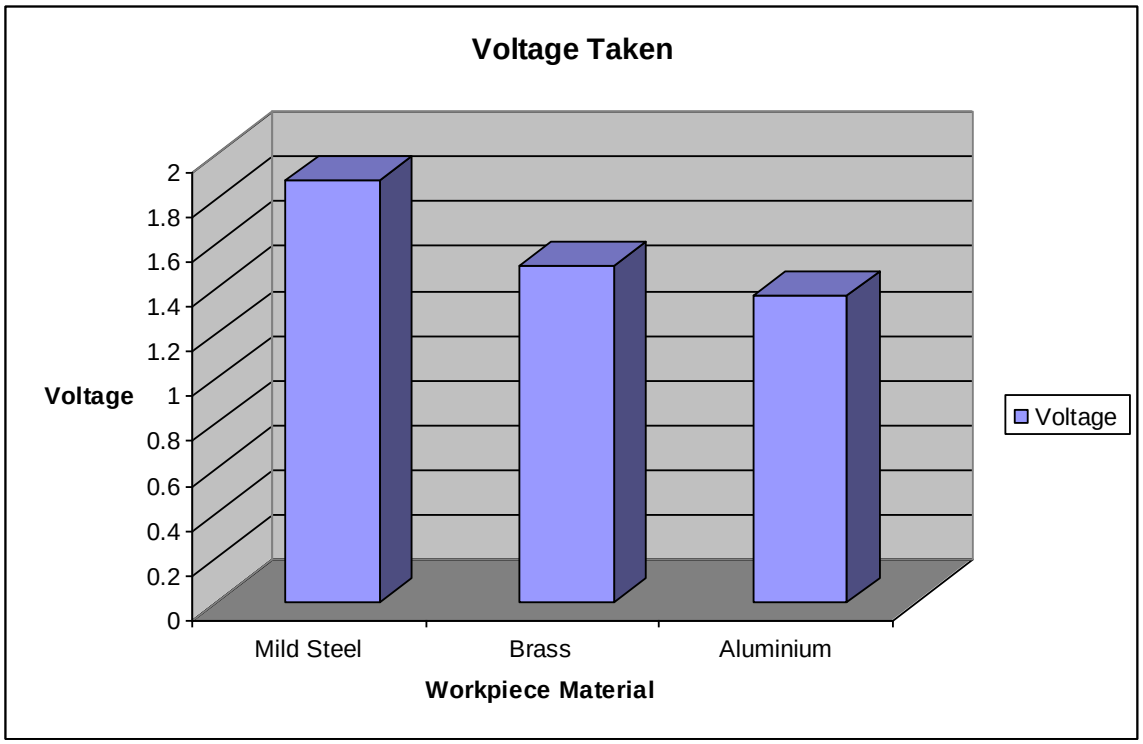

Fig 6.12: Voltage taken during grinding of wheel made of grain size 0.1

Figures 6.11 and 6.12 demonstrate the materials removed and voltages used by W4 respectively. From the experiment it has been found that by using W4, maximum voltage of 1.88, 1.5 and 1.37v was consumed to grind the mild steel, brass and aluminium respectively. It can be seen that using very fine silicon carbide grains with size 0.1 Nm resulted in significantly grinding process modification of W4. Total materials removed by W4 from mild steel and aluminium bars are relatively higher than W1. By using W4 the total material removed from steel and aluminium bars show 2.23 and 1.2 times increase respectively in compare with W1. Using W4 confirmed an increase in Rate of material removed from aluminium bar in compare to C. W4 has shown further improvement of 1.3 time less voltage consumption of aluminium grinding in compare to C, for almost same amount of removed materials.

For brass workpiece removal rate is approximately double than mild steel. It seems the grinding rate of brass is increased considering lower voltage utilised, emphasising an optimised usage of C is for grinding of materials with same properties of brass.

W5 was made by fabrication of parallel grooves by using diamond blade on a wheel with similar properties to W1. The information acquired from W5 grinding process with different bars workpiece are demonstrated in Table 6.13.

Table 6.13: Voltage taken and total material removed by W5

No	Bar	Max. & Min. Voltage (v)	Average Voltage (v)	Total material removed (mm^3)
1	Mild Steel	2.08 2.02	2.05	128.45
2	Brass	1.75 1.72	1.73	30.4
3	Aluminium	1.72 1.65	1.68	115.08

Despite of improvement in total materials removed for all samples, it can be seen that by use of W5 the voltage utilised for all sample bars have slightly increased in compare with W4, thus W5 showed a reduction of voltage taken in compare with C.

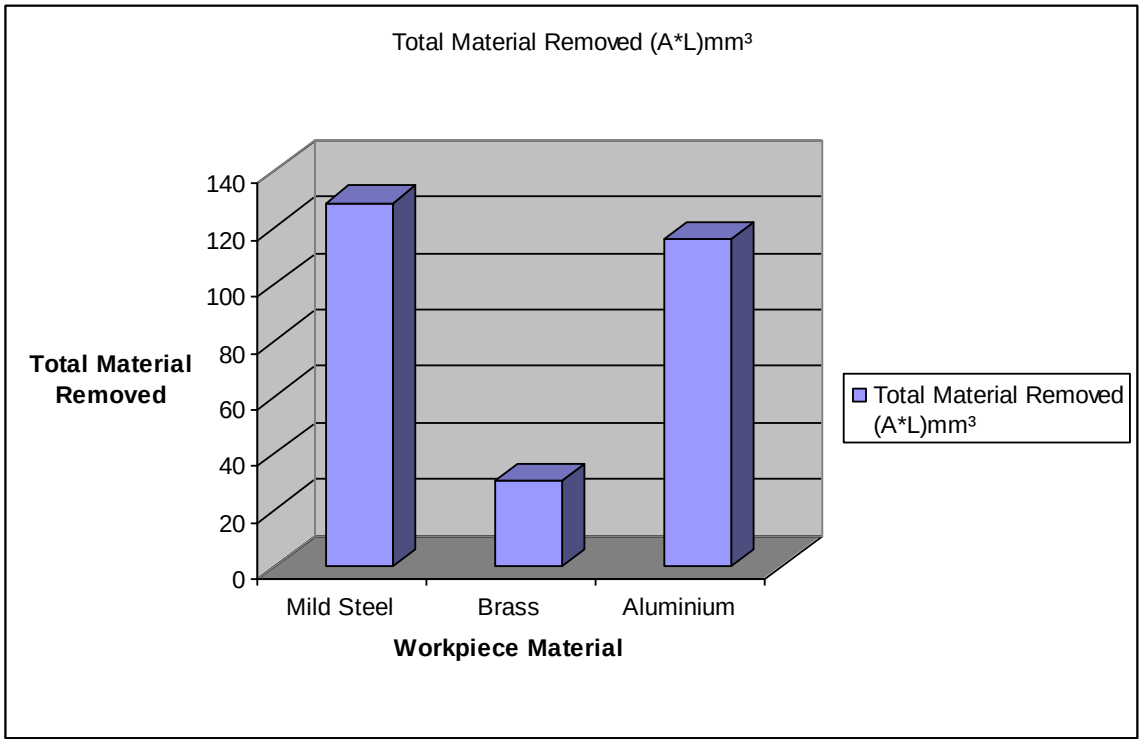

Fig 6.13: Graph of total material removed by the wheel with side lines

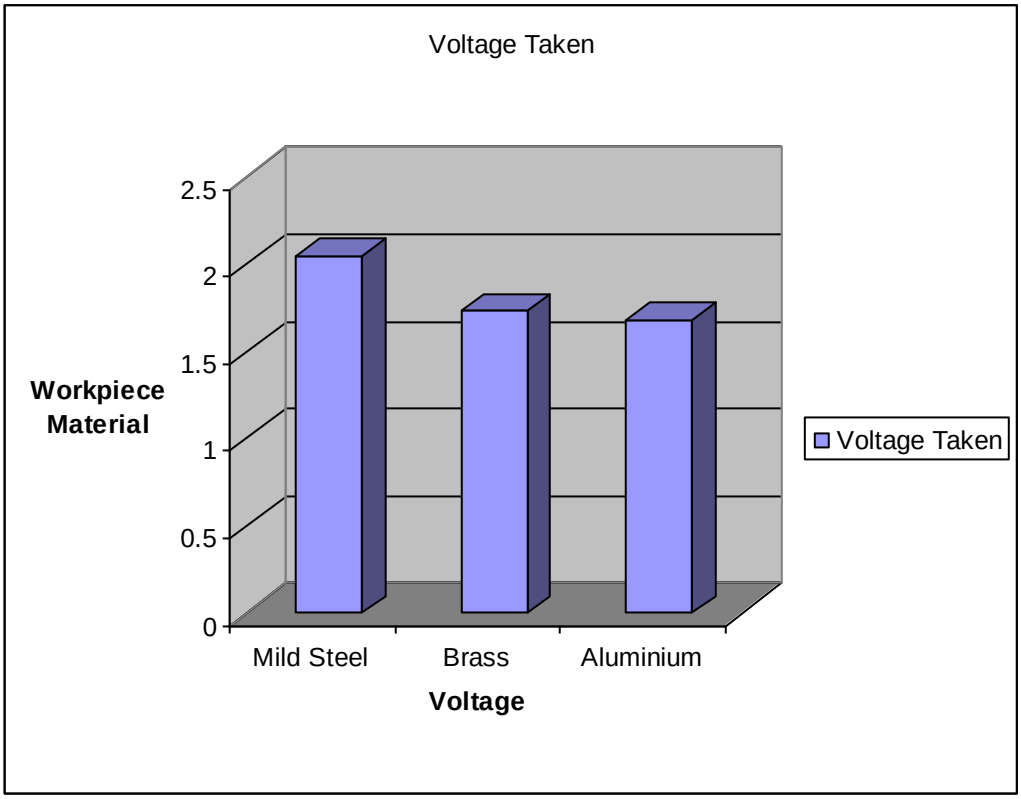

Fig 6.14: Graph of voltage taken during grinding of wheel with side lines

Figures 6.13 and 6.14 demonstrate the material volume removed and consumed voltage respectively. It is recorded that the total material volume removed from brass bar is dramatically lower than other workpieces. Results obtained from W5 grinding have been detailed on section 6.1.3.

Table 6.14: Recorded voltages and total material removed by W6

Sr. No	Bar material	Concumed Voltage (v)	Average Voltage (v)	Total material removed (mm^3)
1	Mild Steel	2.05	2.02	140.45
		1.99		
2	Brass	1.7	1.7	32.4
		1.69		
3	Aluminium	1.73	1.69	128.08
		1.66		

W5 was redesigned to form crossed grooves surface wheel, called W6. Table 6.14 shows data attained during experiment with W6 grinding. The total material volume removed of mild steel bar by W6 was more than the aluminium and brass bars. Since W5 and W6

have shown better performance with lower voltage comparative to other wheels made during this project, therefore throughout of the rest of this study, the research has been focused on C, W5 and W6 performances comparatively and no further experiments were conducted on W1, W2, W3 and W4.

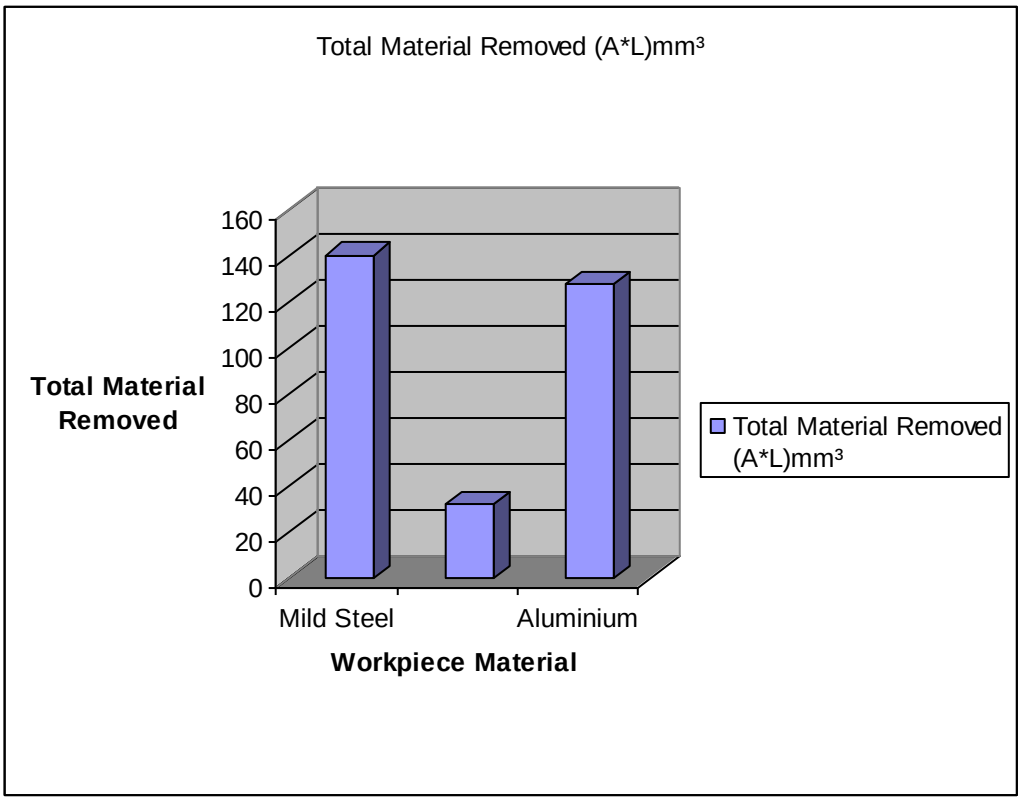

Fig 6.15: Total materials removed by W6

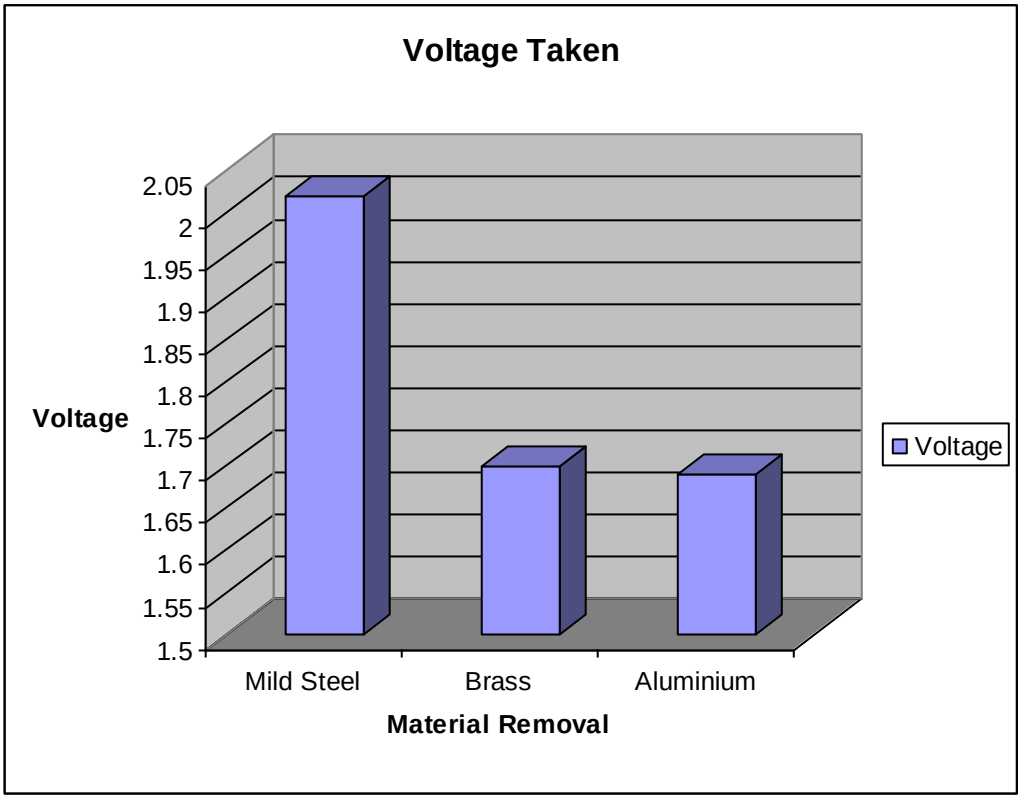

Fig 6.16: Recorded voltages during grinding of various bars by W6

By reviewing all previous grinding wheels, it is apparent that although W6 has used the highest voltage in grinding mild steel (Figure 6.16), it is the first wheel which has grinded more mild steel than brass and aluminium. In this particular case, it has been found that only W6 is not capable to grind brass relatively (Figure 6.15). It may be due to grit size and surface shape of the wheel and materials hardness. Symmetrical surface shape of crossed grooves may be more efficient for materials with higher hardness.

Table 6.15: Work pieces hardness & voltage taken by all grinding wheels

No.	Bars	Hardness (HV)	Voltage (v)						
			C1	W1	W2	W3	W4	W5	W6
1	Mild Steel	0.9062	2.29	1.74	2.02	1.66	1.88	2.05	2.02
2	Brass	0.7089	1.95	1.54	1.7	1.43	1.5	1.73	1.7
3	Aluminium	0.5098	1.77	1.11	1.68	1.31	1.37	1.68	1.69

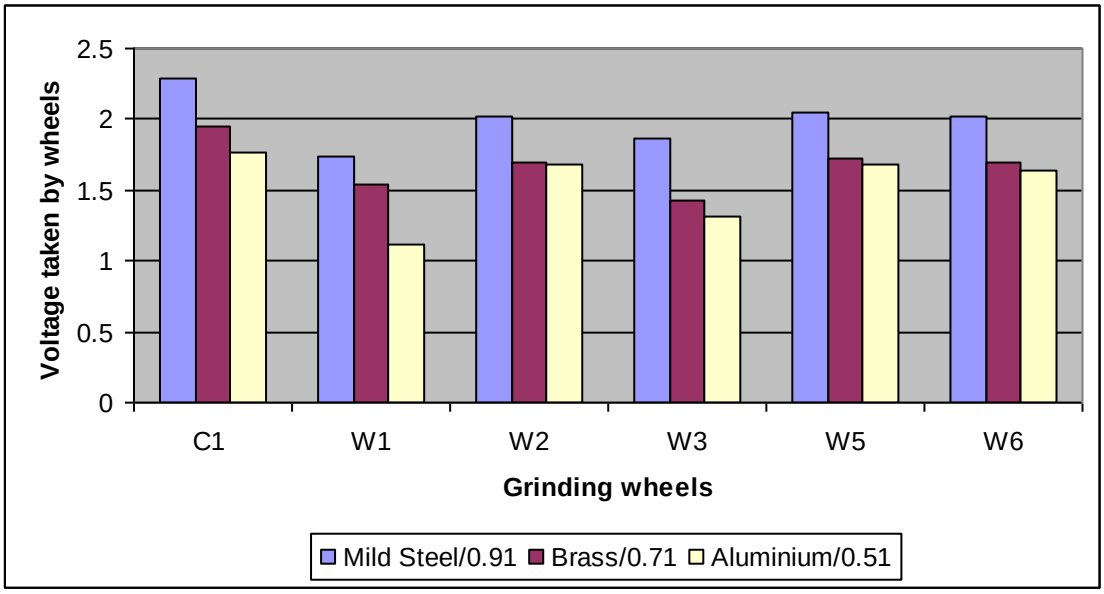

Fig 6.16: Hardness of work pieces material and voltage taken by all grinding wheels

Table 6.15 and Figure 6.16 shows the consumed voltages against a number of materials hardness used in this study. After reviewing above graph, it can be realised that utilised voltages of mild steel, brass and aluminium bars are in descending order respectively according to materials hardness property for all grinding wheels.

It is evident in all wheels the highest voltage has consumed to grind mild steel. Also the voltage taken to grind brass bar is slightly higher than aluminium workpiece. W3 utilised more voltage to grind aluminium than W1. In case of W2 and W4, to grind mild steel approximately same voltage is being utilised.

Table 6.16: Total material removed by all wheels to grind Mild steel, Brass and Aluminium bars

Bars	Hardness (HV)	Volume of material removed (mm³)						
		C	W1	W2	W3	W4	W5	W6
Mild steel	0.9062	210.7	56.6	18.45	6.59	126.5	20.45	140.4
Brass	0.7089	395.5	220	24.4	9.04	28.2	30.4	32.4
Aluminium	0.5098	101.1	86.6	14.08	7.68	103.6	115.08	128.09

It can be noted from Table 6.16 that C is the best wheel to grind brass and mild steel than all other wheels. It is confirmed that W1 made of silicon carbide grain size of 0.25 is the best to grind brass bar comparative to other three wheels. W4 made by very fine and small silicon carbide grain size of 0.1 has grinded more aluminium than all other

grinding wheels. After reviewing W1 to W6 behaviour, W6 was appeared to be the best to grind mild steel than the other wheels made in this project.

It has been found that there is uneven wear on the outer periphery on wheel W2. Material on the outer periphery of grinding wheel is not of accurate thickness (if measure diameter of grinding wheel). Reason behind uneven thickness of grinding wheel is improper mould shape or improper material filled during manufacturing grinding wheel. Because proper standard was not applied in preparing samples due to lack of accurate facilities for manufacturing grinding wheels.

In preparation one mould, clamps were used to hold ring, due to more compressing force applied by clamp, mould preparation can be effected. During manufacturing grinding wheel, material mixed could not have been filled properly between plastic ring and aluminium disc due to lack of quality standard. There was also bit difference of uneven wear on grinding wheel W1 and also there is possibility of air bubbles in filled material in the gap between ring and disc.

Table 6.16 shows wheel W6 grinds mild steel, more than aluminium and brass respectively. By reviewing all studies of previous grinding wheel, W6 is first one to grind more mild steel in comparison with other produced wheels. The temperature during the grinding operation was effectively controlled by coolant application and less wear flats noticed on the wheels. Generally the grinding wheel required less dressing operation and thereby prolonging the wheel life although a more evenly distributed grain structure will facilitate a better performance by allowing better coolant filtration.

Since W5 and W6 have shown better performance with lower voltage comparative to other wheels made during this project, therefore throughout of the rest of this study, the research has been focused on C, W5 and W6 performances comparatively and no further experiments were conducted on W1, W2, W3 and W4.

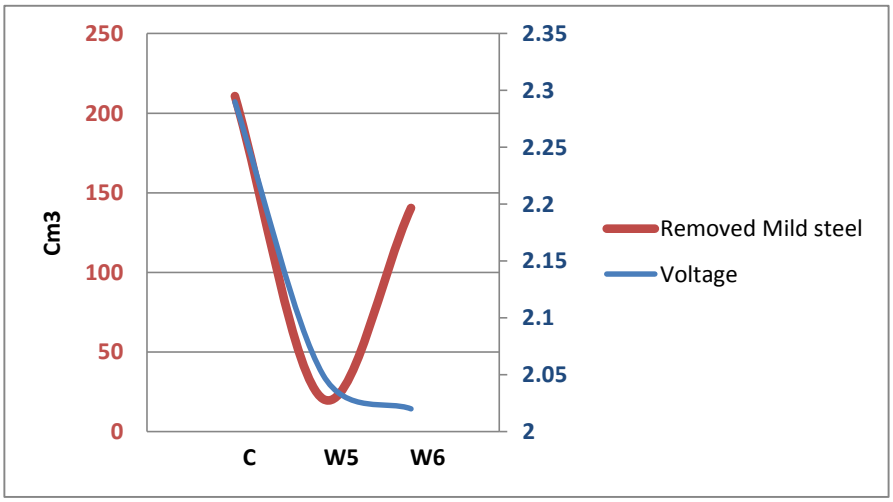

Fig 6.17: Recorded voltage vs. material removed from steel bar using C, W5 & W6

Figure 6.17 demonstrates the materials removed from mild steel bar against voltage taken by C, W5 and W6 comparatively. It has been observed that when C was replaced by W6, the consumed voltage value was significantly decreased from 2.29 to 2.02 v by 13%. The symmetrical surface shape of W6 may lowers stress concentration, consequently reduces shear stress. It should be noted that heat is a result of shear stress, therefore by decreasing shear stress, thermal stress will be lowered and related measuring voltage will be reduced.

In Figure 6.18 total materials volume removed from different bars are plotted along with the utilised voltages by C, W5 and W6. It ease making comparison and behaviour evaluation of C, W5 and W6 by consumed voltages, which is related to stresses and heat, while grinding different workpieces. Stress analysis using FEA profiles of C, W5 and W6 and their behaviour considering consumed voltages have been detailed in section 6.2.

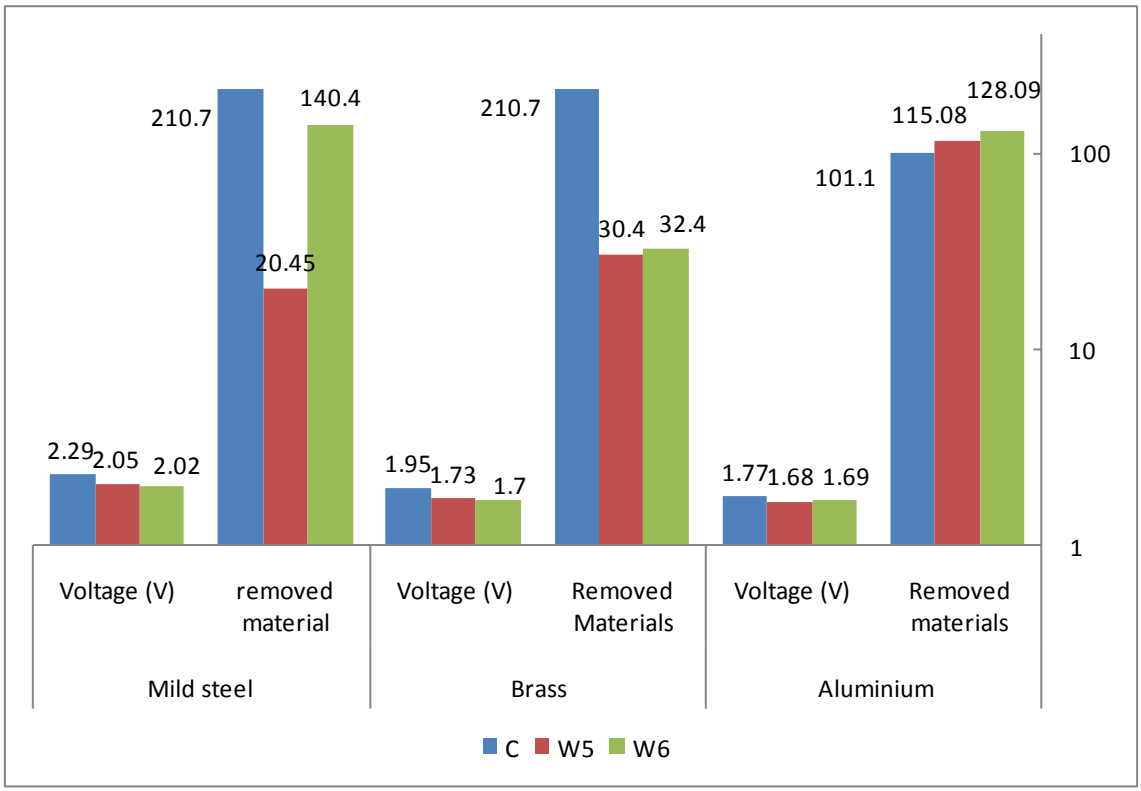

Fig 6.18: Total removed material vs. Recorded voltage by C, W5 & W6

6.2 Simulation results and discussion

The numerical simulation of grinding wheel has been investigated by ANSYS software.

The grinding wheel was modelled. The simulation result matched well with the experimental result at different feed rates and depths of cut. From the experimental analysis results, the boundary condition of the FEA model has been adjusted and fitted the pattern produced by the FEA's modal emulation analysis for different grinding wheels including commercial wheel, encircled by parallel grooves in another type and cross grooves in the third type for grinding of bars with different materials (Aluminium, Brass & Steel).

Figures 6.19,6.20,6.21 shows ansys simulation of boundary conditions for commercial, grooved and crossed grooved wheels. Other photos of simulation wheels are shown in appendix.

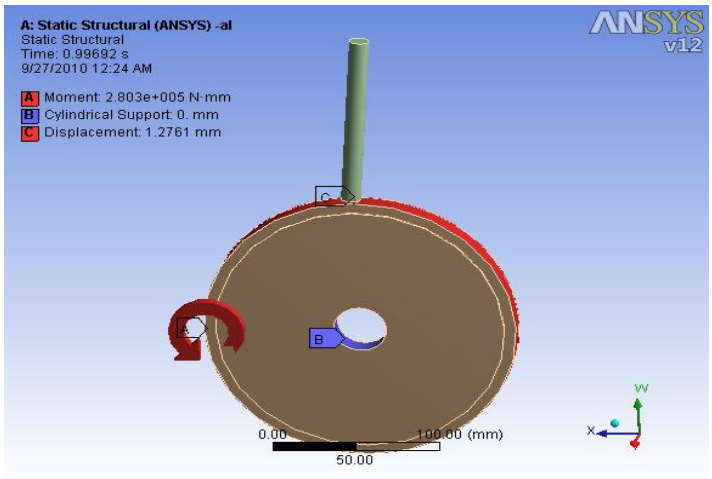

Fig 6.19: Ansys simulation of the commercial grinding wheel highlighting the boundary conditions

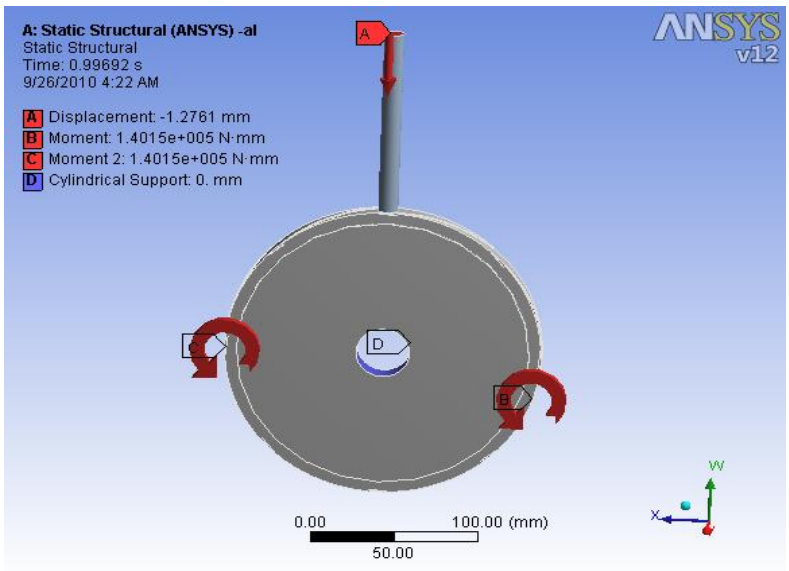

Fig 6.20: Ansys simulation of the grinding wheel with groove highlighting the boundary conditions

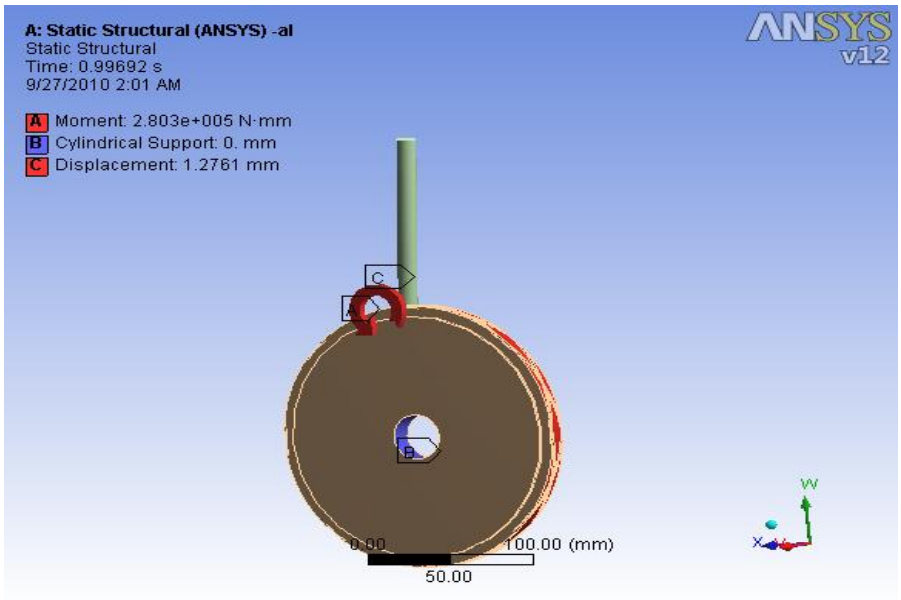

Fig 6.21: Ansys simulation of the grinding wheel with cross groove highlighting the boundary conditions

The dimensions of the grooves were modified to increase the depth of cut and reduce the stress to prevent wheels from overheating and to increase the rigidity. Also it showed the stress levels on the grinding wheel.

Using FEA, different Stress parameters such as von-Mises, principal and shear stresses for C, W1, W2, W3, W4, W5 and W6 were computer-generated by grinding simulation of various bars including; Mild steel, Aluminium and Brass.

The equivalent stress is often called the von-Mises Stress also known as the maximum distortion energy criterion. The von-Mises criteria is a formula for combining 3 stresses in elastic body system which is subject to loads in three dimensions into an equivalent stress, which is then compared to the yield stress of the material. If the von-Mises Stress exceeds the yield stress, then the material is considered to be at the failure condition (Efunda 2011).

The von-Mises Stress mathematically is expressed as,

$$\frac{1}{2}\left[(\sigma_1-\sigma_2)^2+(\sigma_2-\sigma_3)^2+(\sigma_3-\sigma_1)^2\right]\leq {\sigma_y}^2 \qquad (6.15)$$

Where $\sigma_{1,}\,\sigma_2$ and σ_3 are the principal stresses and ${\sigma_y}^2$ is the equivalent stress, or von-Mises Stress.

Minimum and maximum stresses found on design were 904868 N/m^2 and 3.78572e+006 N/m^2 respectively at (-0.0714878 m, -0.0587004 m, -0.007 m). Using FEA, maximum stress on grinding wheel was observed around internal diameter (restrained part). Then less stress found on side faces of grinding wheel and on the periphery of grinding wheel where bar was being grinded by grinding wheel. The results of different stresses obtained from FEA simulation can be seen in Table 6.17. The results of various stresses for different wheels are detailed in sections 6.2.1 to 6.2.3.

Table 6.17: Different Stresses data collected from FEA simulation

Bar	Stress Type	Stress Level	C	W5	W6
Aluminium bar	von-Mises Stress	Max.	25.805	162.47	55.99
		Min.	4.21E-06	3.16E-06	3.76E-06
	Principal Stress	Max.	17.873	76.47	37.194
		Min.	-0.8614	-13.445	-1.0134
	Shear Stress	Max.	14.82	91.891	32.288
		Min.	2.43E-06	1.80E-06	2.09E-06
Steel bar	von-Mises Stress	Max.	25.805	162.47	55.99
		Min.	1.15E-05	8.55E-06	1.36E-05
	Principal Stress	Max.	17.873	77.762	37.194
		Min.	-8.61E-01	-1.34E+01	-1.01E+00
	Shear Stress	Max.	14.82	90.81	32.288
		Min.	6.61E-06	4.89E-06	7.86E-06
Brass bar	von-Mises Stress	Max.	25.805	173.2	55.99
		Min.	5.95E-06	4.30E-06	1.36E-05
	Principal Stress	Max.	13.658	102.64	55.99
		Min.	-8.61E-01	-1.34E+01	5.11E-06
	Shear Stress	Max.	14.82	99.997	37.194
		Min.	3.43E-06	2.46E-06	-1.01E+00

6.2.1 von-Mises stress

During grinding mild steel bar simulation, the commercial wheel, C possessed a maximum von-Mises stress of 25.8 MPa. By using parallel grooves surface wheel, W5 von-Mises stress was increased to 162.47 MPa showing an increase of 6.3 times in von-Mises stress. The von-Mises stress of crossed grooves wheel, W6 was about 55.99 MPa which showed a reduction of about 3 times in compare with W5. Same results have been obtained for aluminium bar. It was evident that von-Mises stress of W5, during grinding simulation of brass bar has been dramatically enhanced to 173.2 MPa in compare with other samples materials. It may be due to brass high wear resistance. Copper and its alloys, such as bronze, brass are the materials which are widely used in friction parts of machines, as bearing liners, bushings, etc. Properties such as high strength and ductility, fatigue strength, wear resistance are necessary for these materials (Sadykov et Al., 1999). FEA profile of

aluminium bar with commercial grinding wheel showing von-Mises stresses are presented in Figure 6.22. FEA profiles of brass and steel are shown in appendix.

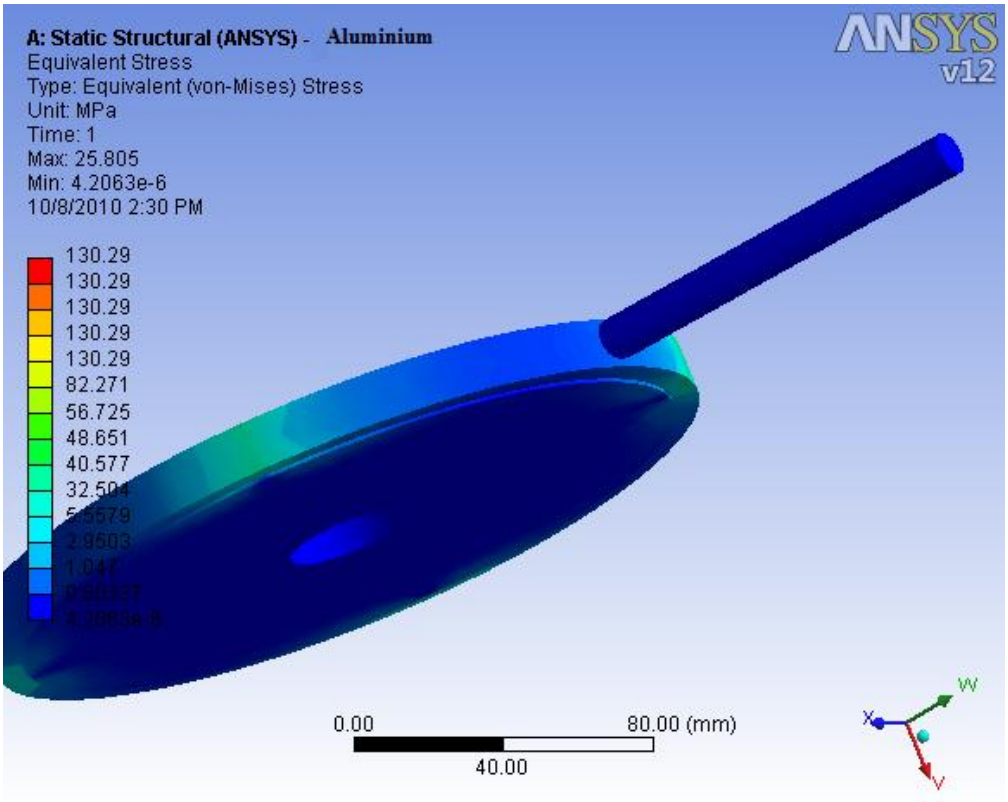

Fig 6.22: FEA profile of aluminium bar with C wheel showing von-Mises stress distribution

6.2.2 Principal stresses

It was observed that the commercial wheel, C leads to the maximum principal stress of 17.87 MPa while grinding mild steel bar. Using W5, maximum principal stress was noticeably increased to 77.76 MPa, showing a rise of 4.3 times in principal stress value. It was noted that principal stress of W6 was about 37.19 MPa which exhibits a significant reduction of 2 times in maximum principal stress in comparison with W5. There was an insignificant slight drop of 1.7% fall of principal stress from 77.76 MPa (mild steel bar) to 76.47 MPa after grinding simulation of aluminium bar with W5. Other results were observed to be the same. It was found that maximum principal stress of W5, during grinding of brass bar has been intensely enhanced by 32% from 77.76 MPa of Steel bar to 102.64 MPa. As it already noted in section 6.1.1 it may be due to brass high wear resistance.

Maximum principal stress of W6 (brass bar) has been recorded to be 55.99 MPa which is noticeably lower than W5 (102.64 MPa) by 83%.

FEA profile of mild steel bar with parallel grooves surface wheel (W5) showing maximum principal stresses are presented in Figure 6.23.FEA profiles of aluminium and brass are shown in appendix.

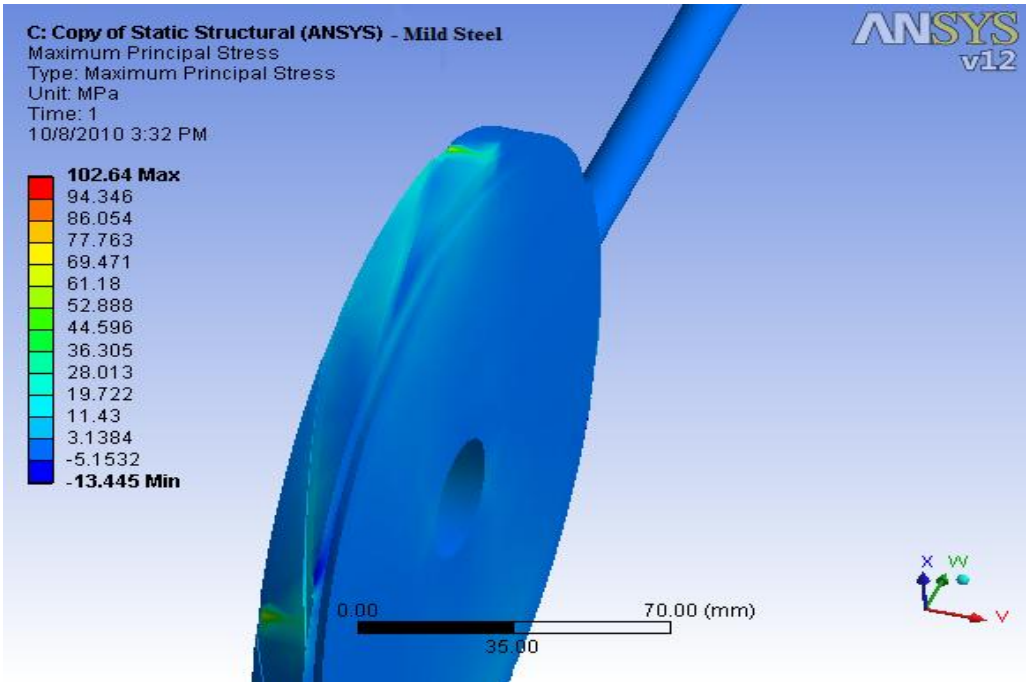

Fig 6.23: FEA profile of steel bar with W5 wheel showing principal stress distribution

6.2.3 Maximum shear stress

The results of shear stresses using FEA modelling on C, W5 and W6 by applying different sample bars are presented in Table 6.17. During grinding aluminium bar simulation, the shear stresses obtained for C, W5 and W6 are 14.82, 91.9 and 32.29 MPa respectively. The effect of using W6 is apparent to decrease maximum shear stress from 91.9 to 32.3 MPa by about 2.8 times.

It is apparent that symmetrical surface shape in crossed grooves wheel has formed a uniformity which in return has lowered the stress concentration in compare with W5. Similar results have been obtained, applying mild steel bar.

As it is previously mentioned in section 6.1.1 and 6.1.2 using brass bar have increased maximum shear stress of W5 and W6 dramatically due to wear resistance of brass.

Maximum shear stresses of C, W5 and W6 were 14.82, 100 and 37.2 MPa respectively, indicating a reduction of 2.7 times in maximum shear stress when W5 was replaced by W6. FEA profile of brass bar with crossed grooves surface grinding wheel showing maximum shear stresses is presented in Figure 6.24. FEA profiles of aluminium and steel are shown in appendix.

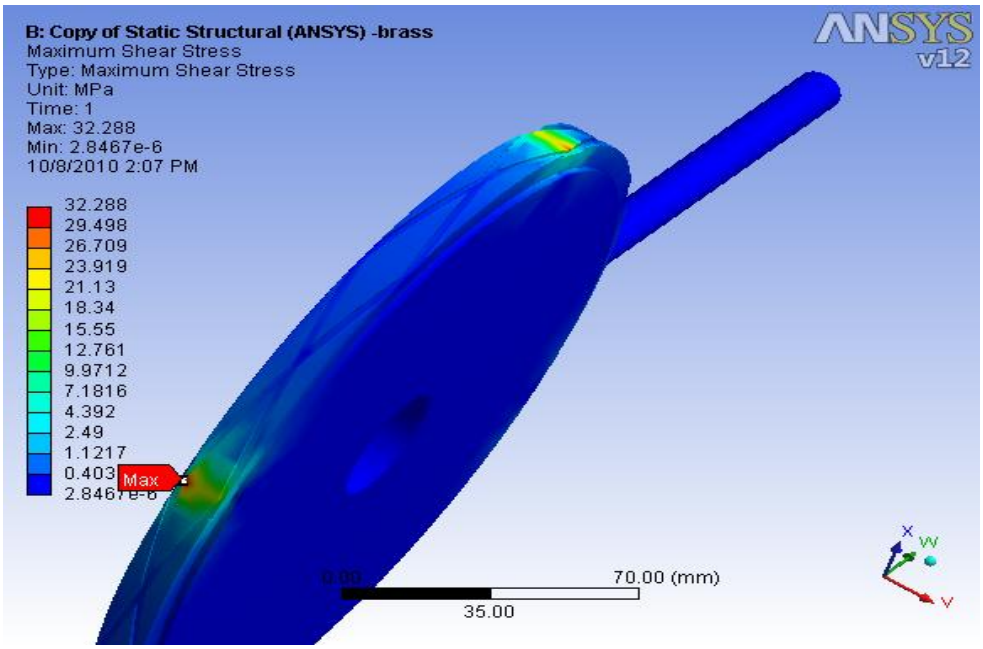

Fig 6.24: FEA profile of brass bar with W6 wheel showing maximum shear stress distribution

For ease of making comparison and evaluation of different stresses the results obtained from FEA profiles for all workpieces including aluminium, mild steel and brass bars are presented in Figure 6.25.

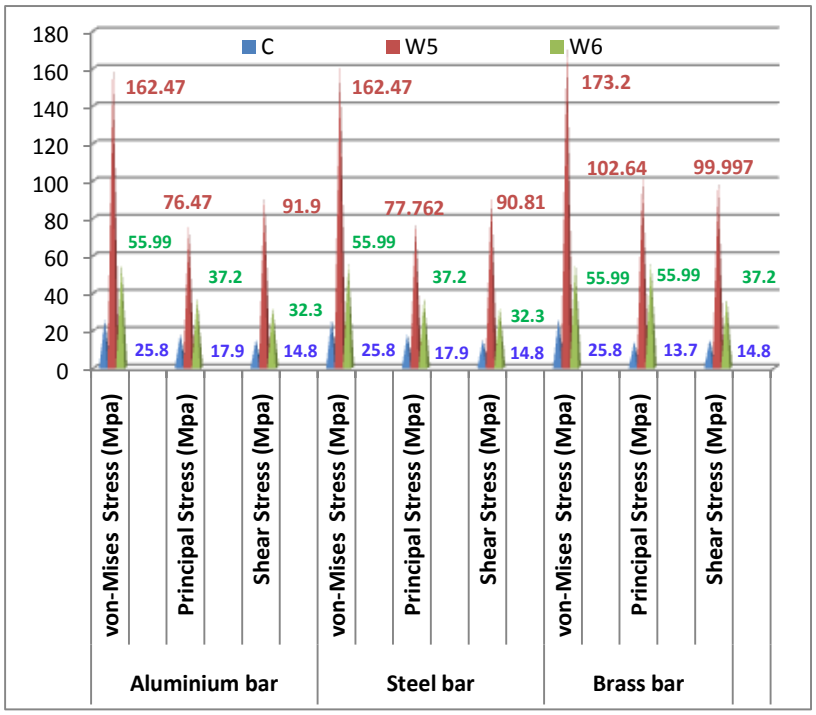

Fig 6.25: Different stresses(maximum) obtained from FEA profiles of C, W5 & W6 for various bars

As it previously noted von-Mises stress can be compared to the yield stress of the materials. If the von-Mises Stress exceeds the yield strength, then the material is considered to be at the failure condition. rule of mixtures formula has been used to calculate stress of grinding wheel which consequently can be compared with con-Mises stress.

In the absence of porosity the longitudinal stress of a two component composite (fibre and matrix) is usually given by a rule-of-mixtures equation:

$$\sigma_c = \sigma_f V_f + \sigma_m V_m \quad (6.16)$$

Where $\boldsymbol{\sigma_c}$ is the flexural stress of produced grinding wheel, $\boldsymbol{\sigma_f}$ *and* $\boldsymbol{\sigma_m}$ is stresses of fibre and matrix respectively. V_f and V_m are the volume fraction of fibre and matrix (Razmara 2008).

To calculate $\boldsymbol{\sigma_c}$ all necessary data from Table 5.1 and section 5.2.1 are extracted into Table 6.18.

Table 6.18: Properties needed to find $\boldsymbol{\sigma_c}$

Materials	Flexural Stress (MPa)	ρ (g/Cm3)	Volume (Cm3)	Volume fraction %
Matrix *(m)*	80	1.18	50.84	73
SiC *(f)*	550	3.21	18.69	27

Using mechanical and physical properties shown in Table 6.18 and applying equation 6.16, σ_c found to be 207 MPa. Hence the strength of produced grinding wheel is extensively higher than the maximum brass von-Mises stress value of 173.2 MPa (Figure 6.26) obtained from FEA profile, resulting 19.5% higher strength in W6.

To study the behaviour of C, W5 and W6 and relation of stresses with voltage consumption, all data obtained from FEA profiles and experimental results are plotted in Figure 6.26.

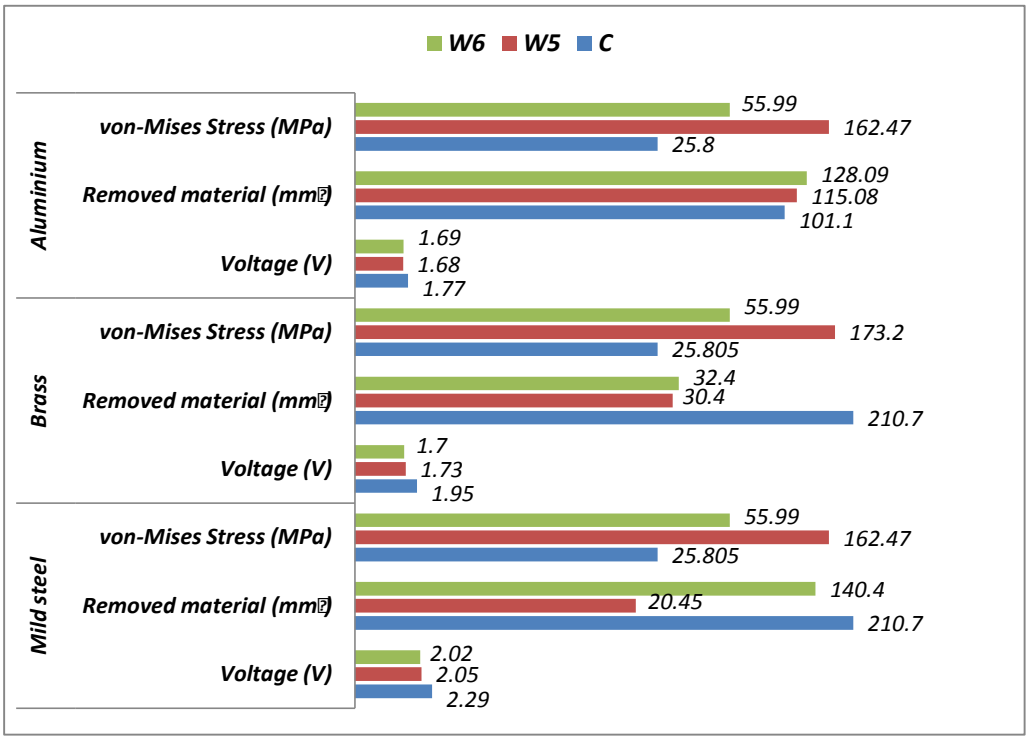

Fig 6.26: Total removed material vs. von-Mises stress and voltage taken by C, W5 & W6

Material removal rate of all workpieces materials, it's different for aluminium according to its properties, because aluminium is the softest material in three workpieces. For brass workpiece material removal rate is approximately double than mild steel. Grinder takes less voltage than to grind more brass than mild steel. It shows that commercial wheel (C) is best for grind brass than other materials by taking less voltage and grinds more material.

Redesigning grinding wheels by making grooves on surface of wheel, material removal rate is increased and less voltage has been used. Also, time for redressing wheels has been reduced. This redesign reduced possibility of clogging particles and grinding wheels can increase grinding time.

With regards to aluminium bar grinding, W6 proved considerable improvement comparative to C and W5. The materials volume removed by W6 showed an increase of 27% and 12% in compare with C and W5 respectively. Hence when C and W5 were replaced by W6 the recorded voltage decrease by about 5% and 2% respectively.

It is evident that W6 is an optimised wheel to grind soft materials like aluminium. It may be due to crossed grooves surface shape and grain size of grit used in W6 production and hardness of bars. Hardness of mild steel, brass and aluminium bars are in sliding order respectively according to material properties of all materials. Voltage taken by all grinding wheels for all bar materials- mild steel, brass, aluminium is also sliding order respectively.

Increasing voltages are also due to increasing friction and temperature. The time involved in producing a chip is extremely short (microseconds).The chips carry away much of the heat generated in grinding process. Only a fraction of the heat produced in grinding is conducted to the workpiece (Kim 1997). The sparks produced when grinding metals are hot chips with oxygen in the atmosphere. Sparks do not occur when any metal is ground in an oxygen-free environment. Sparks colour, intensity and shape depend on the type of metal being ground. If the heat generated due to exothermic reaction is sufficiently high, chips can melt and, owing to surface tension, acquire a spherical shape and solidify as metal particles.

High temperatures in grinding may also cause the workpiece surface to crack. This is known as heat checking. These cracks are usually perpendicular to the grinding direction. Under severe grinding conditions, however, parallel cracks may also appear. Such a surface lacks toughness and has low fatigue and corrosion resistance.

During grinding operations excessive temperature rise can cause tempering and softening of the workpiece surface. Process variables must be selected carefully in order to avoid excessive temperature rise. The use of grinding fluids is an effective means of controlling temperature.

Thus less voltage utilised in W6 is corresponding to less heat produced in W6. Therefore it can be resulted that thermal stresses in W6 has been reduced which in return helps to strengthen W6 structure.

6.3 Grinding wheel optimisation

Grinding process can be optimized by minimizing total production cost, consistent with acceptable workpiece quality. The degree of optimization achievable is often limited by real-world constraints, like Available equipment machine power, wheel wear, workpiece constraints, tolerances, surface finish, thermal damage, mechanical properties The overall grinding process should be examined before attempting to adjust individual process elements like define a workpiece requirements and analyzing grinding process in terms of overall cost and required production rates. Grinding is a complex material removal operation involving many difficult-to-control parameters. The topography of the wheel is determined by wheel structure and dressing conditions. Having defined the grinding process in general terms, the process the process can be optimized (McSpadden 2001).

There are two different approaches available for process optimization.

a) The analytical approach, based on theoretical equations and some empirical information. Attempts to define and model the grinding process in terms of material removal. Treats each active abrasive grain as a miniature cutting tool; which removes material by sliding, plowing, and eventually forming a chip. The most important process elements are abrasive grit size and distribution (number of cutting points per unit area) workpiece speed, wheel speed, and depth of cut.)

b) The experimental approach, which draws on the body of analytical and empirical information available, but also relies on instrumented grinding tests.

Well designed experiment can substantially reduce the number of experiments. Response Surface Methodology can be most efficient if proper attention is given to the choice of experimental design. There is a strong need for standardized test methodologies that can be conducted in a production environment at reasonable costs and without sophisticated instrumentation. There is a need for better analytical models whose results closely match real-world grinding processes. Accurate measurement of wheel performance and wheel wear is a key enabling technology that needs further work and standardization.

During high efficiency grinding process, it is always expected to obtain a relatively large removal rate and to consume least energy simultaneously. Material removal rate of all workpieces materials, it's different for aluminium according to its properties, because aluminium is the softest material in three workpieces (mild steel, brass, aluminium). In this study when the crossed groove wheel is used to grind aluminium bar the material removal rate is increased by 27% and the voltage is reduced by 5% in comparison with the commercial wheel. This improvement in grinding is due to the crossed grooves surface profile and the grain size of grits used in production of the wheel. The wheel with cross grooves is more suitable for grinding soft metals such as aluminium. However commercial wheel seems to be more suitable for grinding harder materials such as steel and brass. Thus the minimum specific energy is chosen as the optimization object, which denotes the total energy consumed in removing unit volume material in unit time.

When keeping the wheel speed and cut depth constant while increasing the feed speed, the grinding heat flowing on unit area of workpiece surface into contact zone will increase. When the heat exceeds certain limits, the workpiece surface temperature will rapidly rise and may result in burning the workpiece. Thus the limitation of heat to the design variables must be considered during optimisation, which indicates that the minimum specific grinding energy (which is a ratio of material removal rate by the average power consumed by grinder) must be optimized without burning the workpiece (Fu 2002).

6.4 Comparison between numerical and experimental results

During the cutting, a substantial thermal energy is produced which enhances the temperature field in the cutting zone, thereby affecting the energy transfer and chip formation processes.

Grinding is a highly dynamic event, involving high velocity impact, indentation or cutting, ploughing and churning of abrasive particles on the workpiece surface. The inertial effects maybe important as they can influence the dynamic strength and toughness of the work. During the cutting, a substantial thermal energy is produced which enhances the temperature field in the cutting zone, thereby affecting the energy transfer and chip formation processes. As the coolant is applied to reduce the temperature of the grinding surface, chemical reactions between the fluid and the solid workpiece are promoted in the elevated temperature environment. This may alter the surface property of the work, which, in turn, changes the behaviour of the work. Those issues are important but are not addressed in the present work. They certainly do deserve our attention for future research.

During the process of grinding, local forces are imposed on the work surface, which, in turn, generates a stress field within the work piece underneath the grinding zone. When the resulting stresses exceed a threshold value (e.g. the fracture strength of the work piece material), micro fracture could take place, and a surface or subsurface damage zone will likely be formed. Finite element method is used to quantify the associated stress generated in the work piece. The finite element method is a versatile and powerful tool for obtaining approximate solutions to mechanics problems associated with non-uniform stress distributions in geometrically complex shapes, where analytical techniques are either too difficult or often impossible to obtain. All stress components, including von-Misses stress, shear stress, principal stress (shear stress is zero) were obtained as a result of the simulation for different types of grinding wheels and material.

Of particular importance are the maximum shear, principal and von-Misses stress. The maximum shear strain energy per unit volume, or von-Mises, theory is applied to elastic materials that allow some form of plastic deformation before fracture occurs. The maximum von-Misses stress ranged from 25 MPa to 173 MPa, shear stress ranged from 14MPa to 100MPa, principal stress ranged from 17MPa to 102MPa for different type of grinding wheels and material. It can be seen that maximum value of von-Misses stress is much higher that other stresses.

Using FEA profile, the maximum von-Mises stress value of brass bar grinded by commercial wheel was found to be 25.8 MPa (Table 6.17). Using grooved wheel the maximum value of von-Mises stress was found to be 173.2 MPa which is an increase of 6.7 times. The von-Mises stress of crossed groves wheel was about 55.99 MPa which showed a reduction of 68% in von Mises stress.

Grinding mild steel bar by commercial wheel, maximum principal stress was 17.87 MPa, but using grooved wheel increase was 4.3 times, 77.76 MPa. Grinding with cross grooved the principal stress was 37.19 which is a reduction of 52% in maximum principal stress as compared with grooved wheel.

The maximum value of shear stress (stress parallel to the surface of the material) was obtained during grinding brass bar with grooved wheel 99.99 MPa , Table 6.17, while minimum value of shear stress was obtained during grinding aluminium bar with commercial wheel. Symmetrical surface shape in crossed grooves wheel has formed a uniformity which in return has lowered the stress concentration in compare with grooved wheel.

Hence the strength of produced grinding wheel calculated as 207 MPa which is extensively higher than the maximum von-Mises stress value obtained from FEA profile, resulting 19.5% higher strength in crossed groves wheel.

During the experiment the grinding wheel was connected to oscilloscope to record voltage consumed to wear bars. The experiments have been performed using commercial wheel, wheels with grain sizes 0.1, 0.2, 0.4, glass fibre, grooves and cross groves wheels. The amount of removed material of ground bars was recorded against the consumed voltage during the experiment, table 6.8.

Because of different material hardness rate of material of removal was different and maximum consumed voltage was different. For aluminium, was 1.77 v, mild steel 2.29 v, brass 1.95v when commercial wheel was used. Grinding aluminium bar with grinding wheel grain size 0.1 the least amount of voltage have been used 1.1v, but the most amount of material removed was with brass bar.

Table 6.16 shows that commercial grinding wheel was the best wheel to grind brass and mild still while wheel with crossed groves is best for aluminium bar. Figure 6.18 shows total materials volume removed from different bars with utilised voltages. The symmetrical surface shape of crossed grooved grinding wheel may be the reason for lowering the stress concentration, consequently leading to a reduction in shear stress.

With regards to aluminium bar grinding, cross grooved wheel proved considerable improvement comparative to commercial and grooved wheel. The volume of materials removed by cross grooved wheel showed an increase of 27% and 12% as compared with commercial and grooved wheel respectively. When commercial and grooved wheel were replaced by cross grooved wheel the recorded voltage decrease by about 5% and 2% respectively.

It is evident that the wheel with crossed groves is the best wheel amongst the ones which have been used in this study for grinding soft materials like aluminium. It may be due to crossed grooves surface shape (e.g. less clogging, less need for dressing wheel) and grain size of grit used in crossed grooves production and hardness of aluminium bar.

The usefulness of the numerical simulation used in this study is that it can perform systematic virtual experiments on the computer for examining the effects of a specific grinding parameters (eg. grinding force, spindle speed, work speed, groove on grinding wheel, particle size, tensile strength of the work piece material) on the final status of the finished part. In this way, the empirical method of performing actual measurements in a laboratory, commonly adopted in the machining community, which is usually a time-consuming and labour intensive effort, can be reduced dramatically to a bare minimum.

Chapter 7

Conclusions and Recommendations for Further Work

7.1 Conclusions

The shape, size and orientation of the abrasive particle of the grinding wheel affect the performance of the grinding wheel during the grinding operations. The abrasive grains distribution of the grinding wheel used were all randomly distributed with irregular shapes. The higher the grit size the less porosity of the wheel and the better the surface finish produce on the workpieces due to more abrasive grains participating in cutting operation of higher grit size although not all the abrasive grains actually participated in the cutting operation. The wheel surface of crossed grooves shape showed a significant improvement in grinding of soft materials e.g. aluminium. The surface shapes and grits materials needs to be investigated for grinding material with higher hardness.

Close examination of the wheel surface under the microscope showed wheel porosity, wear flat on the grain and metal chips from the workpiece adhering to the grain. Both attritions grain wear and microchipping wear of the abrasive grains were noted on the grinding wheel surfaces (dry cutting). In attritions wear, the cutting edges of an originally sharp grain become dull by attrition, developing a wear flat. Wear was caused by the interaction of the grain with the workpiece material, involving both physical and chemical reactions. These reactions are complex and involve diffusion, chemical degradation or decomposition of the grain, fracture at a microscopic scale, plastic deformation, and melting.

Additional wear due to dislodgment of whole abrasive grains from the wheels were also noticed as a result of (a) thermal softening of the resin binder (b) mechanical erosion of the resin binder by the flowing chip and (c) mechanical removal of bond material due to the pressure developed in the voids by the chips due to insufficient volume.

Air cool grinding is generally used for the cut-off as water tends to deteriorate the resin and reduce the life of the cut-off wheel. Cut off grinding operation does not require periodic wheel dressing which is necessary for surface finish grinding operations.

Through these findings the followings can also be deduced:

- Higher grit sizes will produce better surface finish with more dimensional accuracy.
- Less wear and less chips clogging occurred on the wheel after each grinding operation by using coolant.
- The use of coolant result in less dressing condition requirement by the wheel and thus prolonging the wheel life, relatively little or no dressing is required at low depth of cut. The use of coolant was a very effective means of controlling temperature of both the workpiece and that of the wheel during grinding operation.
- From geometrical point of view, the distributions of the cutting grains have a considerably size and dense structure, the spacing will be close and this will result in a smoother surface. The surface finish can be improved by reducing the work speed and increasing the wheel speed. Good surface finish of the workpieces also depends on the rigidity of the machine, well designed spindle bearing and an accurately balanced grinding wheel.

The effective coolant filtration is also necessary to prevent the circulation of abrasive fragments picked up by the wheel which can be severely scratch the surface of the workpiece. Dressing of the grinding wheel also affects the roughness of workpieces. A blunt diamond should be used if a fine surface is required on the workpieces.

Ideally the development of grinding wheels with regular shapes with orderly or evenly abrasive grains distribution for grinding operation will clearly result in better performances of the grinding wheel during the operation due to the fact that the cutting operation of abrasive grains and other process associated with grinding operations e.g. wheel balancing, dressing, cutting forces, coolant filtration etc. will be efficient and the cutting actions will also be more predictable.

- Redesigning grinding wheels by making grooves on surface of wheel, material removal rate was increased and less voltage has been used. Also, time for redressing wheels has been reduced.

With regards to aluminium bar grinding, W6 proved considerable improvement comparative to C and W5. The materials volume removed by W6 showed an increase of 27% and 12% in compare with C and W5 respectively. Hence when C and W5 were replaced by W6 the recorded voltage decrease by about 5% and 2% respectively.

- It is evident that W6 is an optimised wheel to grind soft materials like aluminium. It may be due to crossed grooves surface shape and grain size of grit used in W6 production and hardness of bars.

- Using FEA profile, the maximum von-Mises stress value of brass bar found to be 173.2 MPa. Hence the strength of produced grinding wheel calculated as 207 MPa which is extensively higher than the maximum von-Mises stress value obtained from FEA profile, resulting 19.5% higher strength in W6.

Grinding operation is used as the final step for finishing a product because of their ability of miniature cutting and because of the satisfaction of strict requirements on the surface roughness. Although water tends to deteriorate the resin and reduce the life of the cut-off wheel, coolants are invariably used in finish grinding to dissipate the heat generated and to protect the workpieces from grinding burn. Effective coolant filtration is necessary for efficient coolant performance.

The investigations indicated that the parameters feed rate, depth of cut, grit size types and applications of coolant are the primary influencing factors which affect the surface integrity of the grinding wheel during the grinding operation.

The photographs obtained from the microscope clearly shows reduction in wheel loading with less metal chips adhering to the wheel grains as the coolant filtration had reduced the adhesion of the metal chips. Grinding of mild steel using the wheel of grit size 60 at 20µm depth of cut had more metal chips adhere to its grain it still resulted in giving the best surface finish from the results obtained during the course of performing the experiment due to the fact more grain actually participated in the cutting operation.

The temperature during the grinding operation was effectively controlled by coolant application and less wear flats were noticed on the wheels. Generally the grinding wheel required less dressing operation and thereby prolonging the wheel life although a more evenly distributed grain structure will facilitate a better performance by allowing better coolant filtration.

Grinding power, time constant surface roughness and roundness converge with grinding time despite differences in the dressing conditions employed. This implies that dressing has most effect on the initial grinding stage, while the grinding conditions affect the whole wheel life cycle. Selection of dressing conditions and grinding conditions may be separated. The dressing conditions may be selected to adjust the initial grinding behaviour after dressing and the grinding conditions selected to adjust the grinding behaviour in other stage stages of a wheel redress life cycle. This conclusion is considered to be important for the design of a dressing strategy.

When dressing with very coarse conditions or with a very blunt dressing diamond, more bond fracture is generated on the wheel surface. The result is that wheel wear is increased and workpiece size errors are increased in a positive sense. After dressing with very fine conditions, the wheel wear may mainly be attributed to attritions and microfracture. The wheel wear volume was small. Force and deflection reduction and thermal expansion cause the workpiece size errors to increase in a negative sense. It is concluded that a good dressing operation makes grinding behaviour more stable and gives better grinding quality.

One of the most interesting aspects of the grinding process is that the grinding behaviour can be very different even for the same value of control parameters, such as $v_s, v_w, v_f, a_d f_d$.This is attributed to uncontrollable parameters involved in the grinding operation. The dressing width of the diamond is an uncontrollable parameter and has a strong effect on grinding behaviour. Due to insufficient control of the shape of the dressing diamond, it is necessary to develop a strategy for the selection of dressing parameters, so that effect of the effect of the dressing diamond can be compensated.

7.2 Recommendations for Further Work

The following areas need further investigation:

The wheel surface of crossed grooves shape showed a significant improvement in grinding of soft materials e.g. aluminium. The surface shapes and grits materials needs to be investigated for grinding material with higher hardness.

All the dressing strategies developed in this research are concerned with situations where the grinding conditions remain the same between two dressing operations. If changes of the grinding conditions are required within a wheel redress life cycle, a new method is required to identify the effects of dressing and grinding conditions on grinding behaviour separately, so that the recommended dressing operation can match the wheel self-sharpening action and maintain the grinding wheel behaviour stable.

The methodology for simulating the dressing and grinding needs to be further modified. The grains of the wheel in the simulation were assumed to be a constant diameter. For further research the diameters of the grains should conform to the real distribution of the diameters of the grains.

Therefore the measurement of the diamond shape and simulation with real diamond shape should improve the results. For simulation of the grinding process, the wear process of the grins needs to be further studied. The model for the effect of grinding conditions on the grinding force of a single grain needs to be investigated further.

References

Accurate Corporation, (2011), Silicon Carbide, SiC Material Properties, http://accuratus.com/silicar.htm, Date Cited 2011.

Allanson, D.R., Chen, X., Rowe, W.B. & Mills, B. (1998), Analysis And Simulation Of The Grinding Process. Part IV: Effects Of Wheel Wear, International Journal Of Machine Tools And Manufacture, Vol. 38, Issues 1-2, Pp 41-49.

Alden, & Geo, I. (1914), Operation Of Grinding Wheels In Machine Grinding, ASME Trans., Vol. 36, Pp 451-460.

Armarego & Brown (1964), Oblique Machining with a Single Cutting Edge, Int Journal of Machine Tool Design and Research, Vol. 4, Issue 1,Pages 9-25.

Backer, W. R., Marshall, E.R & Shaw, M.C. (1952), The Size Effect In Metal Cutting, Trans. ASME, Vol. 74, Pp 61-72.

Buttery, T.C. (1973), Grinding Force Predictions Based On Wear Theory, Proceedings Of 13th Int. MTDR Conference, The Macmillian Press, Pp 283-289.

Brecker, J.N. (1974), The Fracture Strength Of Abrasive Grains, Trans. Of The ASME, Journal Of Engineering For Industry, Vol. 96, Issue 4, Pp 1253-1257.

Brinksmeier, E., Heinzel, C. & Wittmann, M. (1999), Friction, Cooling and Lubrication in Grinding, Annals of the CIRP. 48 (2), Pp 1-18.

Cai, R. & Rowe, W.B. (2004), Assessment Of Vitrified CBN Wheels For Precision Grinding, International Journal Of Machine Tools And Manufacture, Vol. 44, Issues 12-13, Pp 1391-1402.

Capello, E. & Semeraro, Q. (2002), Process Parameters and Residual Stresses in Cylindrical Grinding, Journal of Manufacturing Science and Engineering, Vol. 124, Pp 615-623.

Carmona Diaz, E. (2002), Influence of grinding fluids on high efficiency deep grinding of 51CrV4 high alloy steels, MSc Thesis, School of Industrial & Manufacturing Science, Cranfield University. =====

Chen, X. (1996), A Grinding Power Model For Selection Of Dressing And Grinding Conditions Journal Of Manufacturing Science And Engineering, Pp 632-637.

Chen, X & Rowe, W.B. (1996), Analysis And Simulation Of The Grinding Process. Part I: Generation Of The Grinding Wheel Surface, International Journal Of Machine Tools & Manufacture, Volume 36, Issue 8, Pp 871-882. ====

Chen, D.X & Feng, Q. (2009), A Methodology For The Simulation Of Surface-Contact Grinding Tool Topography, Advances In Grinding And Abrasive Technology XV, Key Engineering Materials Journal, Vol. 416, Pp 348-353.

Chen, G., Mei, L., Zhang, B., Yu, C., & Shun, K., (2010), Experiment And Numerical Simulation Study On Laser Truing And Dressing Of Bronze-Bonded Diamond Wheel, Optics And Lasers In Engineering, Vol 48, Issue 3, Pp. 295-304.

Discos De Diamante, (2010), Diamond And CBN Tools, Http://Issuu.Com/Comercial-Toso/Docs/Discos_De_Diamante, Date Cited 2011.

Draper, A.B., Modern Manufacturing Process Engineering, Pp 476-479, ISBN 0-07-046563-0.

Ebbrell, S., Woolley, N.H., Tridimas, Y.D., Allanson, D.R. & Rowe, W.B. (2000), The Effects of Cutting Fluid Application Methods on the Grinding Process, International Journal of Machine Tools & Manufacture, Vol. 40, Pp 209-223.

Efunda, (2011), Failure Criteria: Ductile Materials, http://www.efunda.com/formulae/ solid mechanics /failure_criteria/failure_criteria_ductile.cfm, Date Cited 2011.

Fu, H.J.Xu, (2002) Optimization design of grinding wheel topography for high efficiency grinding,,Journal of Material Processing Technology (129)118-122

Hahn, R. S. (1978), On The Loss Of Surface Integrity And Surface Form Due To Thermoplastic Stress In Plunge Grinding Operations, The Annals Of The CIRP, Vol. 25 1, Pp 203-207.

Hahn, R.S. (1964), Controlled-Force Grinding –A New Technique For Precision Internal Grinding, Trans. ASME, Journal Of Engineering For Industry, Vol. 86, Pp 287-293.

Hwang, J., Kompella, S., Chandrasekar, S. & Farris, T.N. (2003), Measurement of Temperature Field in Surface Grinding Using Infra-Red (IR) Imaging System, Journal of Tribology, Vol. 125, Pp 377-383.

Jackson, M.J., Davis, C.J., Hitchiner, M.P. & Mills, B. (2001). High-Speed Grinding With CBN Grinding Wheels - Applications And Future Technology, Journal Of Materials Processing Technology, Vol. 110, Pp 78-88. =======

Kato, T. & Fujii, H. (1997), Temperature Measurement of Workpiece in Surface Grinding by PVD Film Method, Journal of Manufacturing Science and Engineering, Vol. 119, Pp 689-694. ====

King, R.I. & Hahn,R.S. (1986), Handbook Of Modern Grinding Technology, Champman And Hall.

Kannappan, S. & Malkin, S. (1972), Effects Of Grain Size And Operating Parameters On The Mechanics Of Grinding, Journal Of Engineering For Industry, Pp 833-842.

Komanduri, R. & Hou, Z.B. (2001), A review of the experimental techniques for the measurement of heat and temperatures generated in some manufacturing processes and tribology, Tribology International, Vol. 34, Pp 653-682.======

Koziarski, A. & Golabczak, A. (1985), The Assessment Of The Grinding Wheel Cutting Surface Condition After Dressing With The Single Point Diamond Dresses, International Journal Of Machine Tools, Vol. 25, Issue 4, Pp 313-325.==

Lindsay, R. (1986), Principles Of Grinding, Handbook Of Modern Grinding Technology, Composed By R.I. King And R.S. Hahn, Chapman And Hall, Pp 30-71.====

Loladze, T.N. & Bokuchava, G.V. (1985), Terminological Aspects Of The Grinding Process, ASME, PED, Vol. 16, Pp 401-407.=====

Lortz, W. (1979), A Model Of The Cutting Mechanism In Grinding, Wear, Vol. 53, Pp 115-128.

McSpadden S (2001),Optimizing the Grinding Process for Ceramic Materials, Orak Ridge National Laboratory,Precision Grinding & Finishing in the Global Economy

Malkin S. & Cook N.H. (1971), The Wear Of Grinding Wheels, Part2-Fracture Wear, Journal Of Engineering For Industry, Trans. ASME , Vol. 93, Pp 1129-1133.

Malkin, S. & Anderson, R.B. (1972), Active Grains And Dressing Particles In Grinding, Proceedings Of The International Grinding Conference, Pittsburgh, Pennsylvania, Pp 161-181.

Malkin, S. & Murray, T. (1977), Comparison Of Single Point And Rotary Dressing Of Grinding Wheels, Proceedings Fifth North American Metal Working Research Conference, Pp 278-283.

Malkin, S. (1989), Grinding Technology –Theory And Applications Of Machining With Abrasives, Ellis Horwood Limited.

Malkin, S. & Guo, C. (2008), Grinding Technology: Theory And Applications Of Machining With Abrasives, ISBN 978-0-8311-3247-7, 2nd Edition, Industrial Press, Inc., New York.

Merchant, M.E. (1971), Delphi-Type Forecast Of The Future Of Production Engineering. Annals Of The CIRP, Vol. 19-20, Pp 213-225.

Malkin S., Wiggins, K.L., Osman, M. & Smalling , R, W. (1973), Size Effects In Abrasive Processes, Proceedings Of 13th Int. MTDR Conference, The Macmillian Press, Pp 291-296.

Mark J.Jackson (2011) Machining with abrasives ISBN 978-1-4419-7301-6,Springer New York Dordrecht Heidelberg London

Mindek, R.B. & Howes, T.D. (1996), Slot and Vertical Face Grinding of Aerospace Components. Transactions of the ASME: Journal of Engineering for Gas Turbines and Power, Vol. 118, Pp 620-625.

Müller, B. & Renz, U. (2003), Time resolved temperature measurements in manufacturing, Measurement, Vol. 34, Pp 363-370.

Nakayama, K. & Tamura., K. (1968), Size Effect In Metal-Cutting Force, Trans. Of The ASME, Journal Of Engineering For Industry, Vol. 90, Pp 119-126.

Nakayama, T., Wakuda, M. & Ota, M. (2004), Ultra-High Speed Cylindrical Grinding Using CBN Wheel for High Efficiency, Key Engineering Materials, Vol. 257-258, Pp 273-278.

Nakayama, K. & Brecker, J.N. (1971), Grinding Wheel Elasticity, Trans. ASME, Journal Of Engineering For Industry, Pp 609-614.

Neduet (2011), Determination Of Grain Of A Metal Specimen, Nedians University Of Engineering & Technology, Karachi, Http://Www.Nedians.8m.Com/Metalprac.Htm, Date Cited 2011.

Ono, K. (1961), Analysis On The Grinding Force, Bulletin Of The Japan Society Of Grinding Engineers, Vol. 1, Pp 19-22.

Pande, S. J. & Lal, G.K. (1979), Effect Of Dressing On Grinding Wheel Performance, Int. Jnl. MTDR, Vol. 19, Pp171-179.

Pattinson, E.J. & Chisholm, A.W.J. (1967), The Effect Of Dressing Techniques On Grinding Wheel Wear, Proc.Int.Conf. On Manufacturing Technology, A.S.T.M.E., Univ. Of Michigan, Pp 601-616.

Pattinson, E.J. & Lyon, J. (1975), The Collection Of Data For The Assesment Of A Grinding Wheel Dressing Process''Proceedings Of 15th Int. MTDR Conference, The Macmillian Press, Pp 317-323.

Reliance Diamond Tools, (2011), Technical Information On Diamond Dressers In The Machining Industry, Http://Www.Reliancedia.Com/Technical-Information-Machining-Industry.Html, Date Cited 201.

Rowe, W.B., Chen, X. & Morgan, M.N. (1993), The Identification Of Dressing Strategies For Optimal Grinding Wheel Performance, Proceeding Of The 30th Int. MATADOR Conference, Pp 195-202.

Rowe, W.B. (2001), Thermal Analysis Of High Efficiency Deep Grinding. International Journal Of Machine Tools & Manufacturing, Vol. 41, Pp 1-19.

Shaw, M.C. (1996). Principles Of Abrasive Processing. Oxford: Clarendon Press.=====

Saini, D.P., Wager, J.G. & Brown, R.H. (1982), Practical Significance Of Contact Deflections In Grinding, Annals Of The CIRP, Vol. 31, Issue 1, Pp 215-219.

Sainz, P.A. (2005), Investigation of High Efficiency Deep Form Grinding on 51CrV4 steel alloy. MSc Thesis, School of Industrial & Manufacturing Science, Cranfield University. ======

Saint-Gobain (2009), The Art of Silicon Carbide, Saint-Gobain Ceramic Materials GmbH, http://www.sic.saint-gobain.com/the-art-of-silicon-carbide.aspx, Date Cited 2011.

Salisbury, E.J., Domala, K.V., Moon, K.S., Miller, M.H. & Sutherland, J.W. (2001), Grinding, Part 2: Grinding Wheel Surface Texture Model, Journal Of Manufacturing Science And Engineering, Vol. 123, Pp 582-590.

Scott, W. & Baul, R.M. (1986), Relationship Between Wheel And Workpiece Surface Topographies In Plunge Grinding, The Third International Conference On Manufacturing Engineering, Pp 44-48.

Shaji, S. & Radhakrishnan, V. (2003), A Study On Calcium Fluoride As A Solid Lubricant In Grinding, International Journal Of Environmentally Conscious Design & Manufacturing, Usa, Vol. 11, No. 1. ===

Sheiko, M.N. (2007), Abrasive Wear Of Individual Grits In Diamond Rollers And Sticks And Its Relation To The Overall Tool Wear In Dressing Operations, Journal Of Superhard Materials Vol 29, No. 6, Pp 369-374. ====

Shi, Z. & Malkin, S. (2006), Wear Of Electroplated CBN Grinding Wheels, ASME Journal Of Manufacturing, Science, Engineering, Issue 1, Vol. 128.

Snoeys, R., Peters, J. & Decneut, A. (1974), The Significance Of Chip Thickness In Grinding, The Annals Of The CIRP, Vol. 23, Issue 2, Pp 227-237.

Snoeys, R., Maris, M. & Peters, J. (1978), Thermally Induced Damage In Grinding. CIRP Annals, Vol. 27, Issue 2, Pp 571–581.====

Stephen, M. & Changsheng, G. (2008), Grinding Technology: Theory And Applications Of Machining With Abrasives, Technology & Engineering, 2nd Edition, Industrial Press Inc., ISBN: 0831132477, 9780831132477.====

Stephenson, D.J. & Jin, T. (2003), Physical Basics in Grinding, European Conference on Grinding, WZL Aachen, November 6^{th}-7^{th}.

Stoutk, J. & Sullivan, P.J. (1989), The Analysis Of The Three Dimensional Topography Of The Grinding Process, The Annals Of The CIRP, Vol. 38., Pp 545-548.

Tawakoli, T. (1993), High Efficiency Deep Grinding. Dusseldorf: VDI-Verlag.

Tsuwa, H. (1972), Micro-Structure Of Dressed Abrasive Cutting Edges, Proceedings Of The International Grinding Conference,Pittsburgh, Pennsylvania, Pp 142-160.

Torrance, A. A. & Badger, J. A., (2000), The Relation Between The Traverse Dressing Of Vitrified Grinding Wheels And Their Performance, International Journal Of Machine Tools And Manufacture, Vol. 40, Issue 12, Pp. 1787-1811.

UGWC (1992), The Grinding Data Book, Universal Grinding Wheel Company Limited.

Verkerk, J. (1997), Final Report Concerning CIRP Cooperative Work On The Characterization Of Grinding Wheel Topography , Annals Of The CIRP, Vol. 26, Issue 2, Pp 385-395.

Von Turkovich, B.F. (1970), Shear Stress In Metal Cutting-Force, Trans. ASME Journal Of Engineering For Industry, Vol. 92, Pp 151-157.

Wan, D.P., Hu, D.J., Wang, H.F. & Zhang, Y.H. (2006), Dynamic Monitoring And Intelligent Dressing Of Diamond Wheel For Precision Curve Grinding, Materials Science Forum, Vol. 532-533, Pp 77-80.

Weck, M., Hennes, N. & Schulz, A. (2001), Dynamic Behaviour of Cylindrical Traverse Grinding Processes, Annals of the CIRP, Vol. 50 (1), Pp 213-216

Werner, G. (1978), Influence Of Work Material On Grinding Force, The Annals Of The CIRP, Vol. 27, Issue 1, Pp 243-248.

Werner, G. (1979). Application And Technical Fundamentals Of Deep And Creep feed Grinding. SME Technical Paper. MR 79-319.

Werner, G. & Tawakoli, T. (1988a), High-Efficiency Deep Grinding with CBN. Industrial Diamond Review, Vol. 3, Pp 124-128.

Werner, G. & Tawakoli, T. (1988b), Deep Grinding Narrow Slots with CBN Wheels. Industrial Diamond Review, Vol. 6, Pp 285-288.

Yamaguchi K., Wei, Y. & Takeuchi M. (1999), Development Of DLC Fibre Grinding Wheel. In: Proceedings Of The Vernal Meeting Of The JSPE, Tokyo, P 260.

Ye & Pearce(1984) Some observations on profile wear in creep-feed grinding, Wear, Volume 92,Issue 1,1 December 1983,Pages 51-56.

Zhao, Q., Chen, J., Yao, J. & Zhou, S. (2009), Investigation Of Surface And Subsurface Damage In Diamond Grinding Of Optical Glass Using Hybrid Copper-Resin-Bonded Diamond Wheel, Journal Of Vacuum Science & Technology B: Microelectronics And Nanometer Structures, Vol. 27, Issue: 3, Pp 1489 – 1495.

Appendix

Finite Element Analysis profile of the different grinding wheels used in this project.

Static Structural
Subject:
Date Sunday, September 26, 2010
Comments:

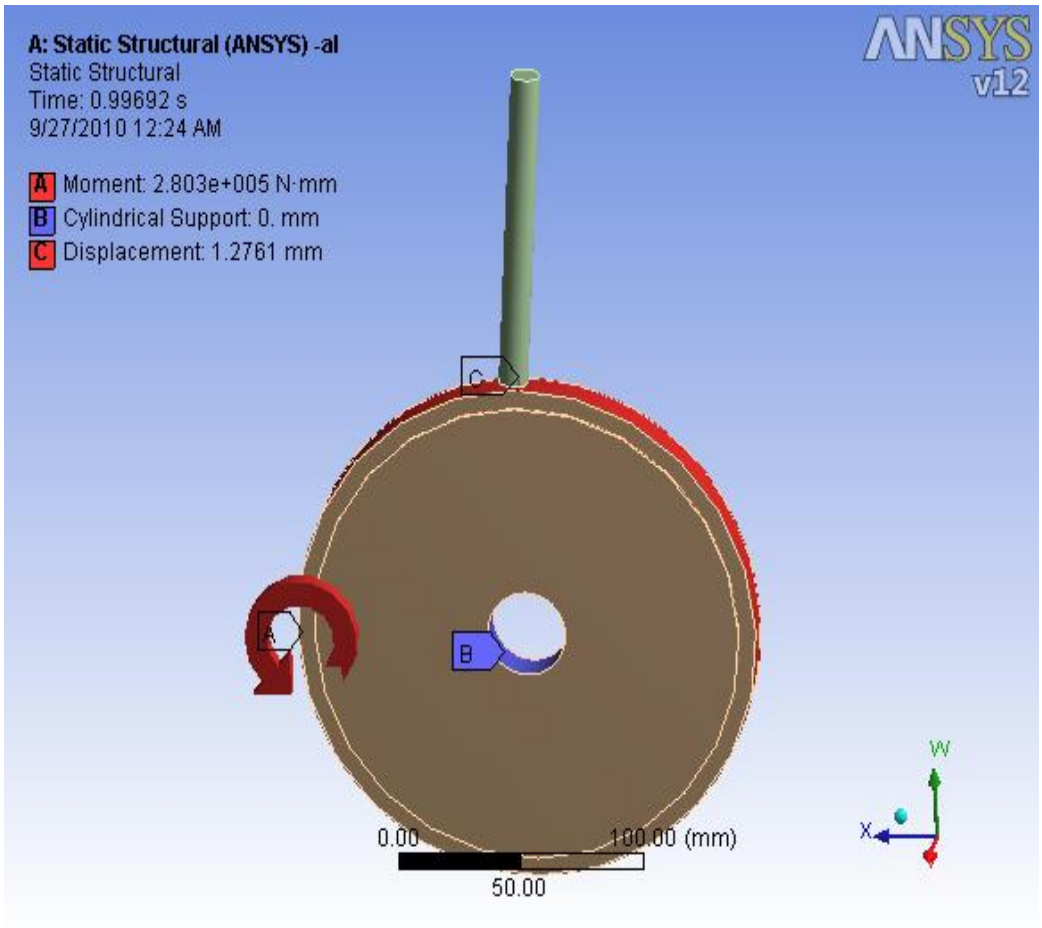

Fig A.1 : Ansys simulation of the grinding wheel highlighting the boundary conditions

Aluminium

Equivalent Stress
Subject:
Date Monday, September 27, 2010
Comments:

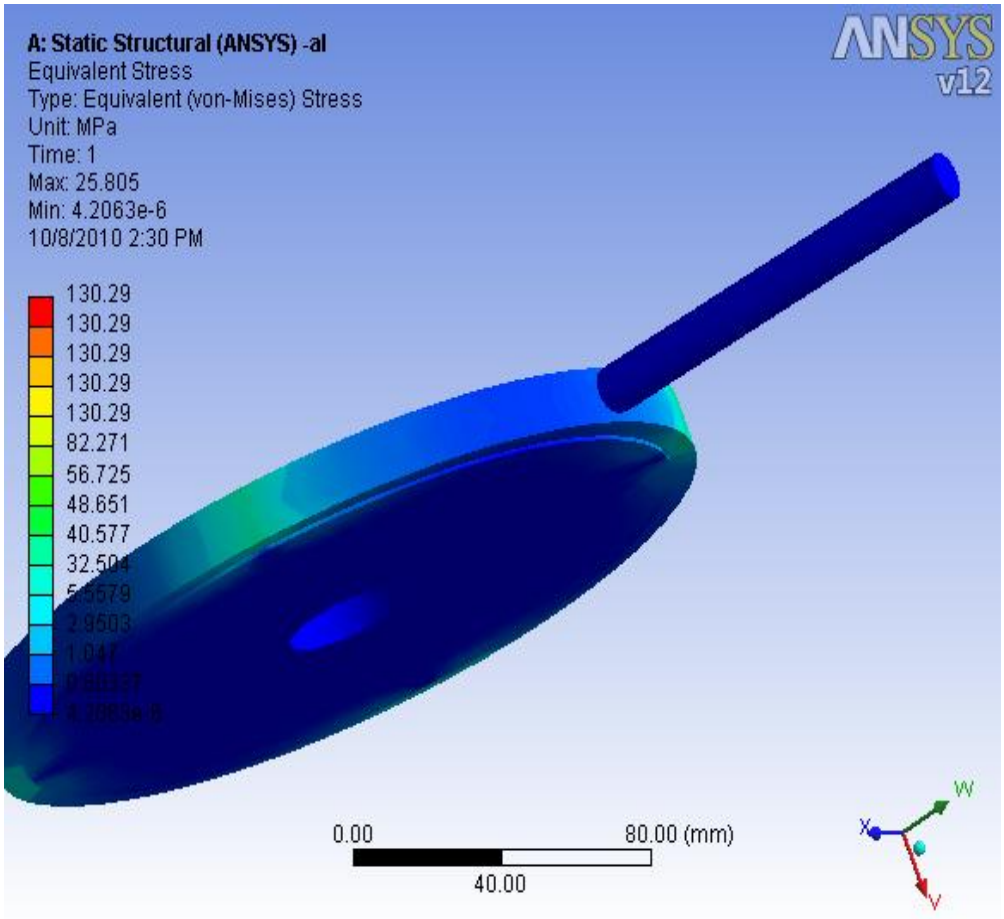

Fig A.2 : FEA profile of aluminium bar with commercial grinding wheel showing von-Mises Stress

Maximum Principal Stress
Subject:
Date Monday, September 27, 2010
Comments:

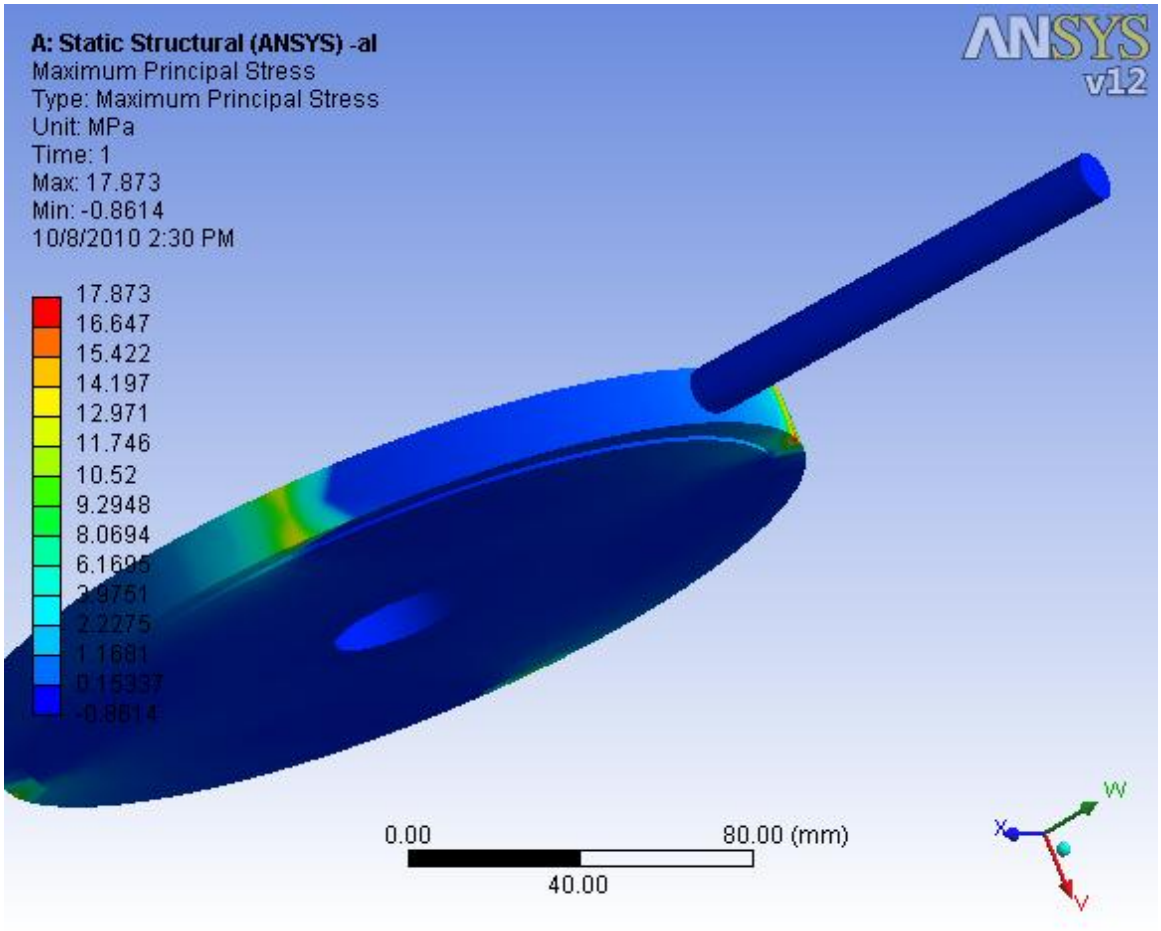

Fig A.3 : FEA profile of aluminium bar with commercial grinding wheel showing Principal Stress

Maximum Shear Stress
Subject:
Date Monday, September 27, 2010
Comments:

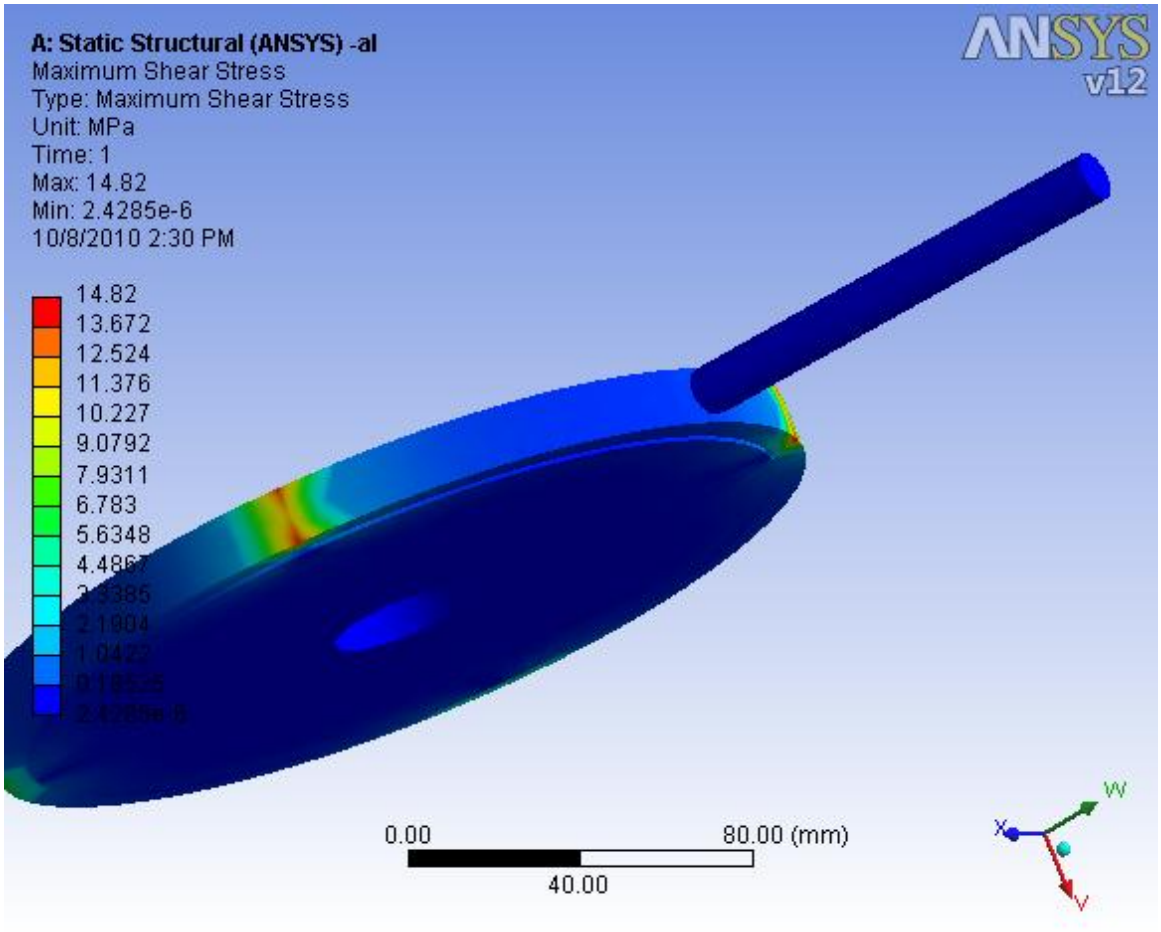

Fig A.4 : FEA profile of aluminium bar with commercial grinding wheel showing Shear Stress

STEEL

Equivalent Stress
Subject:
Date Monday, September 27, 2010
Comments:

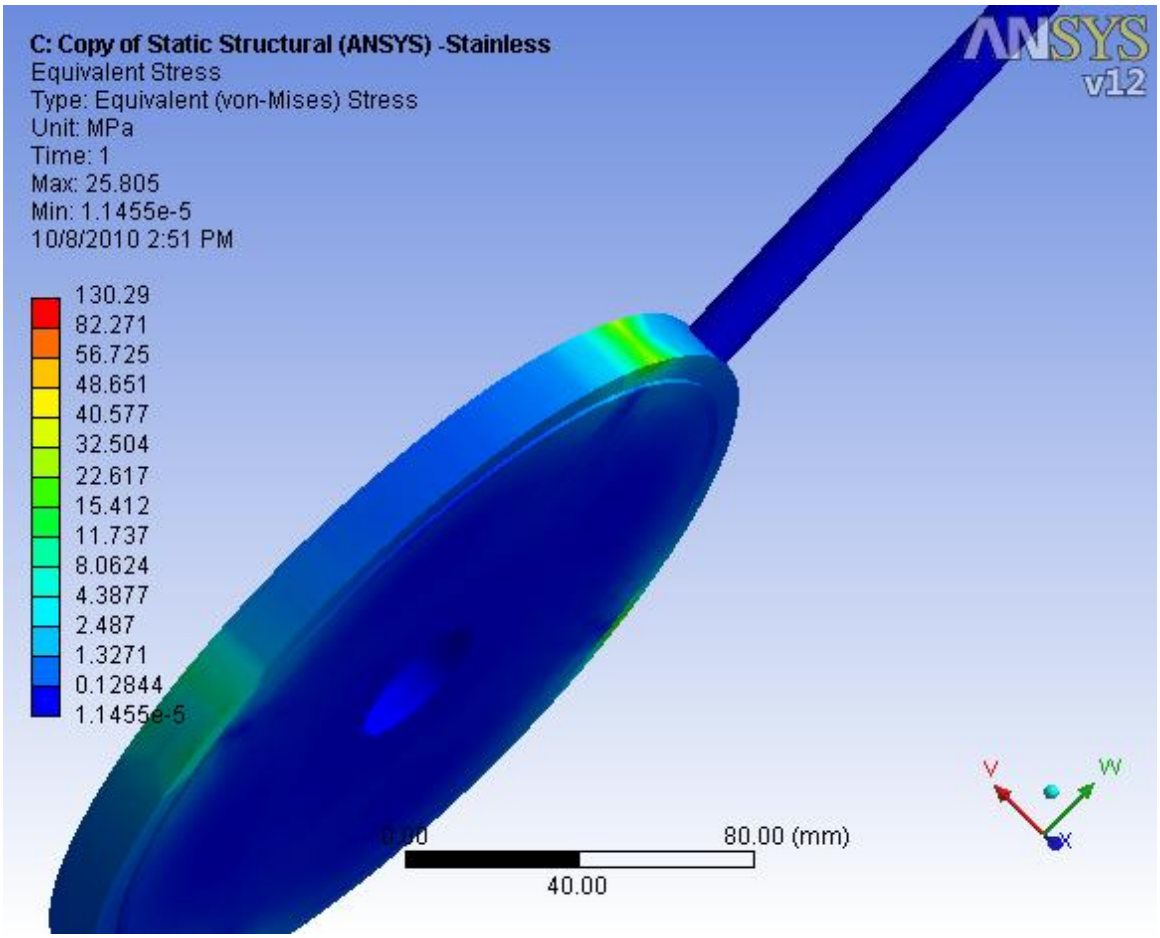

Fig A.5 : FEA profile of steel bar with commercial grinding wheel showing von-Mises Stress

Maximum Principal Stress
Subject:
Date Monday, September 27, 2010
Comments:

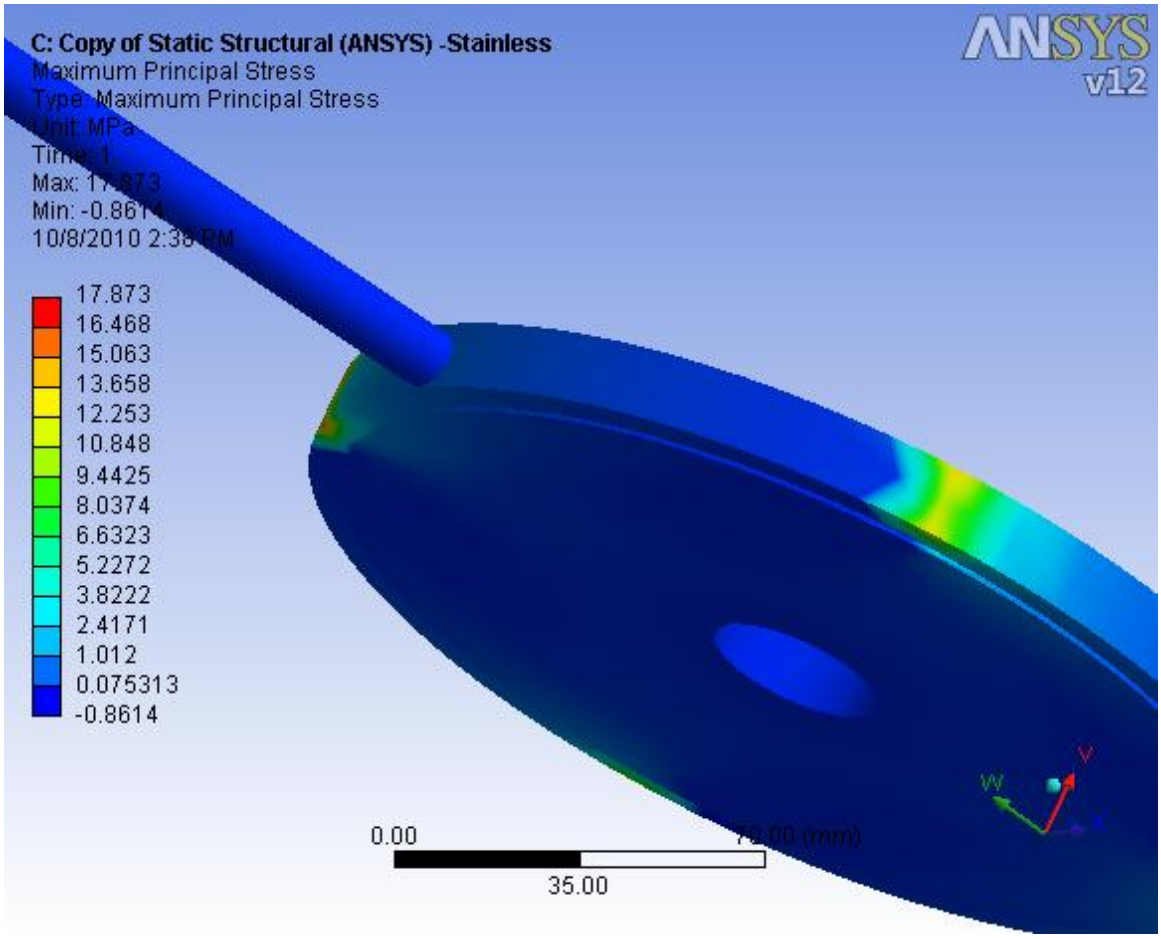

Fig A.6 : FEA profile of steel bar with commercial grinding wheel showing Principal Stress

Maximum Shear Stress
Subject:
Date Monday, September 27, 2010
Comments:

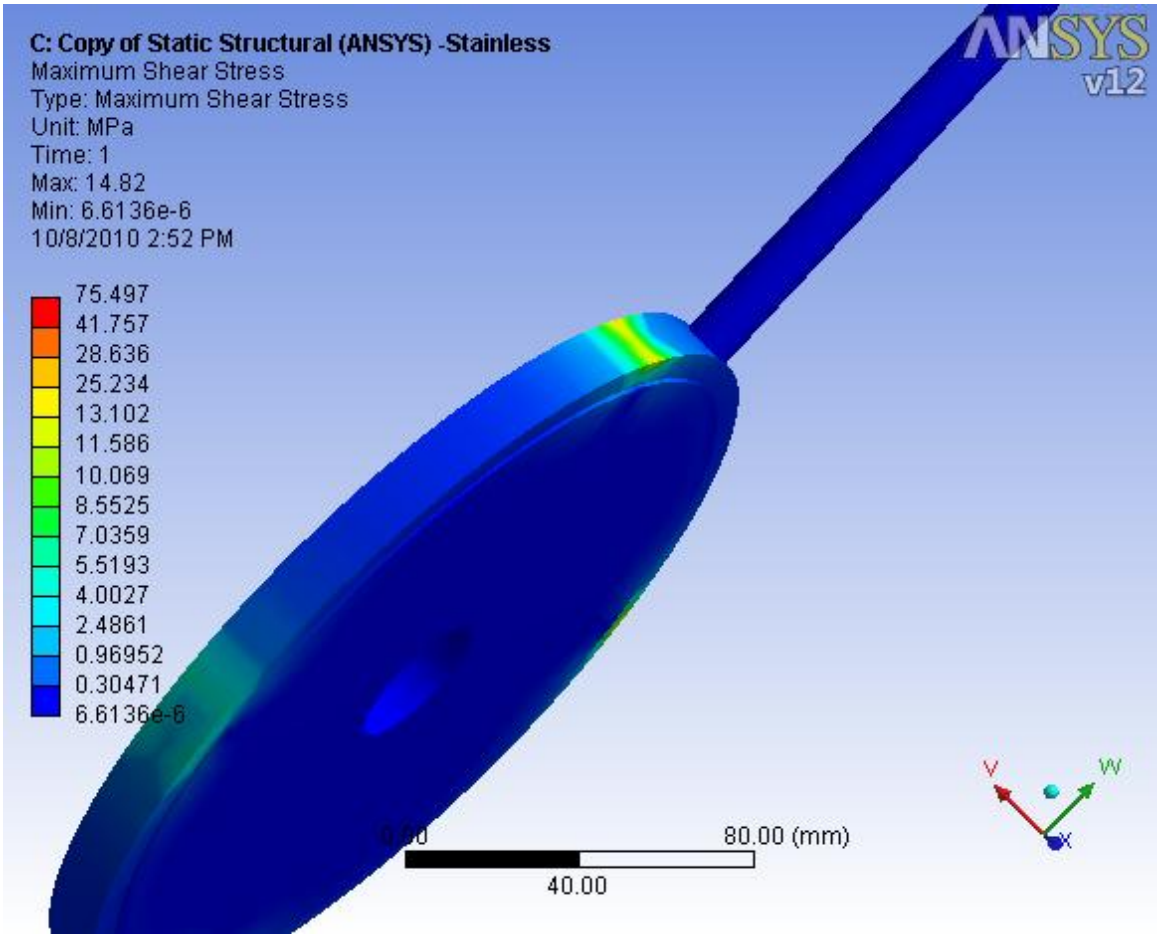

Fig A.7 : FEA profile of steel bar with commercial grinding wheel showing Shear Stress

Brass

Equivalent Stress
Subject:
Date Monday, September 27, 2010
Comments:

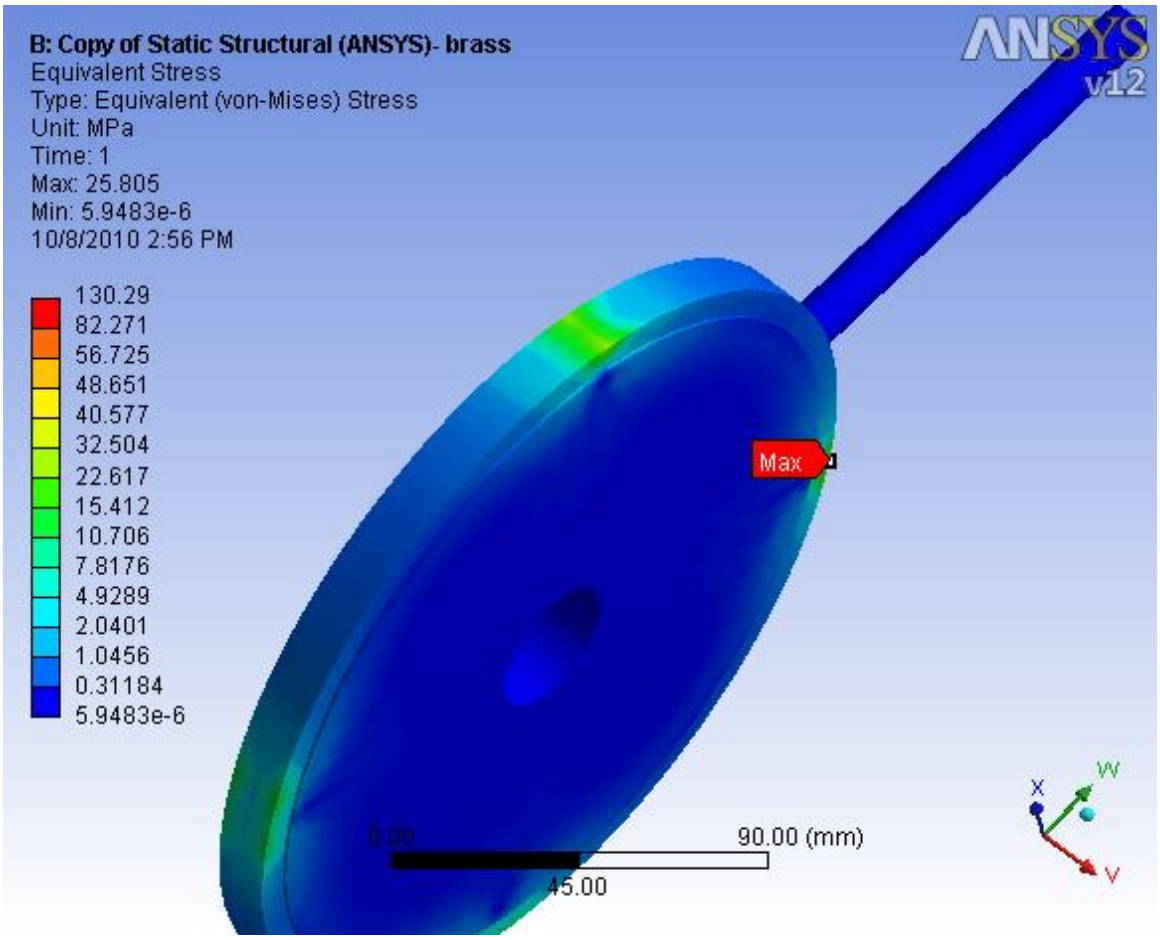

Fig A.8 : FEA profile of brass bar with commercial grinding wheel showing von-Mises Stress

Maximum Principal Stress
Subject:
Date Monday, September 27, 2010
Comments:

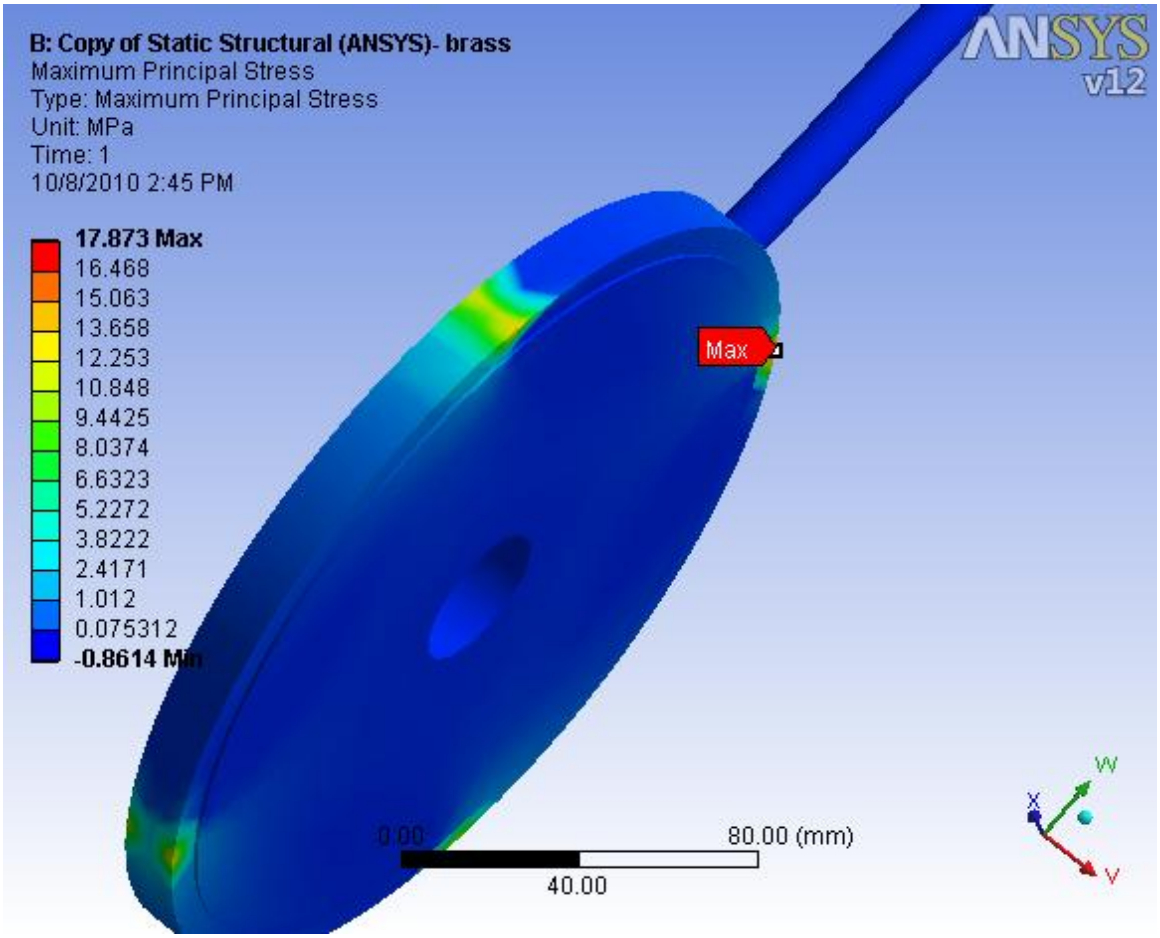

Fig A.9 : FEA profile of brass bar with commercial grinding wheel showing Principal Stress

Maximum Shear Stress
Subject:
Date Monday, September 27, 2010
Comments:

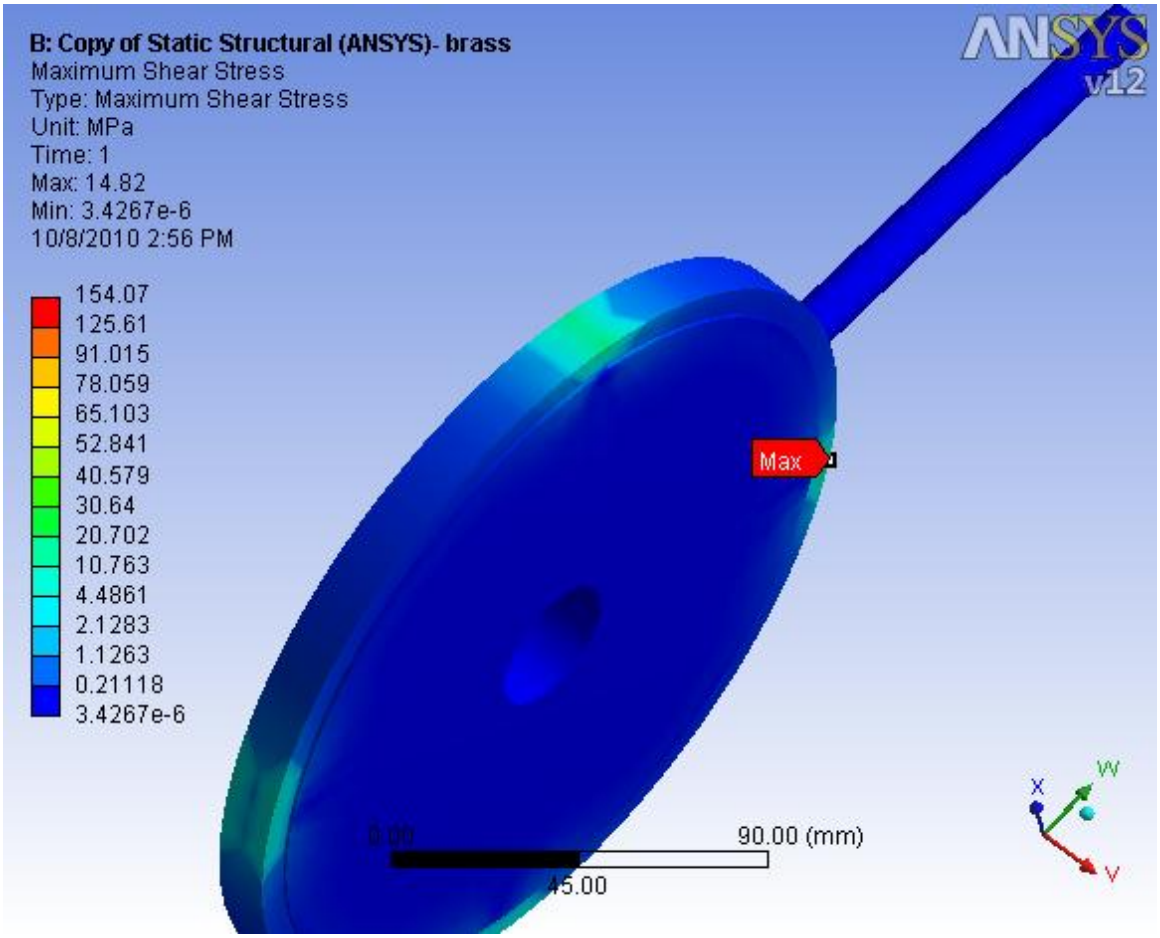

Fig A.10 : FEA profile of brass bar with commercial grinding wheel showing Shear Stress

Equivalent Stress
Subject:
Date Monday, September 27, 2010
Comments:

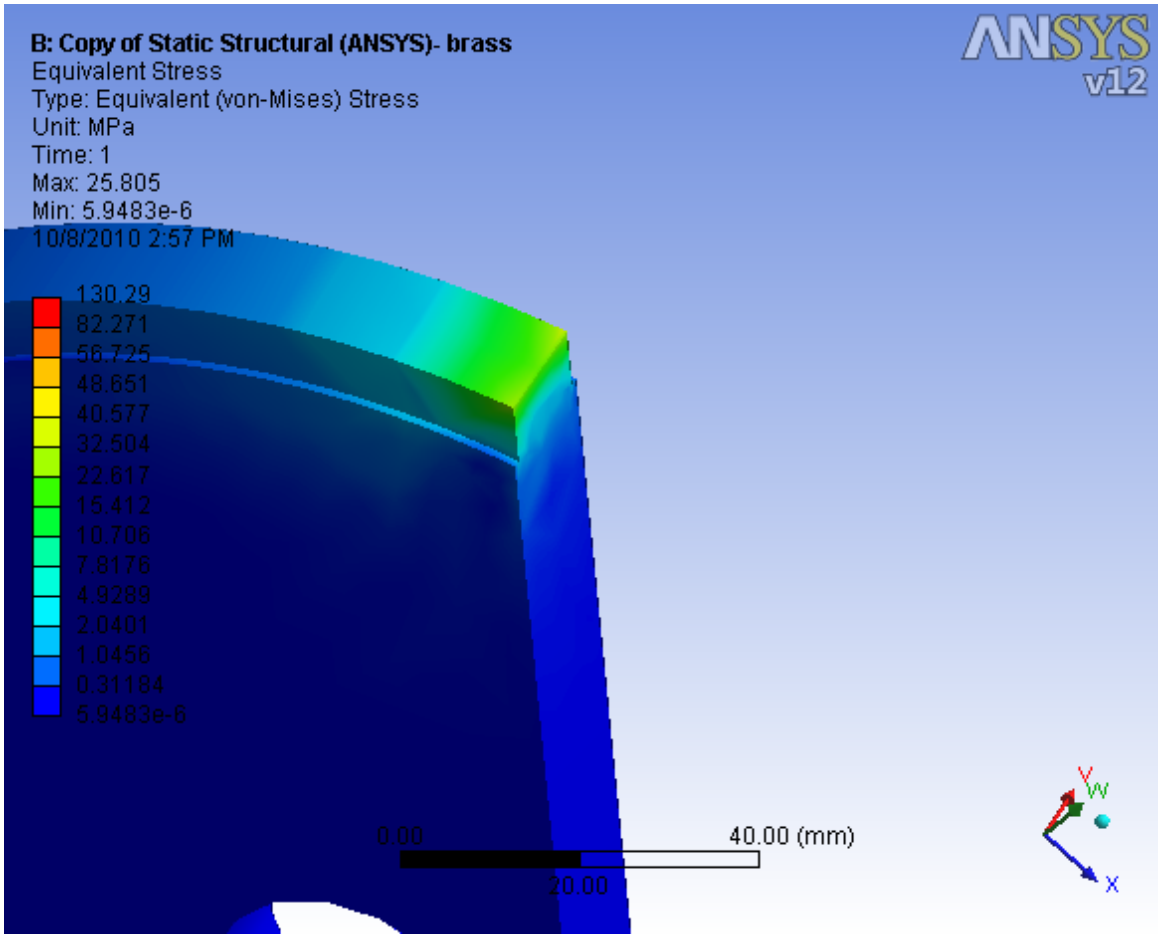

Fig A.11 : FEA profile of brass bar with commercial grinding wheel showing Shear Stress

Static Structural
Subject:
Date Sunday, September 26, 2010
Comments:

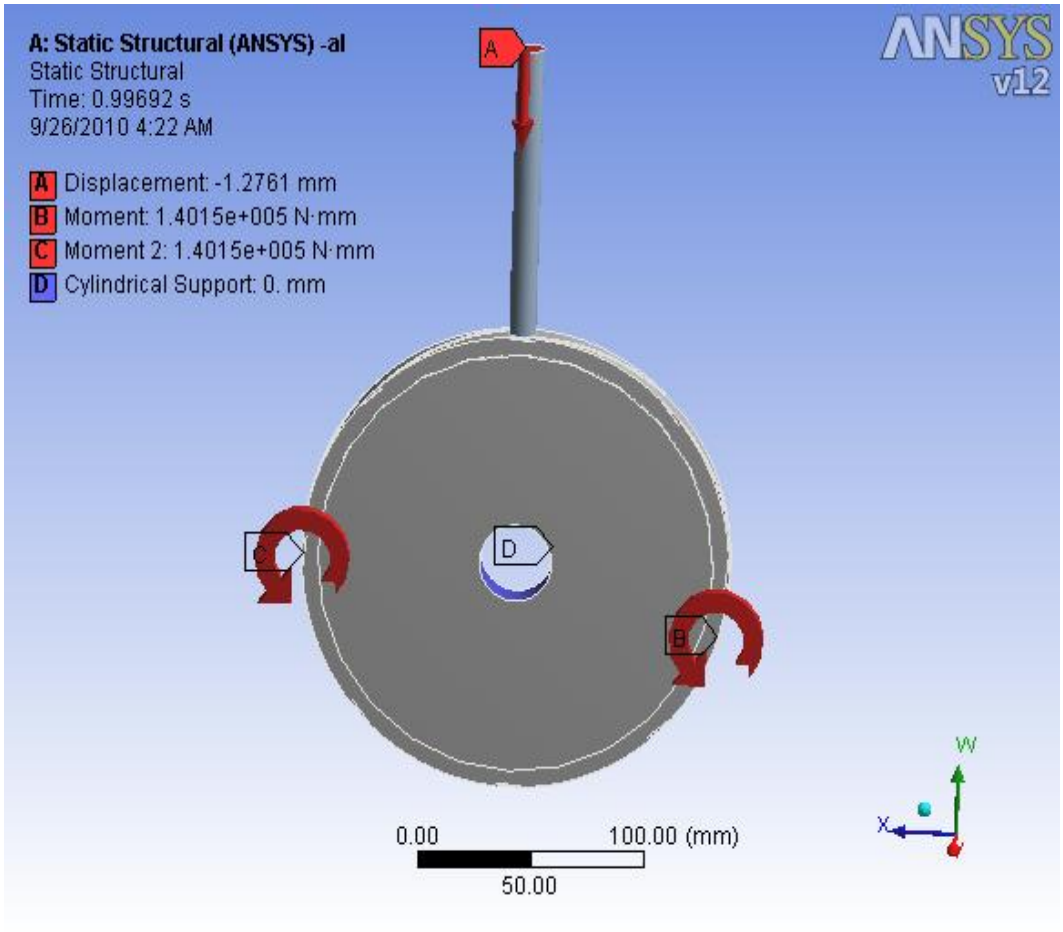

Fig A.12 : Ansys simulation of the grinding wheel with groove highlighting the boundary conditions

Aluminum

Equivalent Stress
Subject:
Date Friday, October 08, 2010
Comments:

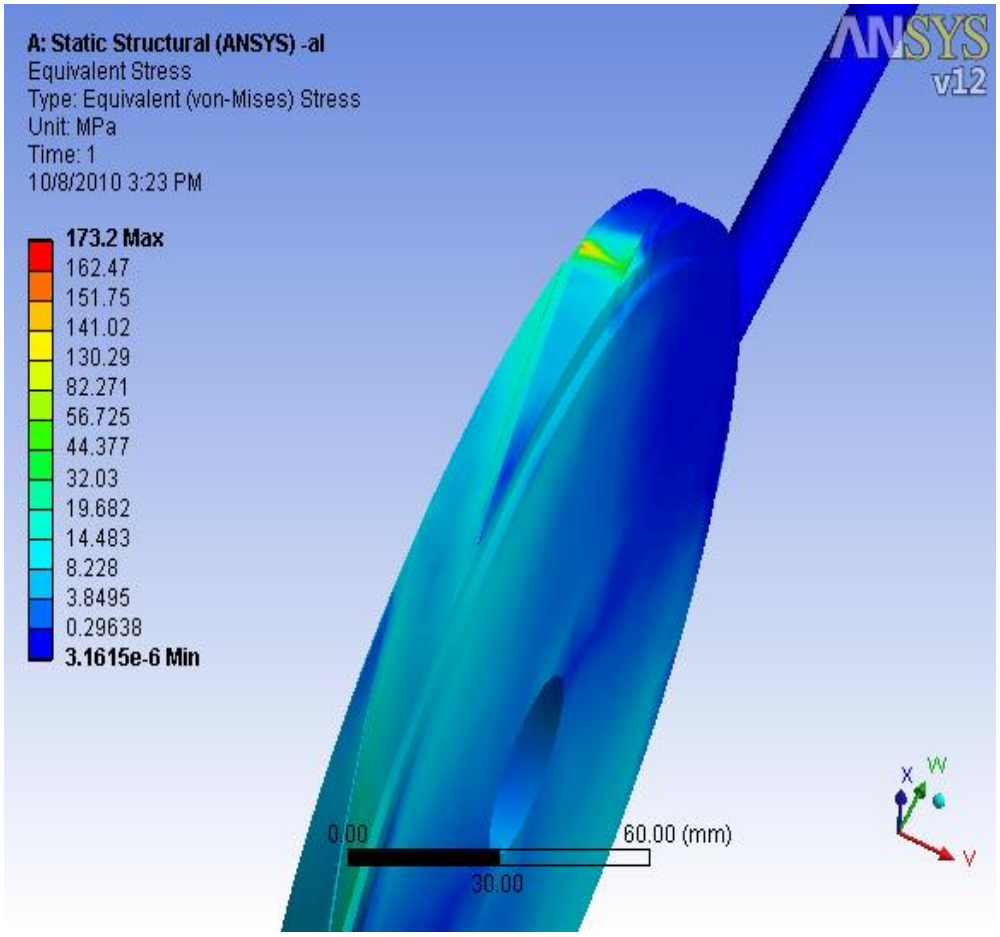

Fig A.13 : FEA profile of aluminium bar with groove grinding wheel showing von-Mises Stress

Maximum Principal Stress
Subject:
Date Friday, October 08, 2010
Comments:

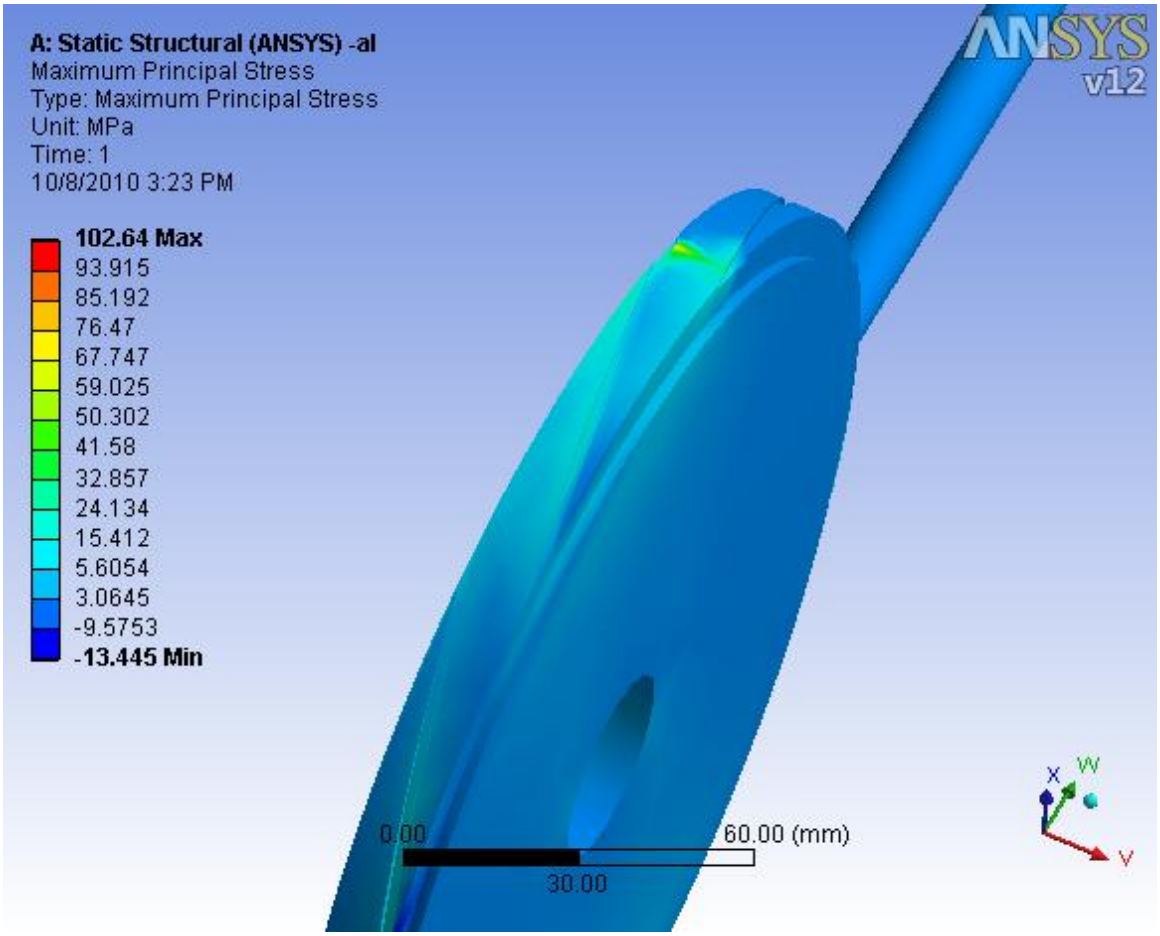

Fig A.14 : FEA profile of aluminium bar with groove grinding wheel showing Principal Stress

Maximum Shear Stress
Subject:
Date Friday, October 08, 2010
Comments:

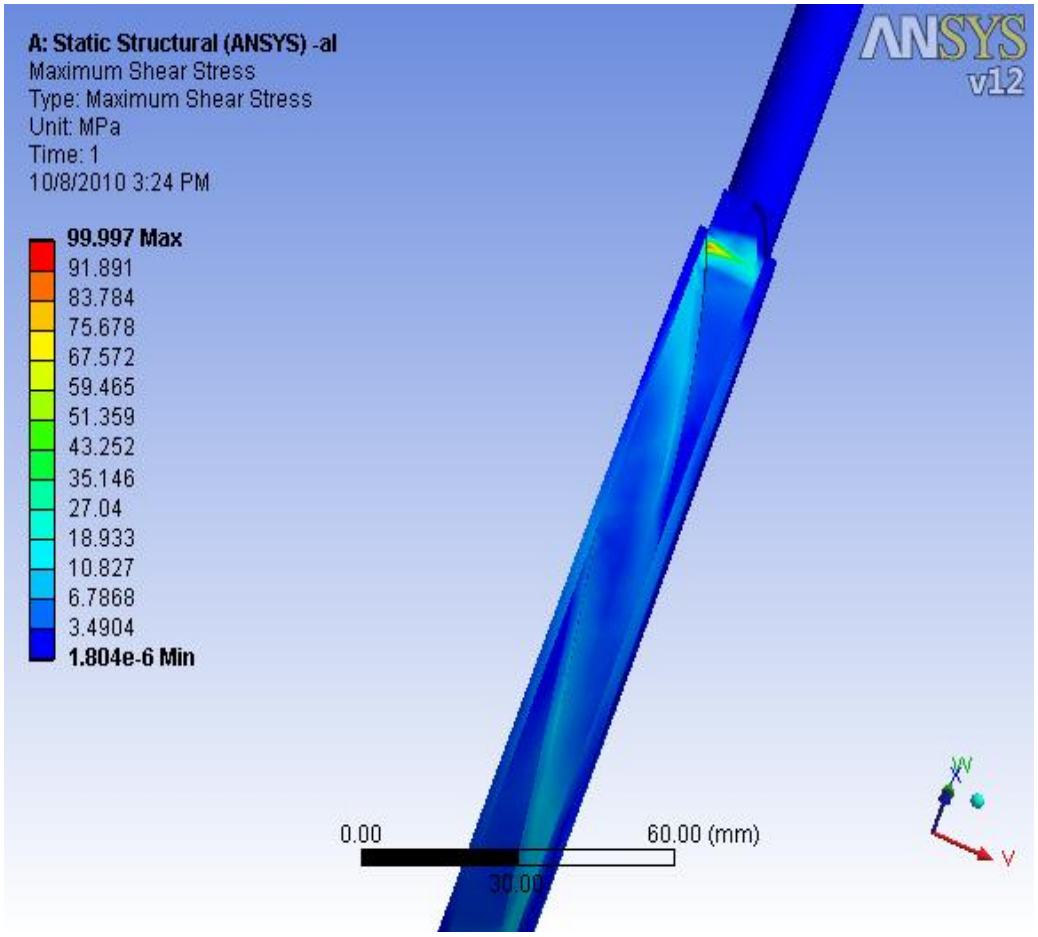

Fig A.15 : FEA profile of aluminium bar with groove grinding wheel showing Shear Stress

Steel

Equivalent Stress
Subject:
Date Sunday, September 26, 2010
Comments:

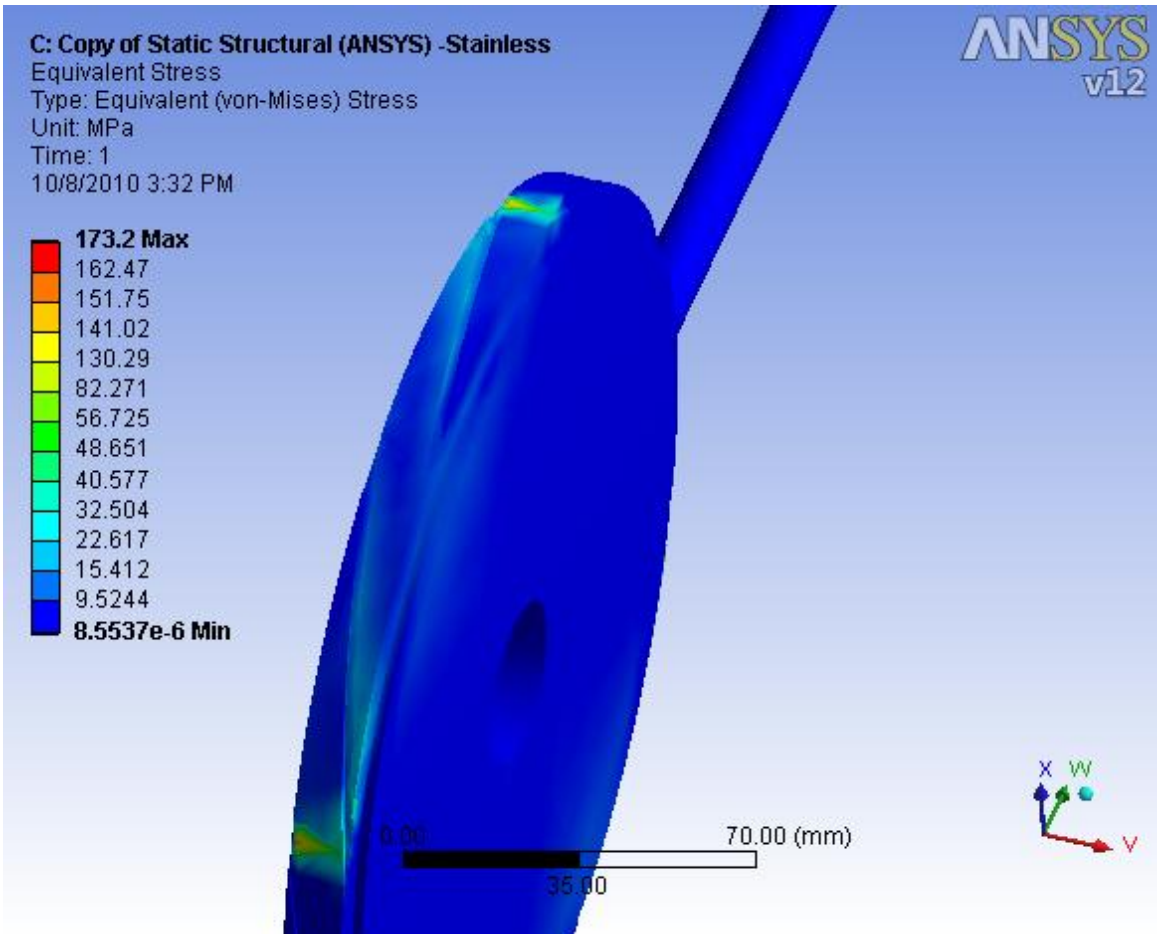

Fig A.16 : FEA profile of stell bar with groove grinding wheel showing von-Mises Stress

Maximum Principal Stress
Subject:
Date Sunday, September 26, 2010
Comments:

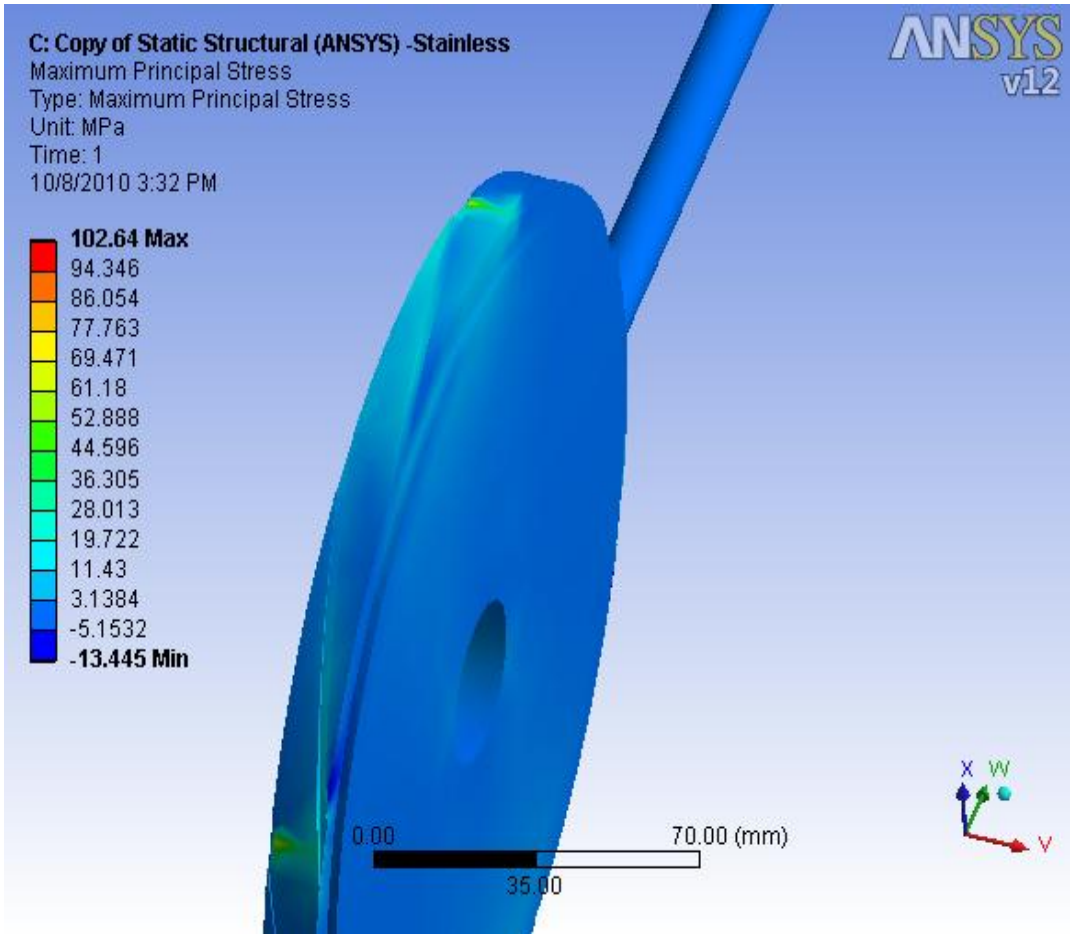

Fig A.17 : FEA profile of aluminium bar with groove grinding wheel showing Principal Stress

Maximum Shear Stress
Subject:
Date Sunday, September 26, 2010
Comments:

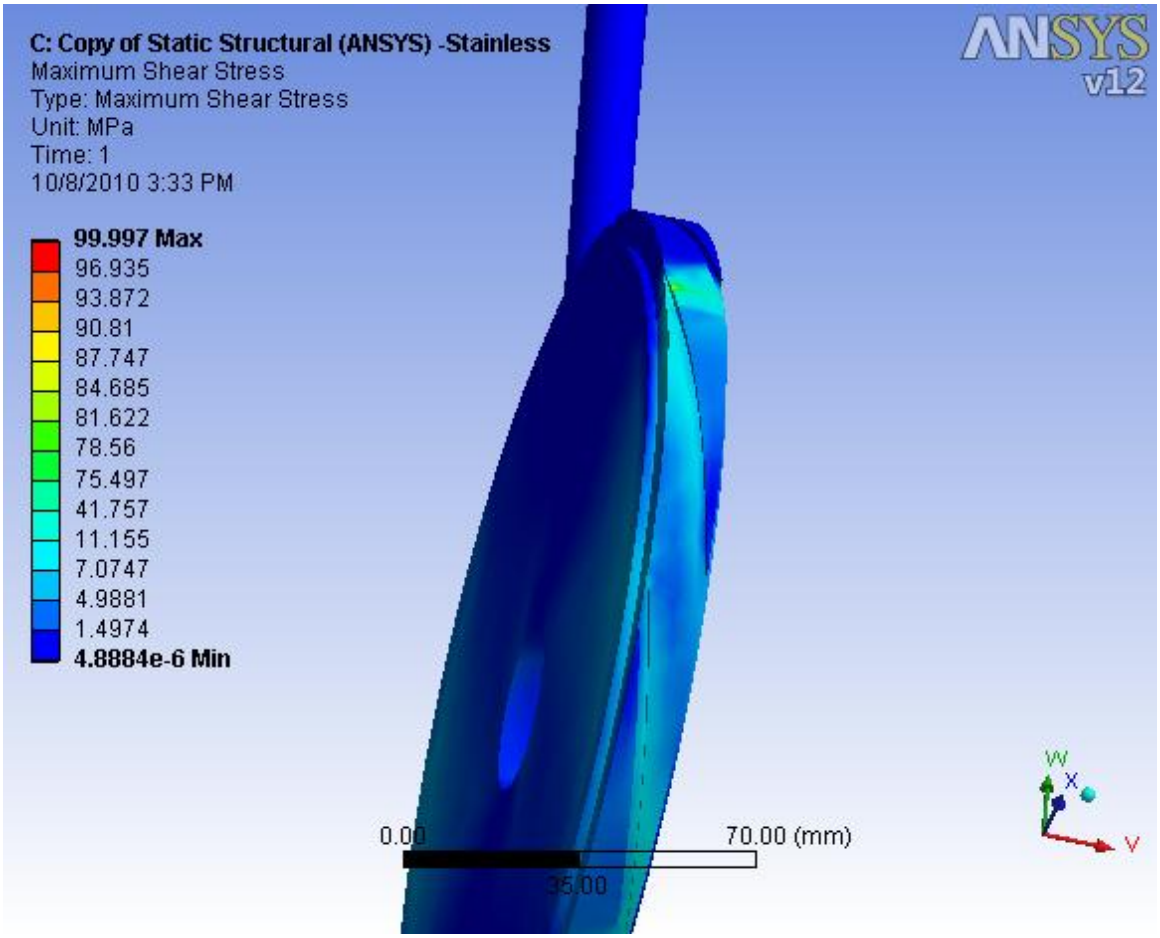

Fig A.18 : FEA profile of aluminium bar with groove grinding wheel showing Shear Stress

Brass

Equivalent Stress
Subject:
Date Friday, October 08, 2010
Comments:

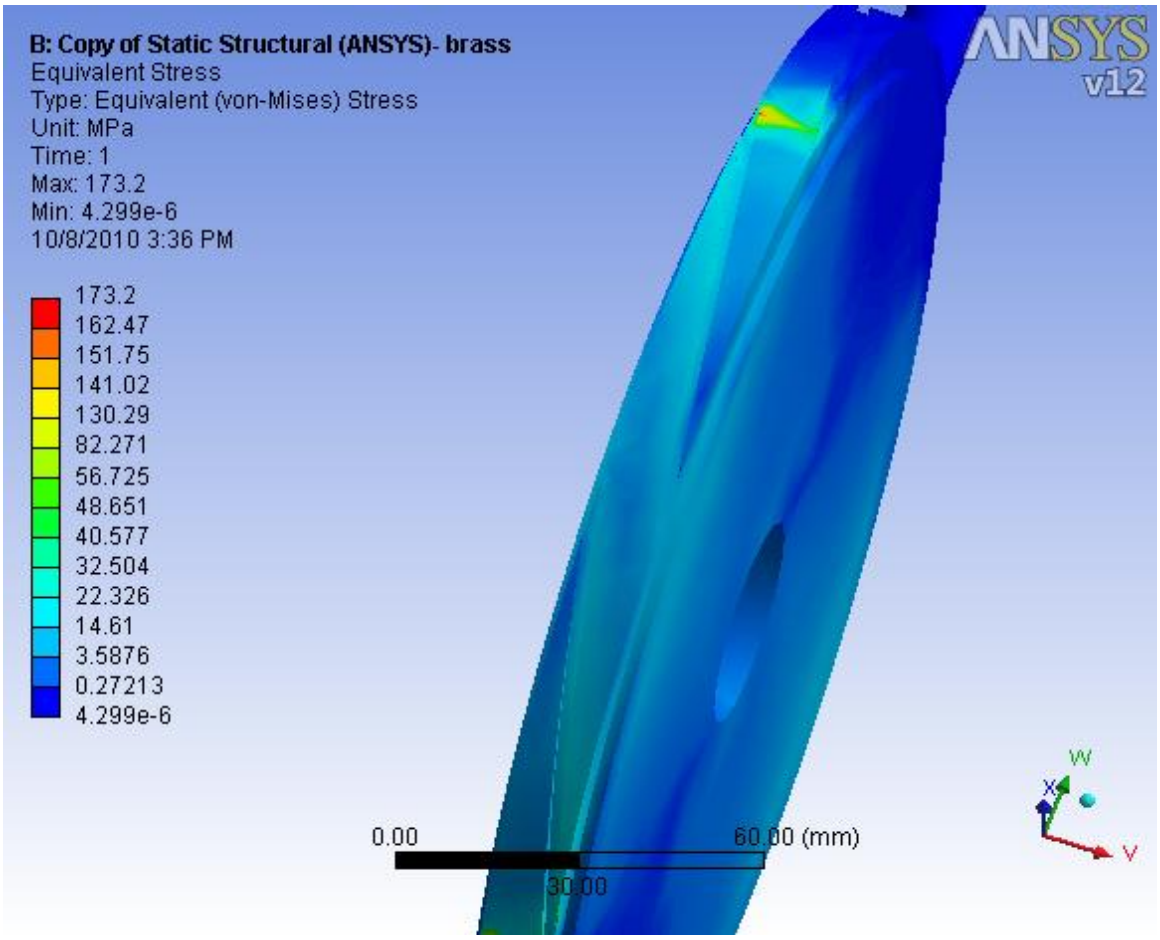

Fig A.19 : FEA profile of brass bar with groove grinding wheel showing von-Mises Stress

Maximum Principal Stress
Subject:
Date Friday, October 08, 2010
Comments:

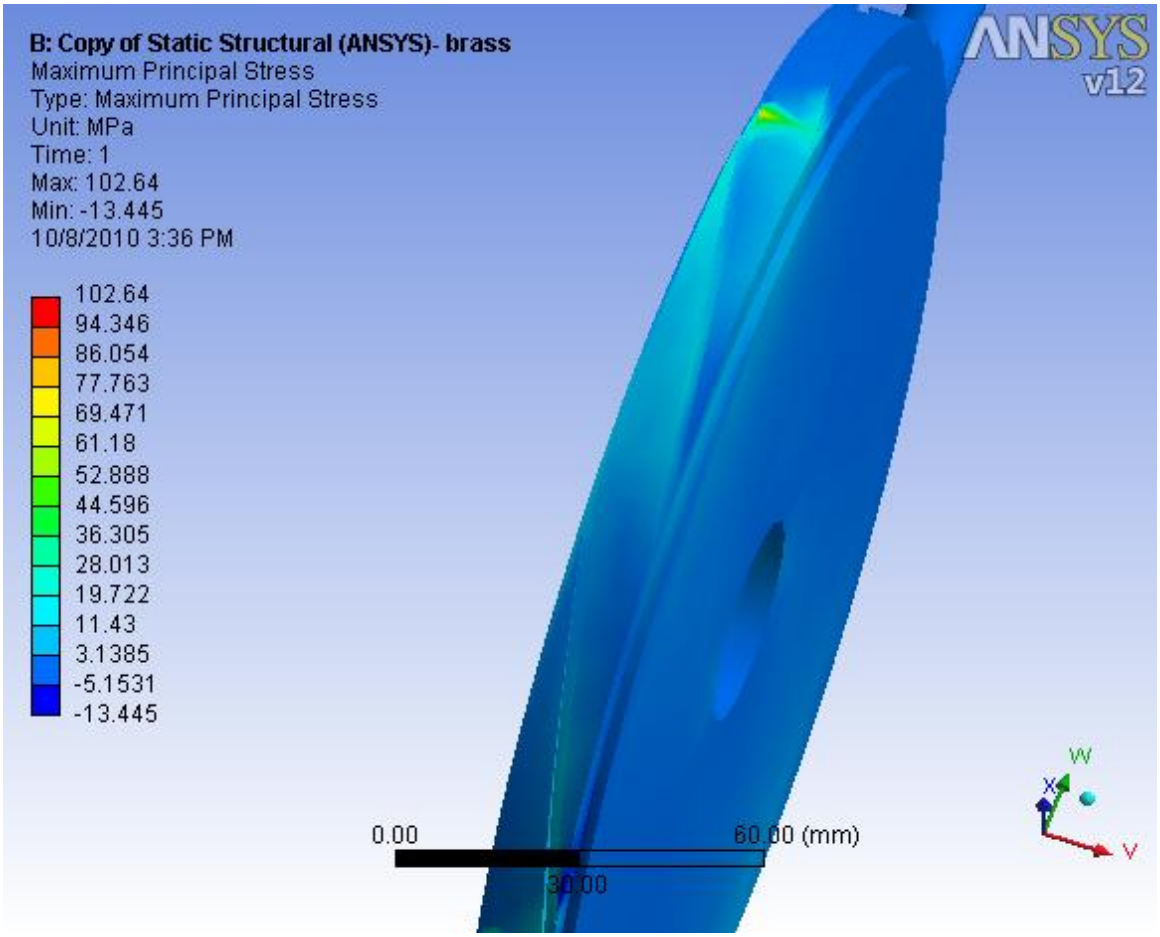

Fig A.20 : FEA profile of brass bar with groove grinding wheel showing Principal Stress

Maximum Shear Stress
Subject:
Date Friday, October 08, 2010
Comments:

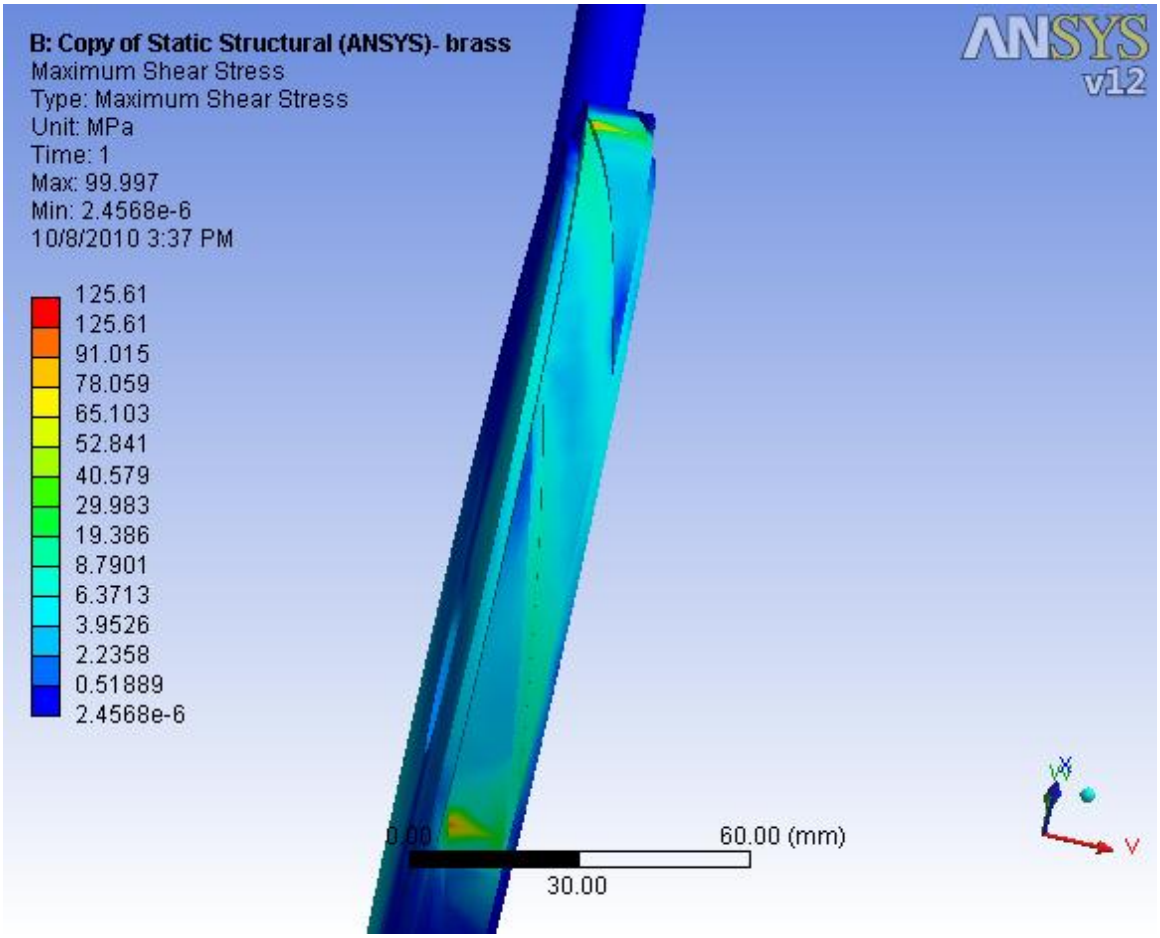

Fig A.21 : FEA profile of brass bar with groove grinding wheel showing Shear Stress

Equivalent Stress
Subject:
Date Friday, October 08, 2010
Comments:

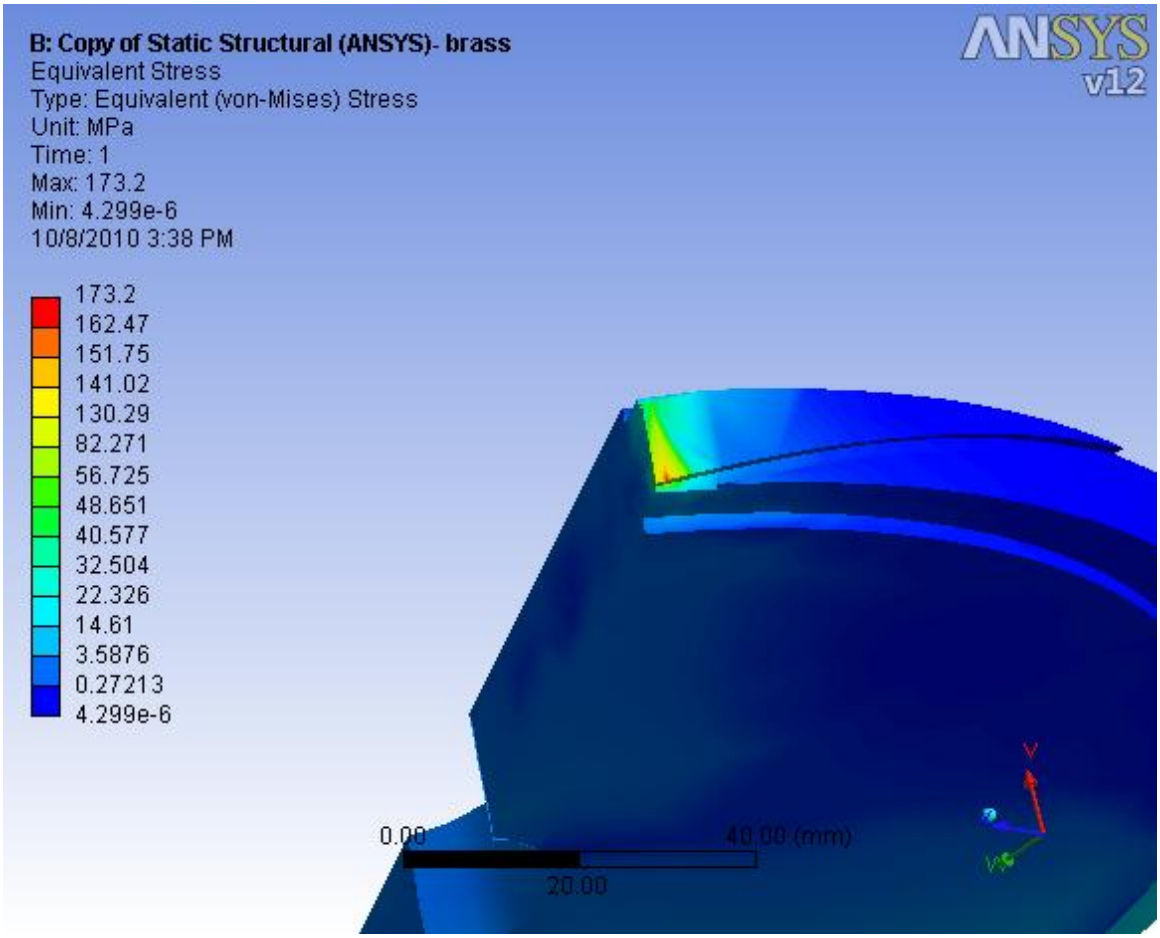

Fig A.22 : FEA profile of brass bar with groove grinding wheel showing von-Mises Stress

Equivalent Stress
Subject:
Date Friday, October 08, 2010
Comments:

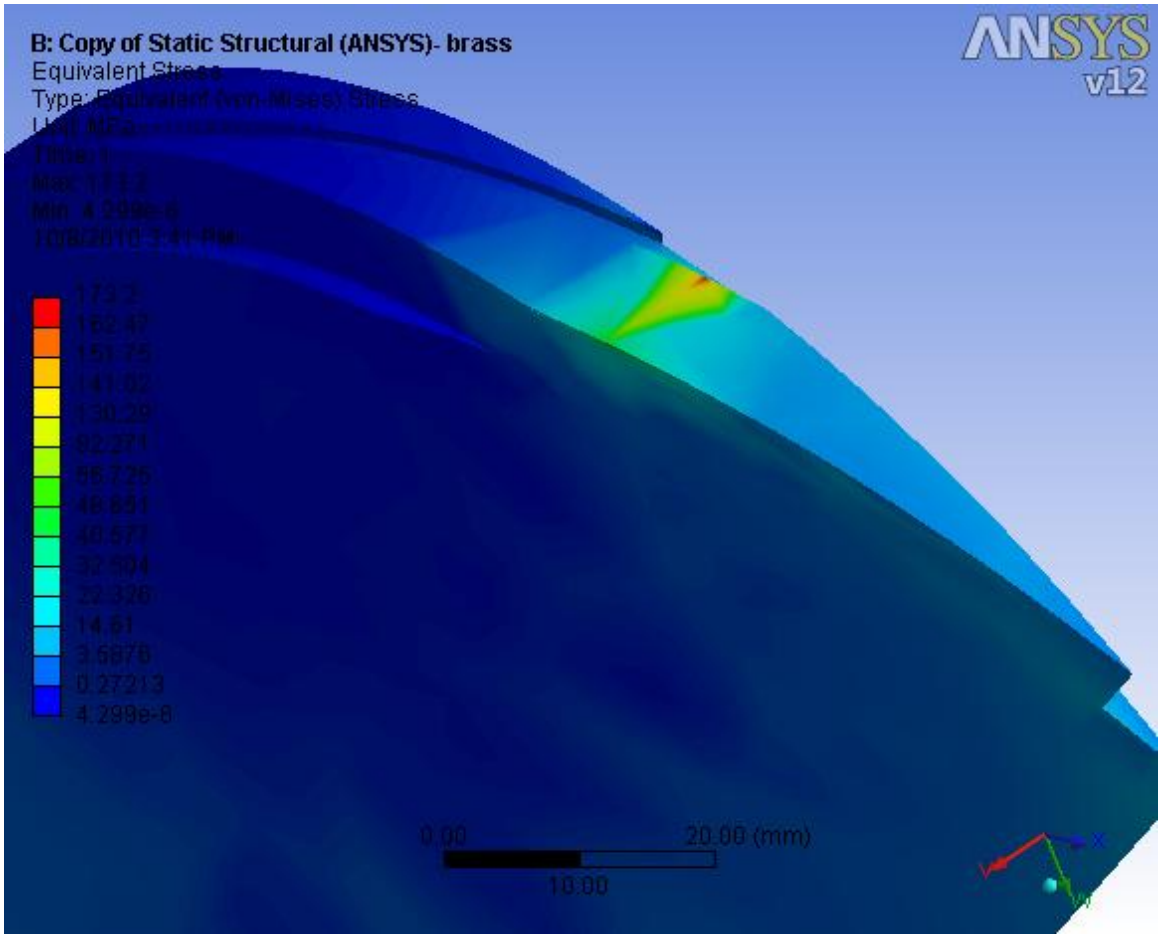

Fig A.23 : FEA profile of brass bar with groove grinding wheel showing von-Mises Stress

Static Structural
Subject:
Date Monday, September 27, 2010
Comments:

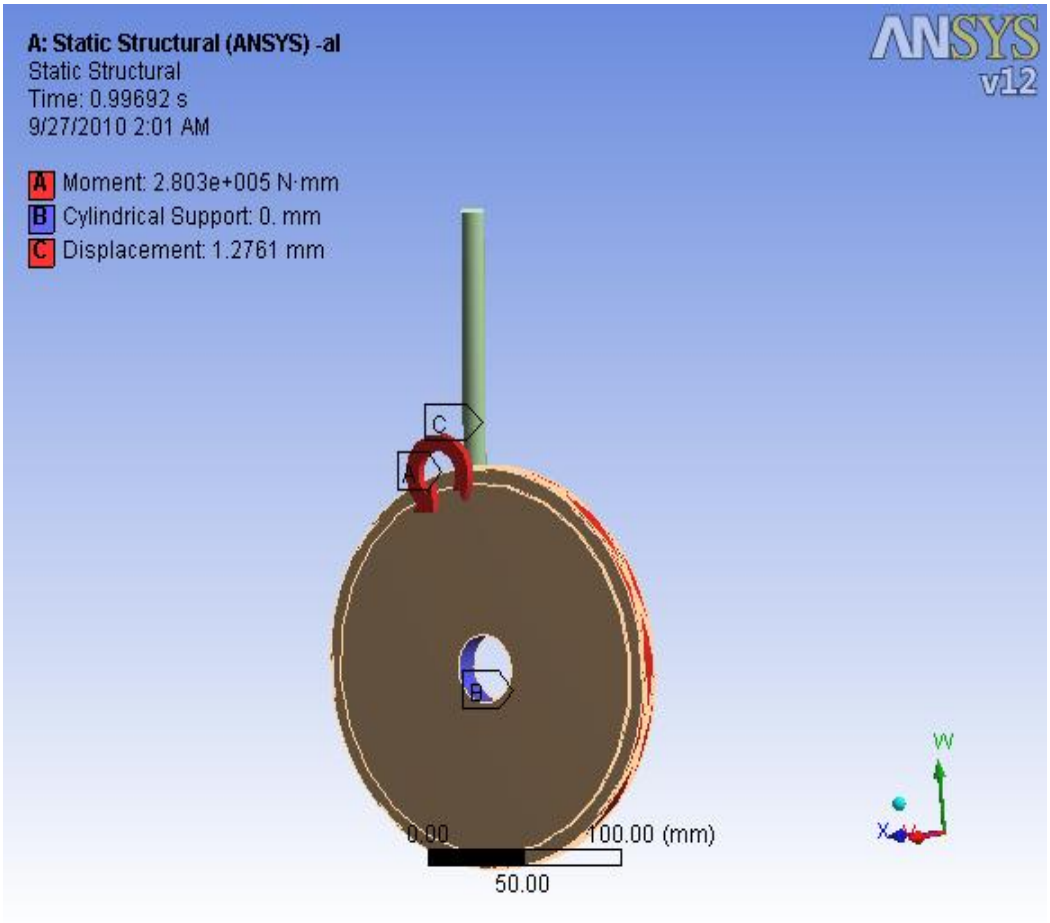

Fig A.24 : Ansys simulation of the grinding wheel with cross groove highlighting the boundary conditions

Aluminum

Equivalent Stress
Subject:
Date Monday, September 27, 2010
Comments:

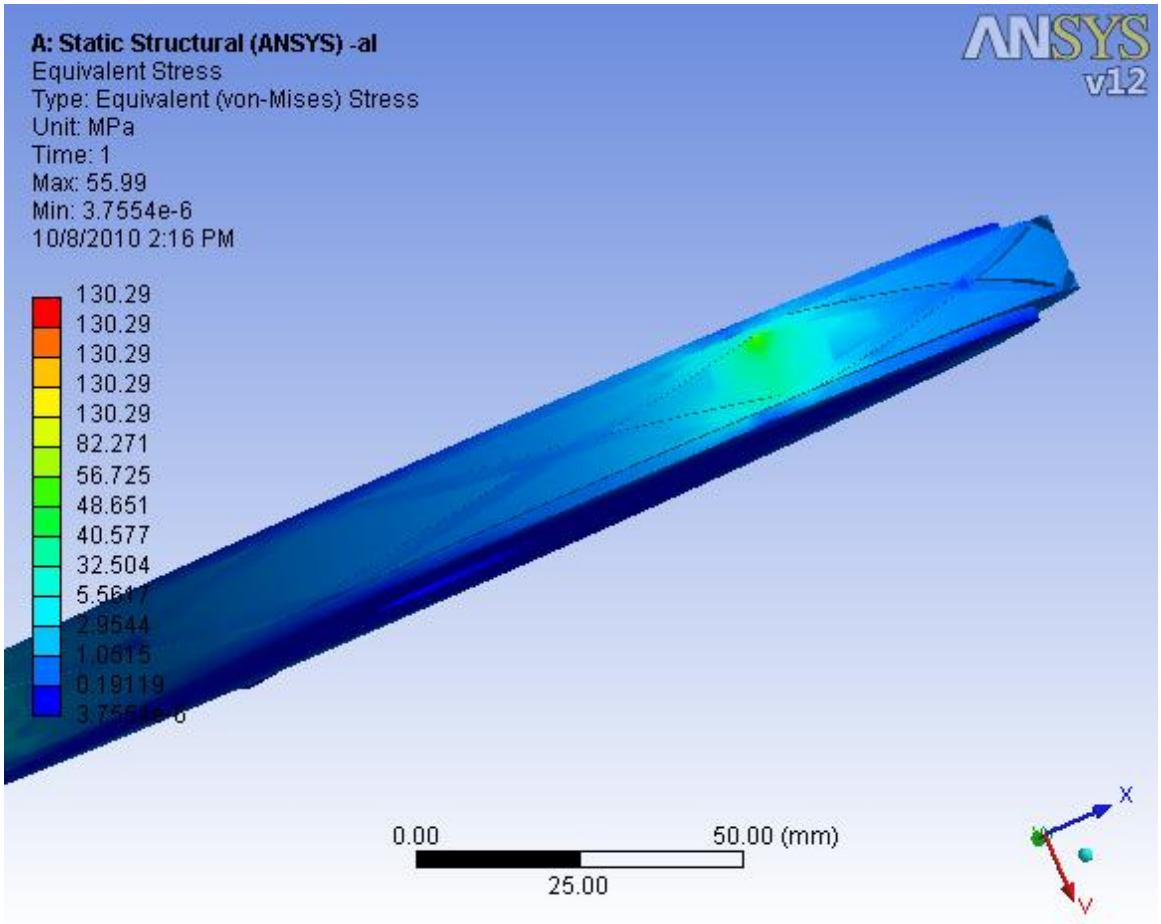

Fig A.25 : FEA profile of aluminium bar with cross groove grinding wheel showing von-Mises Stress

Maximum Principal Stress
Subject:
Date Monday, September 27, 2010
Comments:

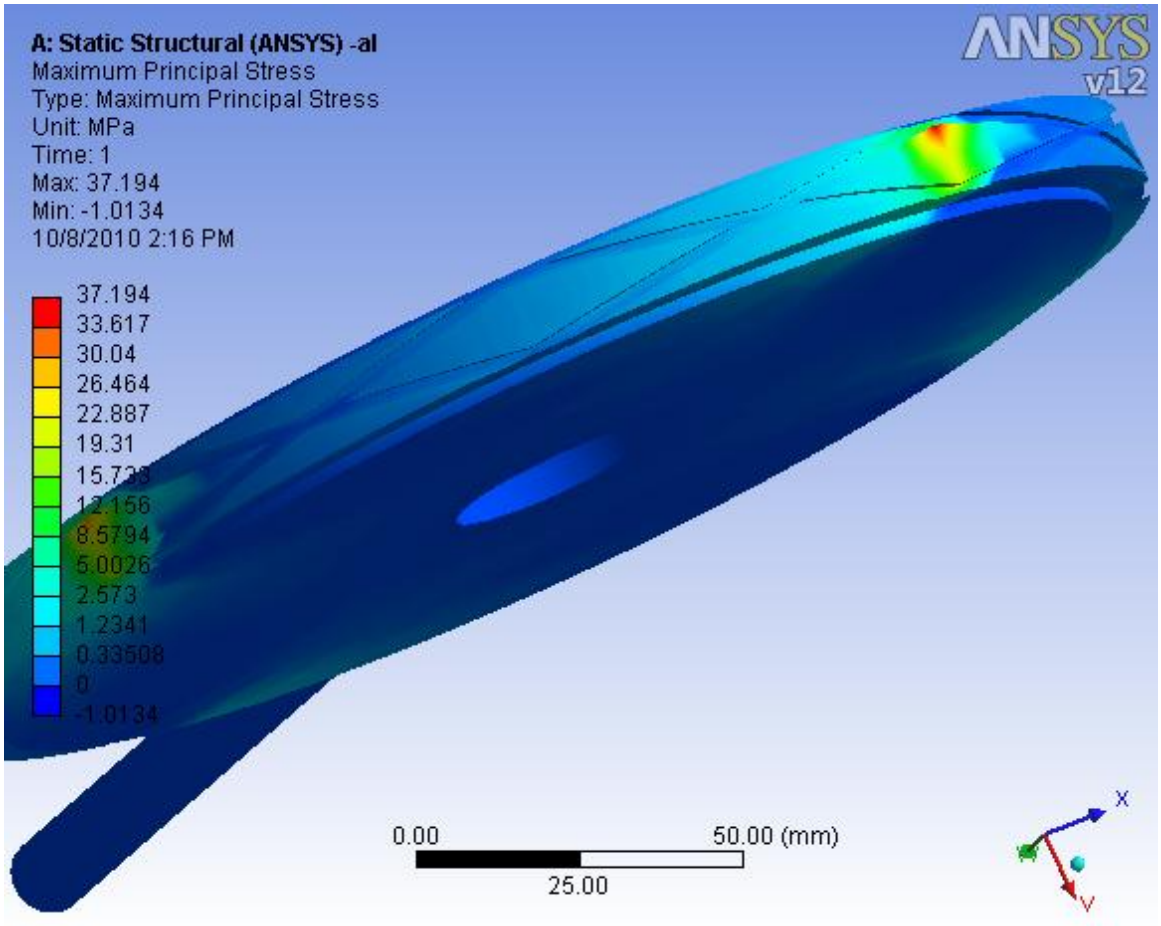

Fig A.26 : FEA profile of aluminium bar with cross groove grinding wheel showing von-Principal Stress

Maximum Shear Stress
Subject:
Date Monday, September 27, 2010
Comments:

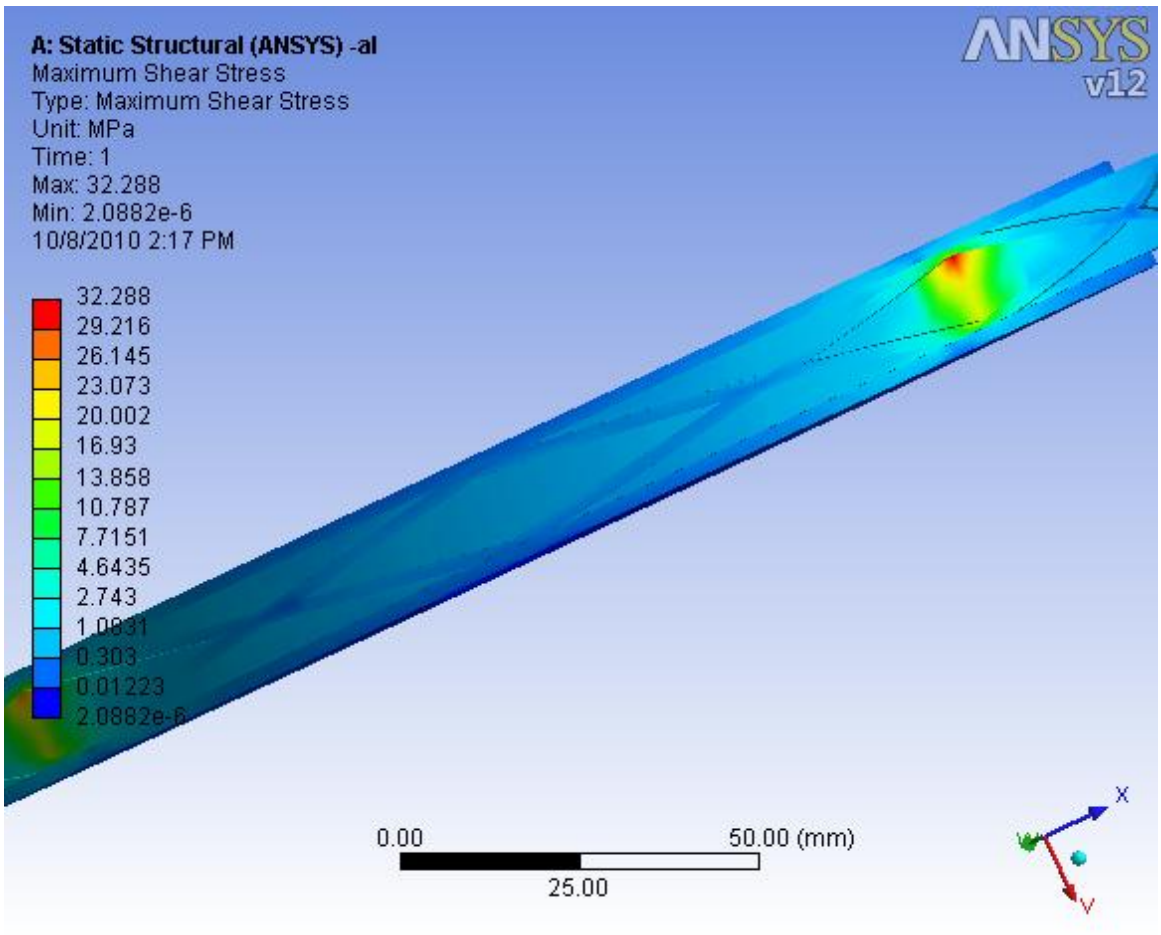

Fig A.27 : FEA profile of aluminium bar with cross groove grinding wheel showing von-Mises Stress

Steel
Equivalent Stress
Subject:
Date Monday, September 27, 2010
Comments:

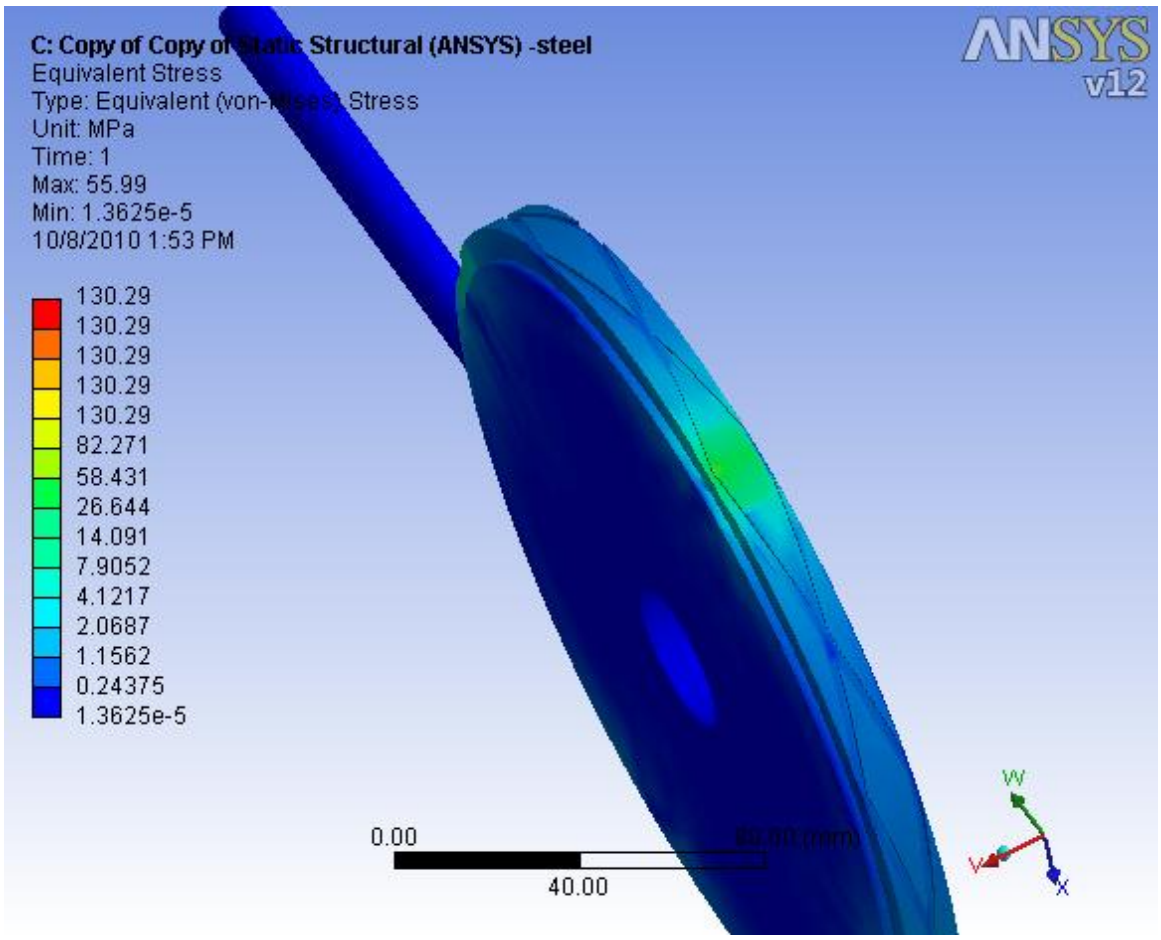

Fig A.28 : FEA profile of steel bar with cross groove grinding wheel showing von-Mises Stress

Maximum Principal Stress
Subject:
Date Monday, September 27, 2010
Comments:

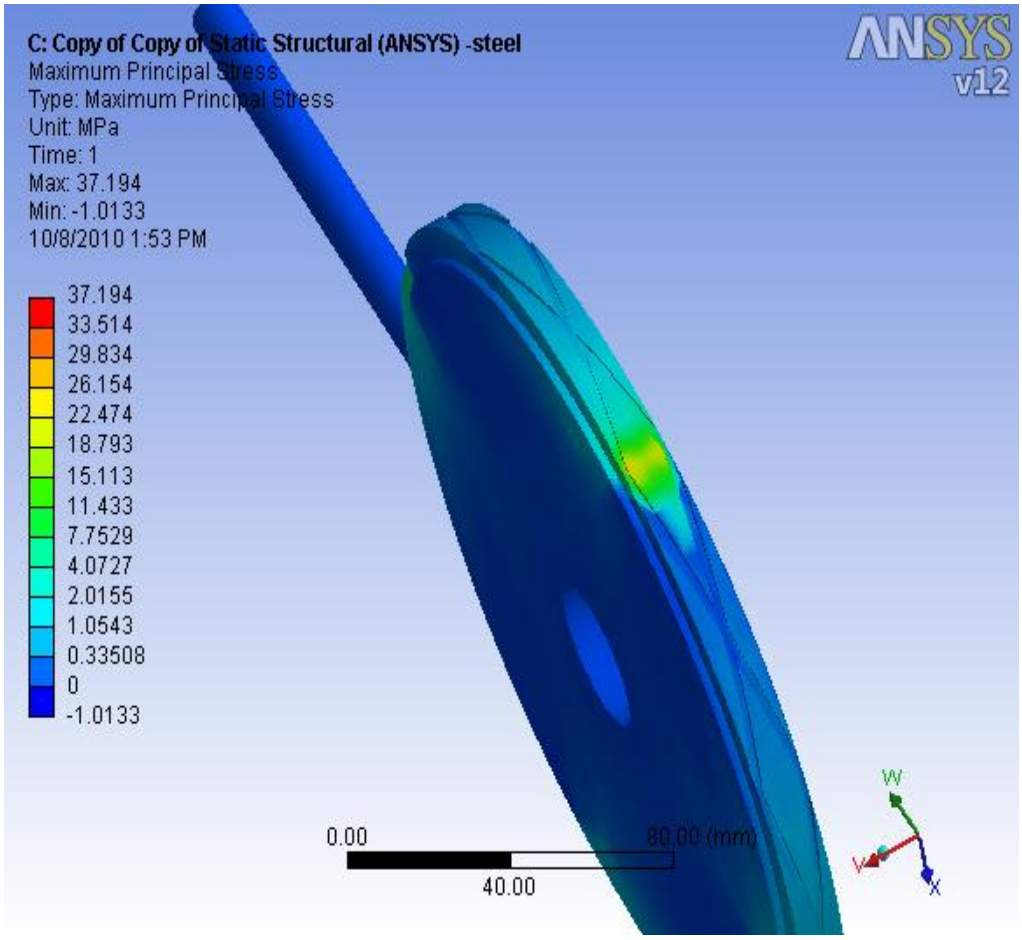

Fig A.29 : FEA profile of steel bar with cross groove grinding wheel showing Principal Stress

Maximum Shear Stress
Subject:
Date Monday, September 27, 2010
Comments:

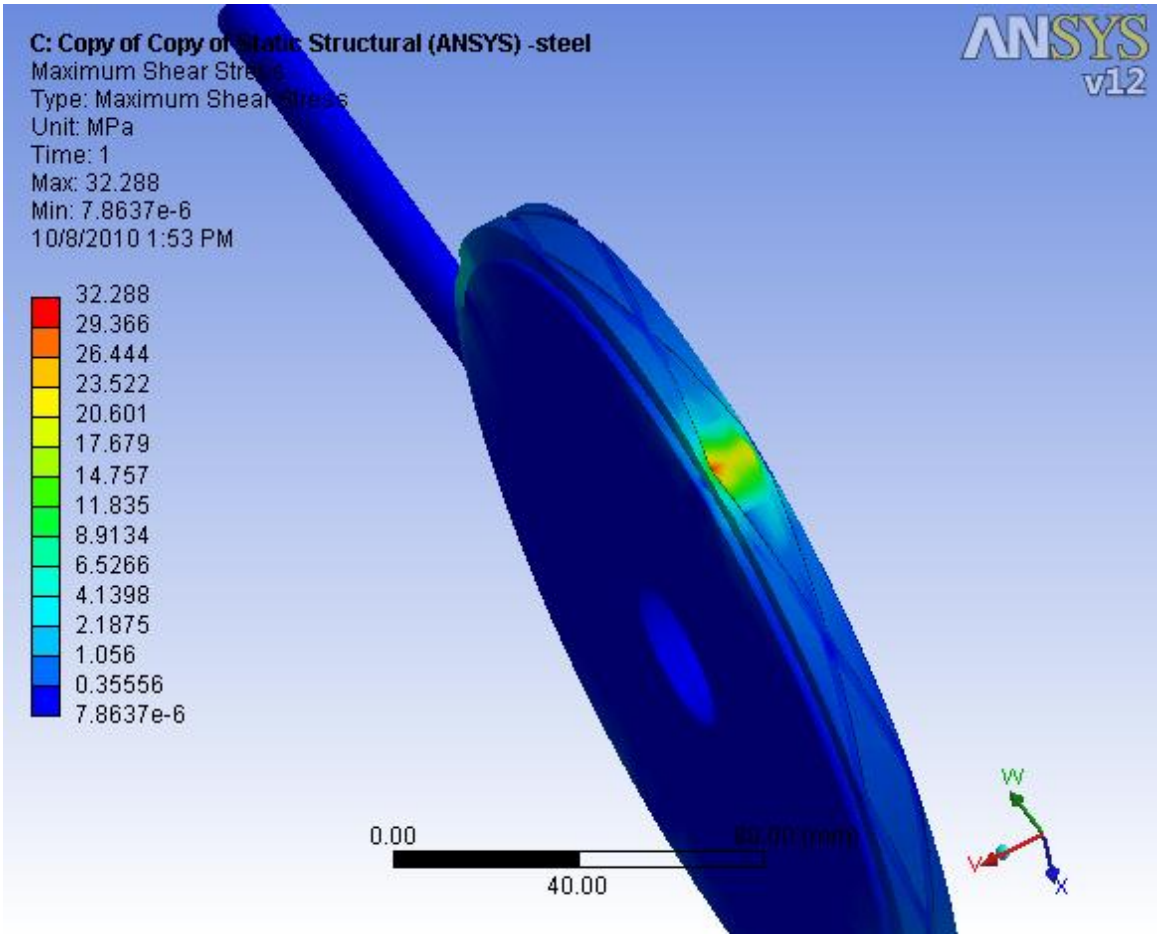

Fig A.30 : FEA profile of steel bar with cross groove grinding wheel showing Shear Stress

Equivalent Stress
Subject:
Date Monday, September 27, 2010
Comments:

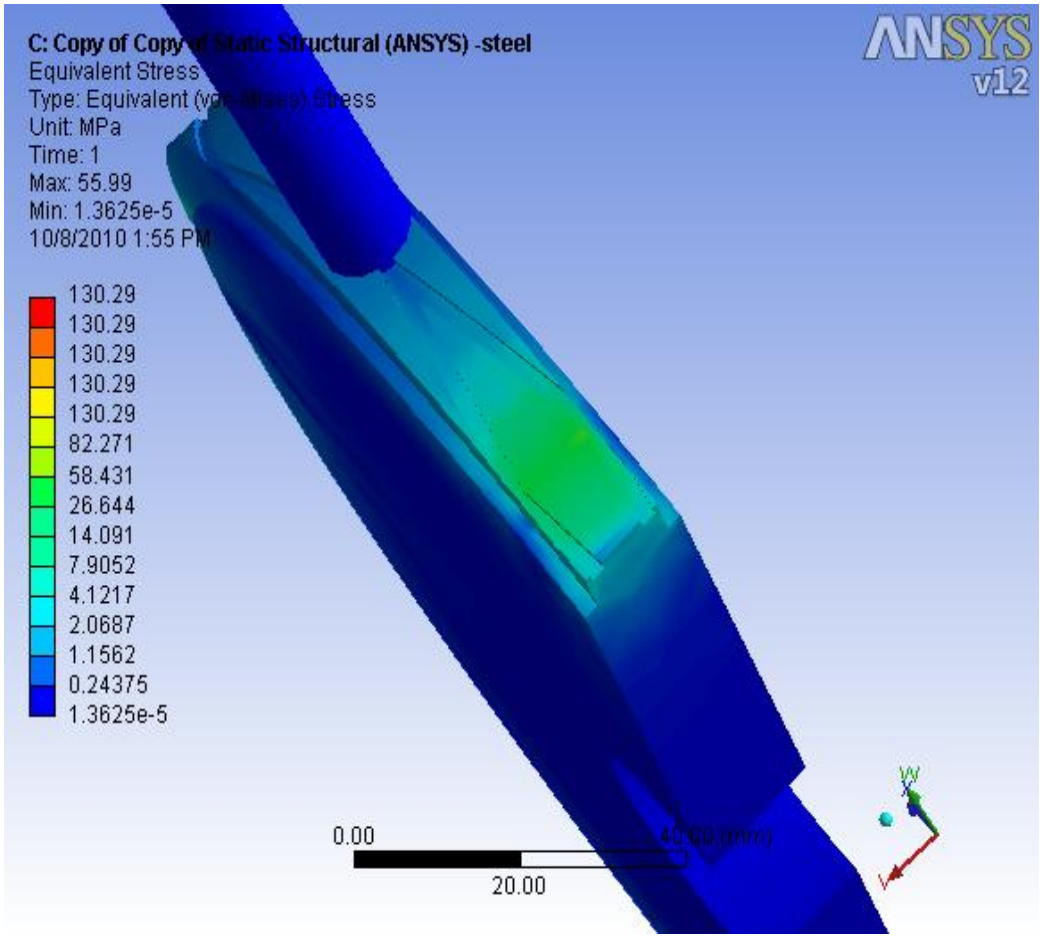

Fig A.31 : FEA profile of steel bar with cross groove grinding wheel showing von-Mises Stress

Brass

Equivalent Stress
Subject:
Date Monday, September 27, 2010
Comments:

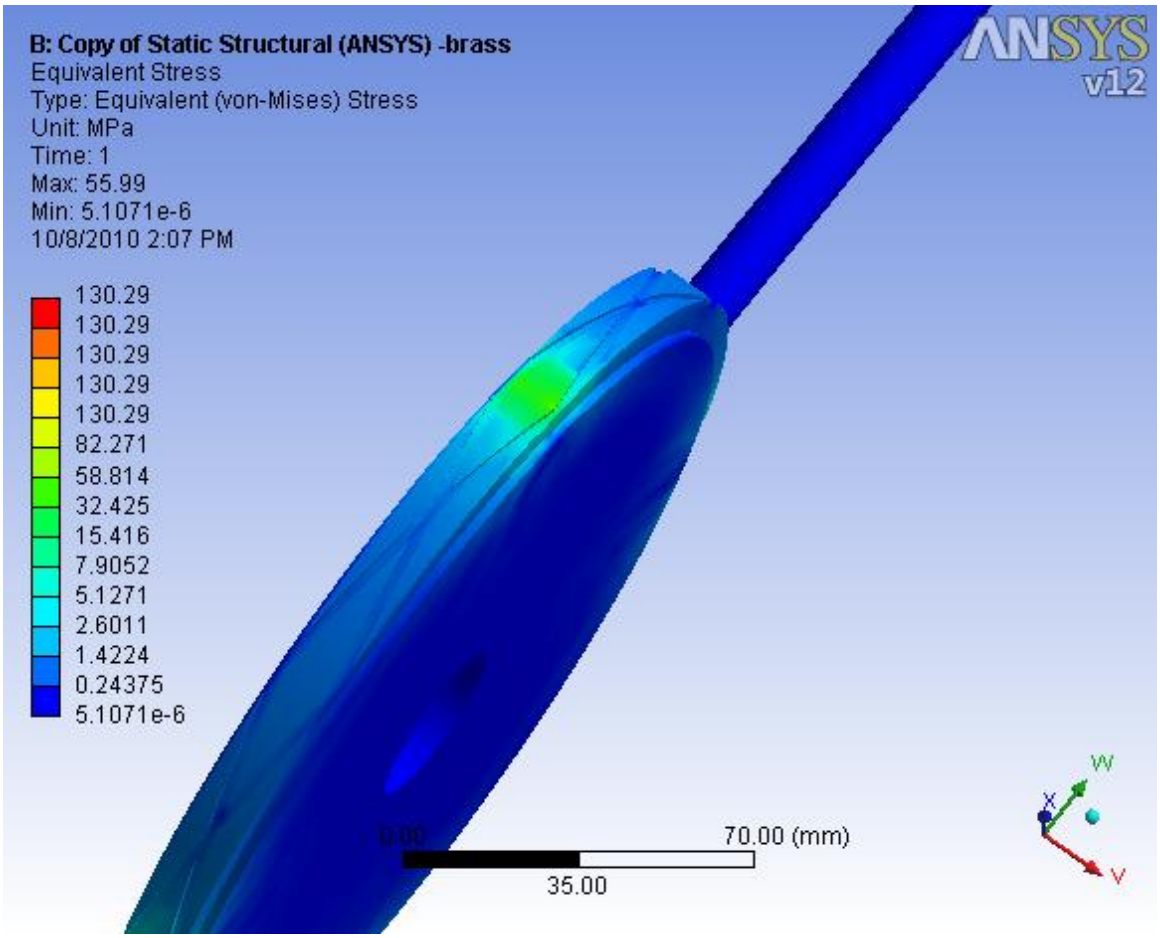

Fig A.32 : FEA profile of brass bar with cross groove grinding wheel showing von-Mises Stress

Maximum Principal Stress
Subject:
Date Monday, September 27, 2010
Comments:

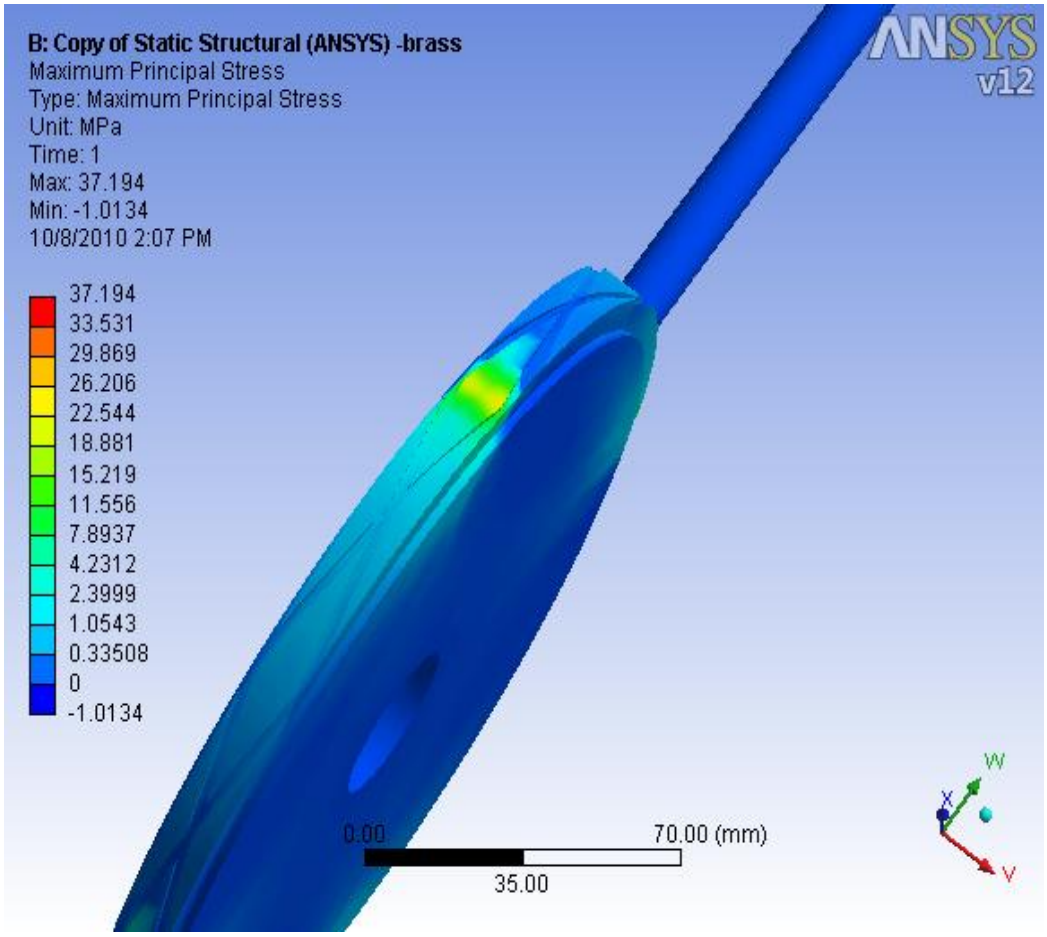

Fig A.33 : FEA profile of brass bar with cross groove grinding wheel showing Principalm Stress

Maximum Shear Stress
Subject:
Date Monday, September 27, 2010
Comments:

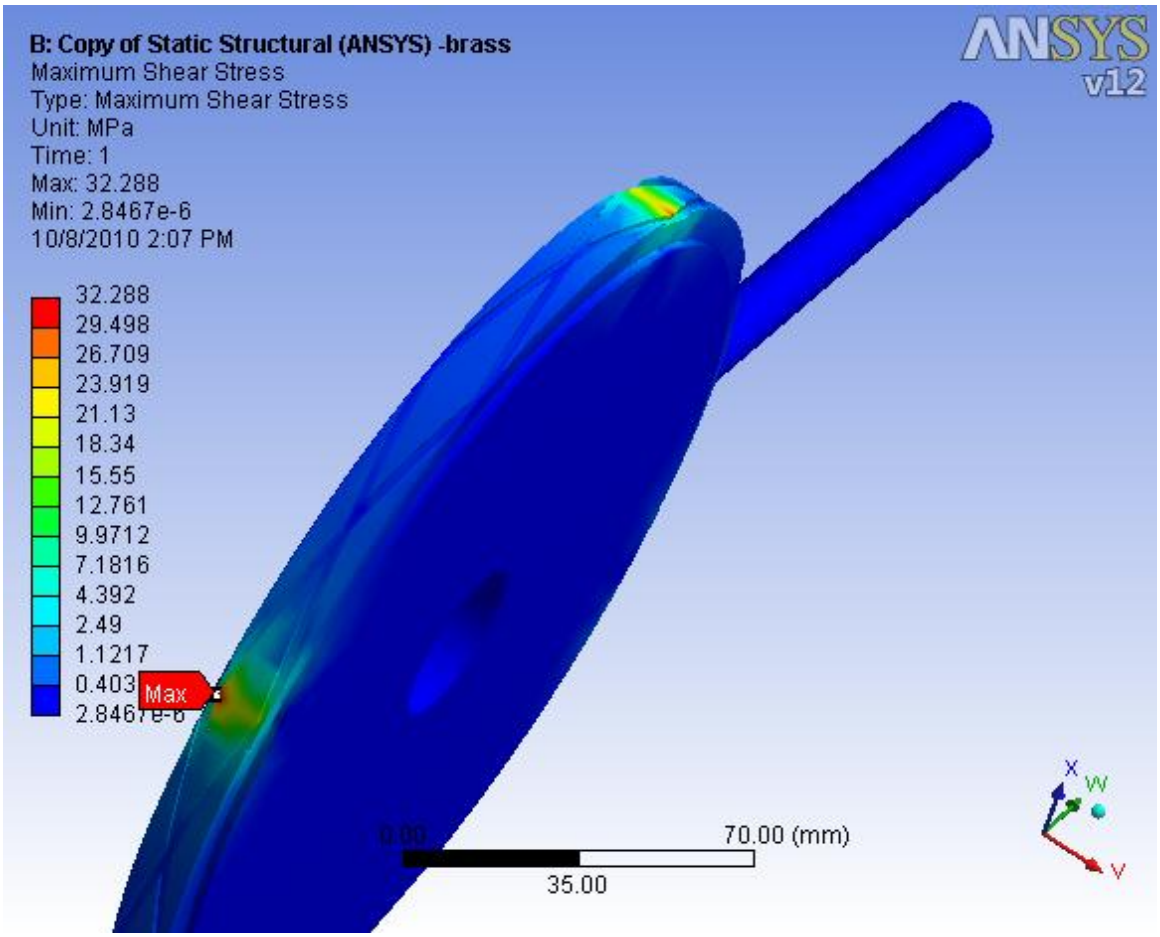

Fig A.34 : FEA profile of brass bar with cross groove grinding wheel showing Shear Stress

Equivalent Stress
Subject:
Date Monday, September 27, 2010
Comments:

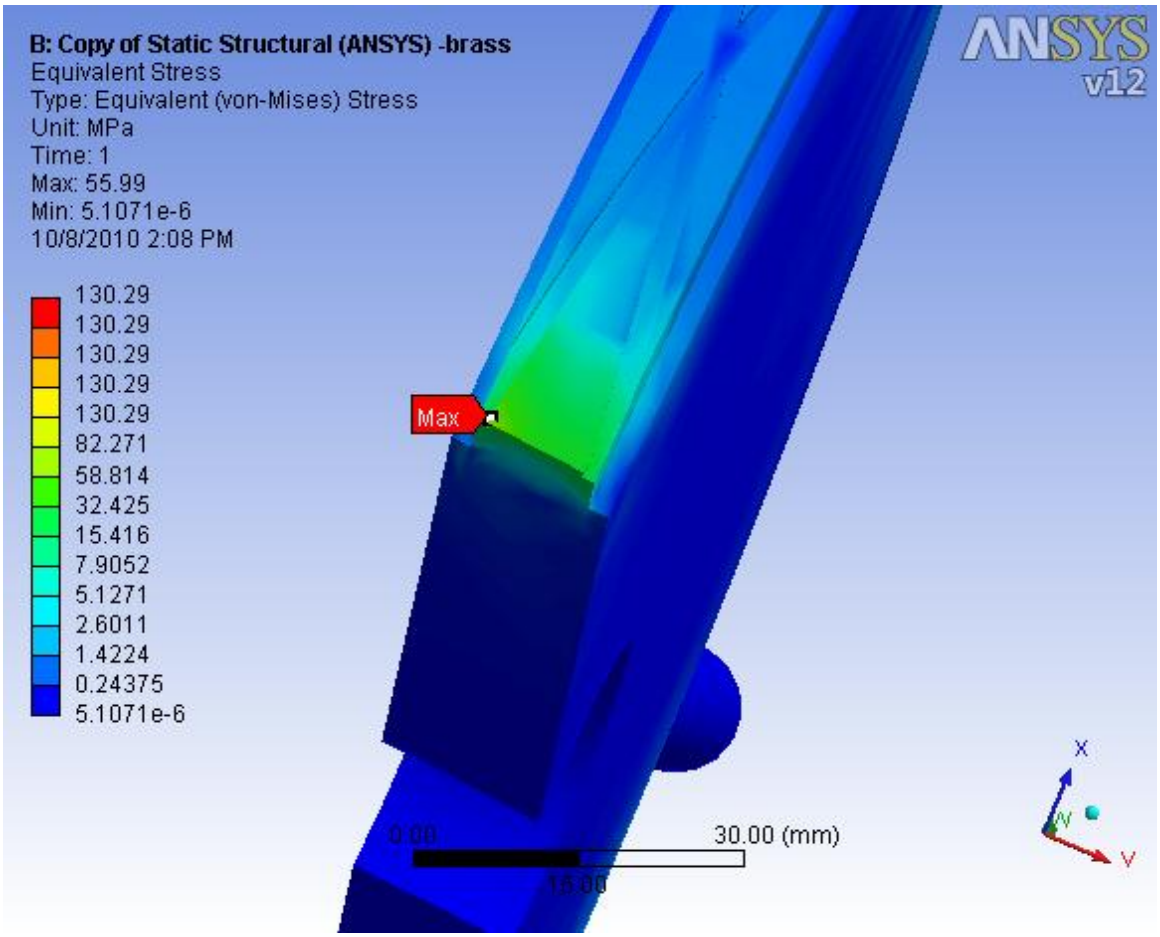

Fig A.35 : FEA profile of brass bar with cross groove grinding wheel showing von-Mises Stress

Equivalent Stress
Subject:
Date Monday, September 27, 2010
Comments:

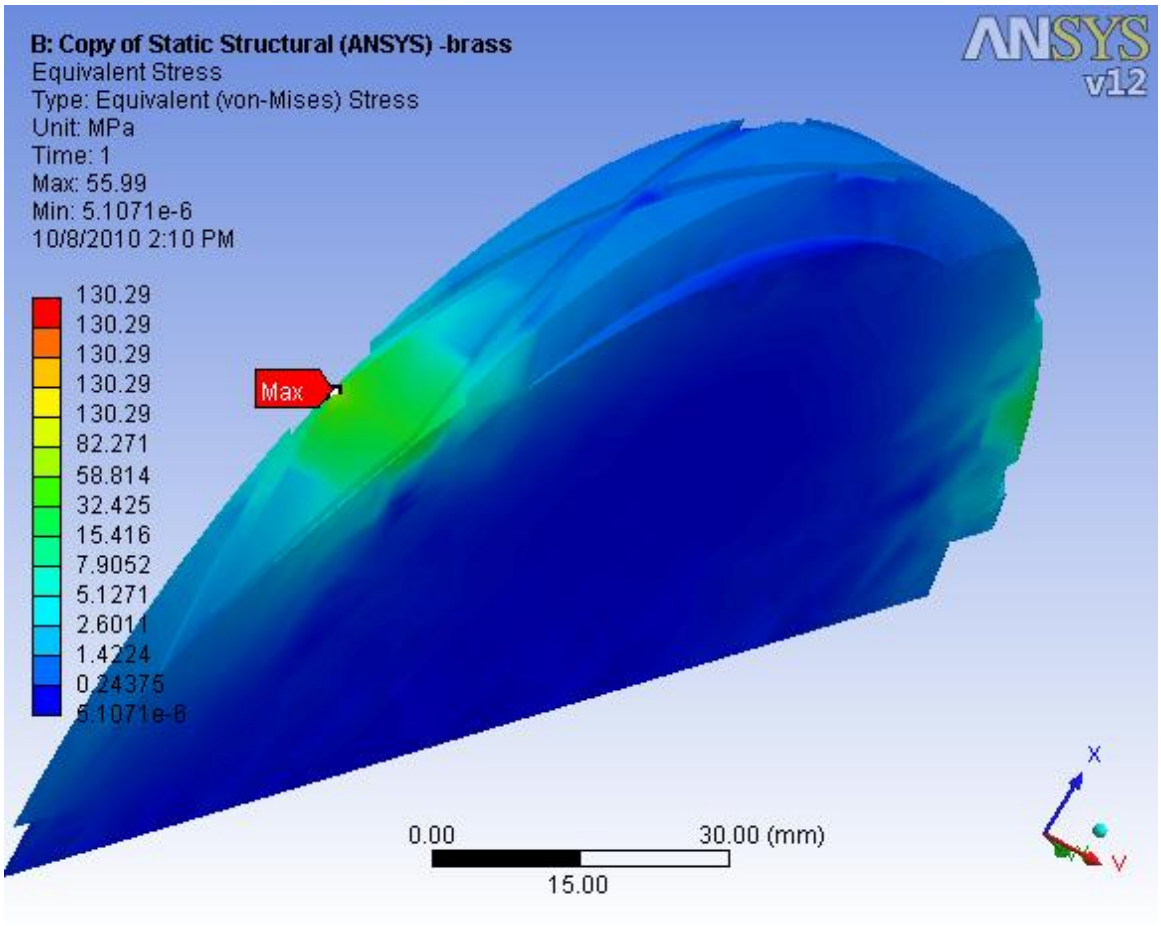

Fig A.36 : FEA profile of brass bar with cross groove grinding wheel showing von-Mises Stress